SOIL ORGANIC CARBON QUANTITY AND DISTRIBUTION IN FROST BOILS IN A CANADIAN HIGH ARCTIC POLAR SEMI-DESERT ECOSYSTEM

A Thesis Submitted to the College of
Graduate and Postdoctoral Studies
In Partial Fulfillment of the Requirements
For the Degree of Doctor of Philosophy
In the Department of Soil Science
University of Saskatchewan
Saskatoon

By

Amanda Muller

PERMISSION TO USE

In presenting this thesis in partial fulfillment of the requirements for a Postgraduate degree from the University of Saskatchewan, I agree that the Libraries of this University may make it freely available for inspection. I further agree that permission for copying of this thesis in any manner, in whole or in part, for scholarly purposes may be granted by the professor or professors who supervised my thesis work or, in their absence, by the Head of the Department or the Dean of the College in which my thesis work was done. It is understood that any copying or publication or use of this thesis or parts thereof for financial gain shall not be allowed without my written permission. It is also understood that due recognition shall be given to me and to the University of Saskatchewan in any scholarly use which may be made of any material in my thesis. Requests for permission to copy or to make other uses of materials in this thesis, in whole or part, should be addressed to:

Head, Department of Soil Science

University of Saskatchewan

Agriculture Building, 51 Campus Drive

Saskatoon, Saskatchewan, S7N 5A8

Canada

OR

Dean, College of Graduate and Postdoctoral Studies

University of Saskatchewan

116 Thorvaldson Building, 110 Science Place

Saskatoon, Saskatchewan S7N 5C9

Canada

DISCLAIMER

Reference in this dissertation to any specific commercial products, process, or service by trade name, trademark, manufacturer, or otherwise, does not constitute or imply its endorsement, recommendation, or favouring by the University of Saskatchewan. The views and opinions of the author expressed herein do not state or reflect those of the University of Saskatchewan, and shall not be used for advertising or product endorsement purposes

ABSTRACT

High Arctic soil organic carbon (SOC) stores are a key component in the global C cycle and are locally important for nutrient cycling in the polar deserts that dominate these regions. Compared to other Arctic regions, we know relatively little about the quantity and distribution of polar desert SOC. Unique frost-driven soil processes in polar deserts result in patterned ground features such as frost boils wherein, SOC-rich patches may develop via diapirism. The objective of this research was to determine whether these patches act as important nutrient sources for vascular plants and how subsurface patches of SOC associated with diapirism contribute to the polar desert carbon pool.

I investigated SOC in 560 frost boils across two polar semi-deserts in the Canadian High Arctic using a field portable visible and near-infrared spectrophotometer. I found frequency of subsurface SOC patches was linked to broad differences in vegetation community. To determine if diapirs provide an enhanced source of plant-available nutrients we used natural abundance and enriched isotope ^{15}N techniques to trace the flow of N through the soil-plant system. When diapir patches were available, the dominant deciduous shrub *Salix arctica* increased its subsurface (i.e., diapir) N uptake, often had greater % cover, and plant root biomass doubled within-diapir. Plant uptake of enriched ^{15}N injected into C-rich soil patches was 2.5 fold greater in diapir than in non-diapir frost boils, also confirming that *S. arctica* is able to access N when these patches are present.

My best estimate of SOC stored in the active layer of High Arctic polar semi-deserts is 8.14 ± 0.45 Pg SOC, or ~73% of SOC stored in the top 30 cm of all High Arctic soils. When subsurface SOC patches were detected in frost boils, those frost boils contained nearly double the SOC compared to those without patches and on average 40% of the SOC was found within the

patch. Thus, despite diapiric frost boils representing only 35% of frost boils, they contribute disproportionately to High Arctic C storage.

ACKNOWLEDGEMENTS

I am grateful for every ounce of guidance from my supervisors, Dr. Eric Lamb and Dr. Steven Siciliano. At every stage, they provided amazing opportunities including epic field seasons, conferences, and support for professional development. Thank you to my advisory committee, Drs. Ken Van Rees, Derek Peak, Angela Bedard-Haughn, Jonathan Bennett, and past member Dr. Jill Johnstone for all the advice and guidance through this process.

Financial research support was provided by the Northern Scientific Training Program and the Natural Sciences and Engineering Research Council (NSERC) of Canada Discovery Grant to SD Siciliano. Polar Continental Shelf Program provided logistical field support. Personal financial support was provided by the NSERC Alexander Graham Bell Canada Graduate Scholarships (CGS D/CGS), and numerous other scholarships administered by the Department of Soil Science, College of Agriculture and Bioresources, and University of Saskatchewan.

Heartfelt thanks to the Arctic field crew - Sarah Hardy, Mitsuaki Ota, Nicole Marleau, and Martin Brummell- for your vis-NIR help, pit dances, and companionship in the field. Thanks to Dr. Greg Henry and his UBC field crew led by Anne Bjorkman for their support in the field. Many thanks to all that were part of my journey in the Soil Environmental Toxicology Lab, Saskatchewan Plant Community Ecology Lab, Department of Soil Science and Department of Plant Sciences. Special thankyous to Richard Nhan, Alix Schebel, Candace Piper and Dr. Steven Mamet for their help and wisdom. Thanks to Saskatchewan Plant Community Ecology Lab for processing samples.

Thank you to all my family for the overwhelming encouragement you provided this ‘scientist’ - especially to my parents Joanne and Murray, and siblings Kayla and Taylor. Finally,

to my husband Deane – thank you for encouraging me, inspiring me and loving me unconditionally throughout this adventure. You are my best friend, my faithful partner and one true love.

TABLE OF CONTENTS

LIST OF TABLES

LIST OF FIGURES

LIST OF ABBREVIATIONS

DOC	Dissolved organic carbon
LM	Local model
MIR	Mid-infrared
NPP	Net primary productivity
PCA	Principal component analysis
PLSR	Partial least squares regression
RM	Regional model
RMSEP	Root mean square error of prediction
RMSEV	Root mean square error of validation
RPD	Ratio of performance to deviation
SOC	Soil organic carbon
SOCC	Soil organic carbon content
SOM	Soil organic matter
vis-NIR	Visible and near-infrared

1. INTRODUCTION

Northern circumpolar soils store approximately 50% of total estimated global soil organic carbon (SOC) (Tarnocai et al., 2009), yet the SOC stores of regions such as High Arctic polar deserts are not well understood and underrepresented in the databases used to quantify Arctic soil organic carbon (SOC) pools (Ping et al., 2008; Tarnocai et al., 2009; Hugelius et al., 2014; Campeau et al., 2014). Polar desert ecosystems dominate the High Arctic (705 000 km^2; CAVM Team, 2003; Walker et al., 2005), and support moisture, temperature and nutrient limited plant communities that often cover <5% of the soils surface (Bliss et al., 1994; Gold and Bliss, 1995; Lévesque, 1997). These polar deserts are thought to contain little SOC relative to other ecosystems in the permafrost region due to a shallow active layer and limited soil development - with 34 ± 16 Pg SOC in the top 0-3 m of High Arctic soils, or 3% of the 1035 ± 150 Pg SOC found in permafrost regions (Hugelius et al., 2014). Nevertheless, given that northern circumpolar regions are experiencing more rapid warming than the global average (Callaghan et al., 2005; Schuur et al., 2008; IPCC, 2013; Schuur et al., 2015), the size and distribution of these SOC stores are both globally important due to the large area covered by these environments and locally important to the plant communities in terms of moisture and nutrient availability.

Complex interactions between vegetation, water/ice and soil redistributes SOC in the soil profile of small (< 3 m) patterned ground features called frost boils (Washburn, 1956; Walker et al., 2004, 2008; Michaelson et al., 2012), common in many polar desert landscapes (Bliss et al., 1994; Lévesque, 1997; Anderson and Bliss, 1998; Ugolini et al., 2006). Due to the heterogeneous

nature of these soils, SOC estimates have a large degree of uncertainty (Ping et al., 2008; Hugelius et al., 2014), and are likely underestimated due to SOC pools in the lower active layer that were previously unaccounted for (Horwath Burnham and Sletten, 2010). Frost boils form from the convective churning action of soil that results from the annual freeze-thaw of the active layer (Walker et al., 2004). A diapir may develop when soil water pools in a concave depression at the base of the active layer under the barren frost boil center and low-density, ice-rich soil develops. SOC may accumulate in this ice-rich concavity above the permafrost table (Shilts, 1978; Cannone et al., 2004; Walker et al., 2004; Boike et al., 2008) as cryoturbation buries SOM or meltwater leaches dissolved organic matter from the surface through the soil profile (Tye et al., 2005; Schaeffer et al., 2013). When the overlying high-density soil in the active layer dries (following snow melt) and becomes more brittle, this soil sinks and the low-density viscous soil material in the lower active layer flows upwards as diapiric injection (Swanson et al. 1999). These diapirs represent a subsurface patch of relatively nutrient-rich soil in an otherwise nutrient-poor polar desert environment, where the majority of High Arctic plants roots are restricted to the upper half of the active layer (Bell and Bliss 1978, Iversen et al. 2015).

The objective of this dissertation is to determine how common subsurface patches of SOC associated with diapirism are in frost boils and how they contribute to the polar desert carbon pool. Furthermore, this dissertation aims to investigate whether these patches act as important nutrient sources for plants such as *S. arctica*. To date this is one of the most comprehensive studies to look at the spatial distribution of active layer SOC in the frost boils of a polar desert ecosystem. With this research I hope to further our understanding of how subsurface Arctic soil environments influence plant community structure. This knowledge will provide important information towards

our understanding of how plants in polar deserts may be able to adapt to climate change in the Arctic.

1.1 Dissertation organization

This dissertation is presented in six chapters, including three research chapters written as manuscripts for publication. Chapter 1 is a brief introduction to the collective topics and objectives of the dissertation. This is followed by a literature review in Chapter 2 that provides a more thorough overview of concepts important to the research chapters including Arctic SOC pools, polar desert ecology and soil processes, and methods of measuring SOC in Arctic soils. The research chapters (Chapters 3-5) are structured so they each have six main sections: preface, abstract, introduction, materials and methods, results, and discussion. The exception to this format is Chapter 3 which also includes a conclusion section as per the guidelines of the journal in which the manuscript was published. While all the sections are standard to journal manuscripts, it is worth noting that the preface section provides the context for each chapter within the manuscript and provides an overview of the various contributions of the chapter co-authors.

The first research chapter, Chapter 3, presents my work developing calibration models relating visible and near-infrared (vis-NIR) spectra of field condition soils and soil organic carbon for characterizing the distribution of SOC in polar deserts using a novel in situ vis-NIR spectrophotometer probe. Chapter 4 examines the distribution of subsurface nutrient patches associated with diapirism in polar deserts and vegetative response to these patches. Specifically, we looked at the root biomass and N uptake of the dominant shrub, *Salix arctica*, in response to these patches. Chapter 5 describes the quantity and distribution of SOC at various spatial scales within polar deserts, and evaluates the contribution of subsurface SOC patches, indicative of diapirism, to the polar desert SOC pool. Following the research chapters is a synthesis chapter

(Chapter 6). This chapter summarizes the key findings of this dissertation and explores avenues for future research that would deepen our understanding the role of these subsurface patches in a changing arctic climate

One of the original objectives of the study was also to characterize the belowground plant community on frost boils with and without diapir horizons using next-generation sequencing; while the samples were processed and sequenced, these data were not incorporated into the research chapters due to the time-consuming sample processing, and the complexity of bioinformatics pipeline and subsequent statistical analysis of the data. A detailed description of the laboratory methods used are outlined in Appendix 5.

2. LITERATURE REVIEW

2.1 Soil organic carbon pools in the Arctic

Permafrost soils are estimated to contain more than 44% of the global estimate of soil organic carbon (SOC) and the polar regions are warming more rapidly than the global average (Jobbagy and Jackson, 2000; Schuur et al., 2008; Tarnocai et al., 2009; IPCC, 2013; Hugelius et al., 2014; Schuur et al., 2015). The exacerbated warming of the Arctic relative to lower latitudes is a result of numerous carbon-climate feedback mechanisms driven by changes in albedo and the release of carbon as CO_2 or CH_4 from the warming and thawing permafrost (IPCC, 2007; Schuur et al., 2008; Jeffries et al., 2012; Schuur et al., 2015). Quantifying polar soil organic carbon pools for global estimates and understanding the carbon-climate feedbacks that control the vulnerability of those pools to decomposition are important for global carbon-climate models (Davidson and Janssens, 2006; Schuur et al., 2008; Koven et al., 2015; Schuur et al., 2015).

Global SOC pool estimates to 1 m depth converge at ~1500 Pg (Amundson, 2001; Scharlemann et al., 2014). Typically these estimates, upscaled based on soil taxonomy or ecosystems, have been restricted to shallow sampling depths. Estimates in the 0 to 100 cm soil depth range from 1220 – 2946 Pg SOC (Bohn, 1982; Post et al., 1982; Sombroek et al., 1993; Jobbagy and Jackson, 2000; Amundson, 2001) and a single study examining the 0 to 300 cm depth reported 2344 Pg SOC (Jobbagy and Jackson, 2000). Few studies examining the size and distribution of SOC in regions defined by soil permafrost, tundra vegetation or geographic Arctic boundaries contributed to these global SOC pool estimates. Thus, polar SOC pools were likely

underestimated and only contributed modestly to global estimates with 191.8 Pg (Post et al., 1982), 114 Pg (Jobbagy and Jackson, 2000), 64.7 Pg (Scharlemann et al., 2014) estimated for the 0 to 100 cm depth, and 144 Pg for the 0 to 300 depth (Jobbagy and Jackson, 2000).

It has only been relatively recently that studies have recognized the influence that permafrost and the Arctic climate have on carbon accumulation and storage, and have investigated the size and distribution of SOC pools in permafrost soils at regional and northern circumpolar scales (see review by Ping et al., 2015). In North America, significant efforts have been made to quantify SOC pools in Alaska (Michaelson et al., 1996, 2013; Bockheim et al., 2003; Bliss and Maursetter, 2010; Johnson et al., 2011), Canada (Tarnocai, 1998; Hugelius et al., 2010), and North American Arctic (Ping et al., 2008). Tarnocai et al. (2009) compiled the Northern Circumpolar Soil Carbon Database (NCSCD) for one of the first detailed assessments of SOC in entire northern permafrost region. Soil organic carbon was initially estimated at 1024 Pg for the top 0-300 cm depth which is equivalent to 44% of the estimated belowground global carbon pools for that depth (Jobbagy and Jackson, 2000; Tarnocai et al., 2009). The NCSCD has since been updated to include more pedons to the 0-300 cm depth (Hugelius et al., 2013b; a), yet estimates for that depth remain similar (1035 Pg SOC) (Hugelius et al., 2014).

2.1.1 Soil organic carbon pools in polar deserts and semi-deserts

Barren environments make up 39% of the non-glaciated arctic (2.21×10^6 km^2) and dominate the High Arctic (Bliss and Matveyeva, 1992). Despite the large area covered by these environments, these areas are underrepresented in the databases used to quantify Arctic SOC pools (Ping et al., 2008; Tarnocai et al., 2009; Hugelius et al., 2014). It has long been recognized that vegetative barrens of the High Arctic contain less SOC relative to other circumpolar ecosystems due to their poorly developed soils (Bliss and Matveyeva, 1992; Ping et al., 2008; Horwath

Burnham and Sletten, 2010; Hugelius et al., 2014). Recent estimates suggest High Arctic soils contain 34 ± 16 Pg SOC in the top 0-3 m of soils, or approximately 3% of the 1035 ± 150 Pg SOC found in permafrost regions (Hugelius et al., 2014).

Soil organic carbon content (SOCC; kg C m^{-2}) estimates for these regions have a large degree of uncertainty (Ping et al., 2008; Hugelius et al., 2014), which can in part be attributed to the limited number of studies available estimating SOC pools (Table 2.1). Additionally, the heterogeneous nature of these permafrost affected soils requires a sufficiently large number of pedons to capture the fine-scale spatial variation required for upscaling SOC estimates (Banerjee et al., 2011; Mishra and Riley, 2012; Campeau et al., 2014)

Comparisons between SOC pool estimates are difficult to make as the spatial extent and the sampling depths differ between each study. The earliest SOC estimates for polar deserts and semi-deserts estimated SOC based only on surface soils and the estimates differed substantially (Table 2.1). Miller et al. (1983) estimated that polar deserts across the Arctic contained 10.87 Pg SOC with 0.09 kg C m^{-2} in polar deserts, and 7.2 kg C m^{-2} in semideserts (Miller et al., 1983). In contrast, the more widely cited Bliss and Matveyeva (1992) study estimated much less SOC (0.863 Pg SOC) for a slightly smaller area, with a 160% difference in SOC measured in polar desert soils and 146-176% difference in polar semi-deserts (Bliss and Matveyeva, 1992).

More recent studies have looked at SOC within only the active layer (Horwath Burnham and Sletten, 2010), or within the active layer and perennial frozen permafrost soils (Ping et al., 2008; Hugelius et al., 2014). As expected, SOC estimates in these newer studies are larger as they typically account for deeper pools of SOC that were previously unaccounted for (Table 2.1). Horwath Burnham and Sletten (2010) found that SOC pools in the high Arctic polar deserts and polar semi-deserts of Greenland were likely underestimated due to lower active layer SOC pools.

They found that 57% and 31% of active layer SOC was stored below 25 cm in polar deserts and polar semi-deserts, respectively. Additionally, SOC was extremely variable within both ecosystems with SOC ranging from 0.5 to 5.3 kg m^{-2} (average 2.2 kg m^{-2}) in polar deserts and ranging from 1.5 to 19.5 kg m^{-2} (average 7.9 kg m^{-2}) in polar semi-deserts (Horwath Burnham and Sletten, 2010). Due to the heterogeneous nature of these permafrost affected soils and the limited number of studies available with sufficient numbers of pedons to capture the fine-scale spatial variation required for upscaling SOC estimates (Banerjee et al., 2011; Lamb et al., 2011; Mishra and Riley, 2012; Campeau et al., 2014), the most recent SOC estimates for the High Arctic have a relatively large degree of uncertainty given the small size of the SOC stocks (Ping et al., 2008; Hugelius et al., 2014). Regardless, in the High Arctic active layer SOC is clearly an important carbon store as most SOC is stored in the upper metre of the soil (24±8 Pg SOC) with 10±3 Pg SOC concentrated in the top 0 to 0.3 m (Hugelius et al., 2014). Estimates of SOC stocks in deeper soil layers in the High Arctic are lower, 7±5 and 3±3 Pg SOC in the 1–2 m and 2–3 m depth ranges, respectively (Hugelius et al., 2014).

2.2 Polar desert distribution and plant ecology

Northern polar deserts and semi-deserts are characterized by cold, dry desert-like conditions and sparse vegetative cover (Bliss et al., 1984; Lévesque, 1997; Walker et al., 2005). The most barren communities make up approximately 25% of the non-glaciated Arctic (1.268 x 10^6 km^2), most of which are found in the High Arctic regions of Canada, Greenland, and Russia (CAVM Team, 2003; Walker et al., 2005). While the full northern circumpolar extent of these regions varies depending on how the different vegetation types, soil types or geographic boundaries associated with these barren environments are classified and mapped (Table 2.1), collectively the polar deserts and semi deserts cover approximately 40% of the arctic or 2.21 x 10^6 km^2 (Bliss and

Matveyeva, 1992). Polar desert ecosystems have low mean annual temperatures ranging from -20°C to -6°C, low annual precipitation of <100 mm to 200 mm (Ecological Stratification Working Group, 1995), and the presence of a thick permafrost layer (Tedrow, 1966; Cruikshank, 1971; Ping et al., 2015).

Winters are long, dark and most of the precipitation falls as snow. The summer growing season is short, less than two and a half months, and soils dry within 2-3 weeks following snow melt (Bliss, 2000). Cryoturbation is the dominate soil process in all permafrost environments, including polar deserts, and it refers to any soil movement caused by the annual freeze-thaw of active layer (Bockheim and Tarnocai, 1998; Ping et al., 2015). This frost driven soil movement is commonly associated with patterned ground such as small frost-heave features called frost boils (Walker et al., 2004). Soils are often classified as Regosolic Turbic Cryosols (Bliss et al., 1994; Soil Classification Working Group, 1998) as they have very little soil development, low fertility, have very little visible evidence of soil organic matter and when present, soil horizons that are irregular or poorly developed (Tedrow, 1966; Cruikshank, 1971).

Table 2.1. Estimates of soil organic carbon storage in circumpolar barren environments by various authors

Study	Region	Description	Area	Surface ¶		Active Layer#		Active Layer + Permafrost	
			x 10^6 km^2	kg SOC m^{-2}	Pg SOC	kg SOC m^{-2}	Pg SOC	kg SOC m^{-2}	Pg SOC
Miller et al (1983) †	Arctic	Polar desert	0.80	0.091	0.07	-	-	-	-
	Arctic	Polar semi-desert	1.50	7.2	10.80	-	-	-	-
Bliss and Matveyeva (1992) ‡	High Arctic	Polar desert	0.847	0.010	0.008	-	-	-	-
	High Arctic	Semi-desert	1.005	0.453	0.455	-	-	-	-
	Low Arctic	Semi-desert	0.358	1.118	0.400	-	-	-	-
Ping et al. (2008) §	N.A. Arctic	Barren uplands	0.207	2.9	0.6	16.0	3.3	21.1	4.4
	N.A. Arctic	Rubblelands	0.371	0.8	0.3	2.9	1.1	3.4	1.3
	N.A. Arctic	Mountains	0.161	0.7	0.1	3.8	0.6	3.8	0.6
Horwath Burnham and Sletten (2010)	High Arctic	Desert	0.847	0.93	0.79	2.55	2.16	-	-
	High Arctic	Semi-desert	1.005	5.25	5.28	7.83	7.87	-	-
Hugelius et al. (2014)	High Arctic	Geographic region	1.0	10	10 ± 3	-	-	24	24 ± 8

† Total SOC calculated by multiplying area by SOCC (kg m^{-2})

‡ SOM values converted to SOC by dividing by 2

§ Barren uplands, rubblelands and mountains refer to the B1, B2, and B3-4 units of the Circumpolar Arctic Vegetation Map, respectively. The barren upland estimate was calculated based on Ping et al. (2008) supplemental.

¶ Sampling depths were ~25 cm – Bliss and Matveyeva (1992), Horwath Burnham and Sletten (2010); 30 cm – Hugelius et al. (2014); undefined – Miller et al (1983), Ping et al. (2008)

Sampling depths were 68-75 cm – Horwath Burnham and Sletten (2010); undefined – Ping et al. (2008)

These conditions limit the diversity and productivity of the plant communities (Bliss et al., 1984; Bliss and Matveyeva, 1992; Bliss, 2000). Plant communities of North American polar deserts and semi-deserts have been extensively described (Bliss and Svoboda, 1984; Muc et al., 1989; Batten and Svoboda, 1994; Bliss et al., 1994; Lévesque, 1997). In polar deserts and semi-deserts plant richness is low (6-10 vascular plants) (Bliss and Gold, 1999), plant cover is sparse and growth forms are restricted to cushion plants, rosettes, low growing graminoids, and prostrate shrubs (Bliss and Matveyeva, 1992). Polar deserts tend to lack woody shrubs and have substantial amounts of bare patterned ground. Vascular plant cover is often less than 5%, average cover of mosses and lichens is <1% (Bliss et al., 1984; Bliss and Matveyeva, 1992), and net annual productivity is 0.8 g m^{-2} (Bliss et al., 1984). The most common vascular plants in polar deserts are cushion forbs such as *Minuartia rubella* and *Saxifraga oppositifolia*, the rosette species *Papaver radicatum, Saxifraga spp.* And *Draba spp.*, and graminoids such as *Luzula confusa, L. nivalis and Puccinellia angustata* (Bliss and Matveyeva, 1992; Walker et al., 2005).

Plant community development and species distribution are related to microenvironments created by patterned ground as well as mesoscale differences in topography, slope and substrate (Anderson and Bliss, 1998). Generally, we find increased plant cover associated with cryptogamic crusts composed of lichens, bryophytes and cyanobacteria, as these crusts these help to retain soil moisture, stabilize soils and host nitrogen-fixing organisms (Gold and Bliss, 1995; Bliss and Gold, 1999; Stewart et al., 2011b; Michaelson et al., 2012). Anderson and Bliss (1998) found within the patterned ground of polar deserts that the margins of frost boils have increased plant cover and cryptogamic crusts and provide favourable microsites for seedling establishment compared to the more exposed frost boil centers. More broadly, there are limited areas within the polar desert ecosystem, such as the site investigated in this dissertation (Figure 2.1), where improved

temperature and moisture conditions allow for increased cover of vascular plants, increased cryptogamic crusts, and species more typical of polar semi-deserts (Bliss et al., 1984, 1994; Bliss and Gold, 1999). The vegetation of polar semi-deserts is patchy with 5-25% vascular plant cover, 30-60% cover of lichens and mosses (Walker et al., 2005), and net annual productivity is 35-45 g m^{-2} (Bliss and Matveyeva, 1992). Vascular species richness is greater than polar deserts, with sufficient moisture to support prostrate shrubs *Salix arctica*, *Dryas integrifolia*, *and Cassiope tetragona*, sedges *Eriophorum triste* and *Carex rupestrisa*, and a wider variety of graminoids and low growing forbs (Bliss et al., 1994; Walker et al., 2005). *Dryas integrifolia* and *Salix arctica* tend to dominate plant communities on non acidic substrates, and *Salix arctica* and *Luzula sp.* tend to dominate communities on acidic substrates (Walker et al., 2005)

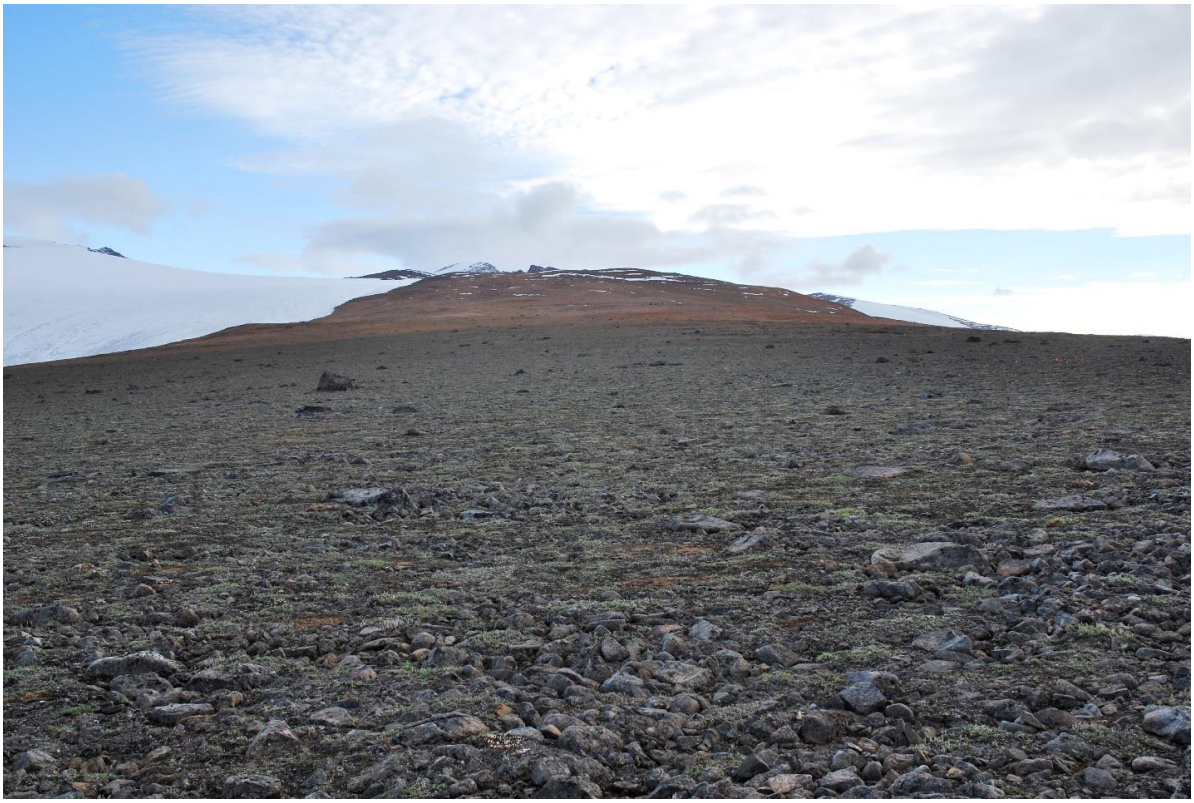

Figure 2.1 Patterned ground and scattered plant cover at a polar semi-desert site located at Alexandra Fiord, NU, CA (78°51'N, 76°06'W). Photo Credit: Amanda Muller.

2.2.1 *Salix arctica*

Salix arctica is a deciduous dwarf or prostrate shrub ubiquitous at the site investigated in this dissertation (Figure 2.2; Batten and Svoboda, 1994; Bliss et al., 1994) and across the northern circumpolar Arctic. It grows in a wide variety of Arctic habitats from wet bogs to frost-heaved patterned ground (Aiken et al., 2007). This low growing plant is generally 3-25 cm in height, with elliptic- oblanceolate to more obovate-circular leaves. The adaxial leaf surfaces can be slightly glossy or dull with pillose or silky hairs along the margin, and adaxial leaf surfaces are covered in pillose or short-long silky hairs (Aiken et al., 2007). *S. arctica* is dioeceous with male and female catkins on separate plants, and disperses seeds by wind (Aiken et al., 2007). This species can be extremely long lived, with specimens in Greenland dated to 236 years (Savile, 1979) and one Canadian specimen older than 270 years (Boulanger-Lapointe et al., 2014). Most of the aboveground biomass in a typical *Salix arctica* consists of low stems resistant to wind abrasion, with over 60% of total biomass belowground (Maessen et al., 1983). The species was observed to root laterally up to 20-30 cm away from the stem and as deep as 20 cm on ancient beach ridges (Lamb et al., 2016). This species is known to form ectomycorrhizal associations (Kohn and Stasovski, 1990).

The high and low Arctic appear to be greening as shrubs respond to a warmer climate (Beck and Goetz, 2011; Myers-Smith et al., 2011, 2015; Walker et al., 2012). Deciduous shrubs, such as *S. arctica,* respond strongly to experimental warming by increasing leaf size, plant height (Hudson et al., 2011), and overall plant cover (Walker et al., 2006). Site-specific habitat conditions influence the response of *S. arctica* to climate warming (Jones et al., 1999; Boulanger-Lapointe et al., 2014). Recruitment and establishment of seedlings is common in the glacier forelands as glaciers rapidly retreat; however, *S. arctica* seedling recruitment and growth is reportedly strongly limited by water

availability in dry environments (Boulanger-Lapointe et al., 2014). Plant performance may also differ depending on the sex of the plants due to their differential costs of reproduction (Jones et al., 1999). In dry habitats, female plants had increased peak season gas exchange in response to experimental warming, whereas this was depressed in males (Jones et al., 1999).

Figure 2.2 Prostrate growth of *Salix arctica* with a female catkin at a polar semi-desert site located at Alexandra Fiord, NU, CA (78°51'N, 76°06'W). Photo Credit: Amanda Muller.

2.3 Polar desert soil processes and patterned ground

Polar desert soils are strongly influenced by the low mean annual temperatures and the presence of a thick perennially frozen permafrost layer (Tedrow, 1966; Cruikshank, 1971; Ping et al., 2015). Cryoturbation is the dominate process in these environments and it refers to any soil movement caused by the annual freeze-thaw of active layer (Bockheim and Tarnocai, 1998; Ping et al., 2015). The annual heave of soils during the seasonal freezing and subsequent settling of soils when they thaw contributes to the development of patterned ground (Walker et al., 2004).

Patterned ground is common in polar deserts and often manifests in the form of frost boils (Bliss and Matveyeva, 1992; Bliss et al., 1994; Lévesque, 1997; Anderson and Bliss, 1998; Ugolini et al., 2006), a term that encompasses a range of small frost-heave features including sorted and non-sorted stripes, circles and polygons (Walker et al., 2004, 2008)

Frost boils are small (< 3 m) frost heave features (Washburn, 1956; Walker et al., 2004, 2008; Michaelson et al., 2012) that are characterized by circular patterns of barren or sparsely vegetated mineral soil with vascular plant cover restricted to the margins of the boil (Cannone et al., 2004; Walker et al., 2004; Michaelson et al., 2012). The centers of frost boils have fine to medium textured soils that are subject to active cryoturbation and are often raised relative to the more stable margins of the feature (Walker et al., 2004; Ugolini et al., 2006). The vegetated margins of the frost boils also tend to have fine mineral soils, though organic soil horizons may also develop (Walker et al., 2004). These finer soils are segregated from stony borders comprised of coarse fractions ranging from pebbles to boulders; these coarse boundary zones often act as avenues for root penetration at depth (Ugolini et al., 2006).

In High Arctic deserts, complex interactions between vegetation, water/ice and soil redistributes SOC in the soil profile. Frost boils form from the convective churning action of cryoturbation that results, in part, from the annual freeze-thaw of water in the active layer migrating to the permafrost table, freezing and upheaving the fine to medium textured soils in the frost boil centers (Walker et al., 2004). Bockheim (2007) summarized four common cryoturbation models contributing to the formation of frost boils a) the convection-cell equilibrium model (Mackay, 1980), b) the differential frost-heave model (Peterson and Krantz, 2008), c) the diapirism model (Swanson et al., 1999) and d) the cryostatic model (Vandenberghe, 1992). While each of these models describe different mechanisms that frost action influences soil movement, they are

all mediated by temperature gradients and freeze-thaw cycles (Walker et al., 2004). Perhaps, more importantly the cryoturbation processes described by these models have been linked to SOM storage as soil organic carbon (SOC) is transported to depth (Bockheim and Tarnocai, 1998; Bockheim, 2007; Horwath et al., 2008; Michaelson et al., 2008) and physically protected from decomposition under permanently frozen and anaerobic conditions (Walker et al., 2004; Davidson and Janssens, 2006).

Generally, the trajectory of particles in frost boils is can be described as circular (Figure 2.3)(Mackay, 1980; Walker et al., 2004; Bockheim, 2007). Starting in the center, particles are carried downward from the raised frost boil center towards the margin of the frost boil via soil creep (Walker et al., 2004). From the top of the frost boil margin particles and SOM, and DOC are carried downwards via soil movement and leaching, respectively. Organics accumulate at the base of the active layer in a thawed depression underlain with permafrost (Walker et al., 2004; Horwath et al., 2008). The presence of ice lenses in the frost boil causes a portion of the SOM from the thawed base to be heaved upwards towards the surface of the frost boil center where it becomes available as substrate for microbial activity to decompose and release nutrients for plants (Walker et al., 2004).

Landforms interact as soil particles and SOC move between the frost boil and an inter boil regions (Walker et al., 2004). These interactions are primarily mediated by the different characteristics of frost boil centers and margins areas already described. The interaction between climate and soils is bidirectional. Soil texture influences the formation of ice lenses, and ice lenses influence the soil by causing soil heave and particle sorting (Walker et al., 2004). There are more complex interactions between vegetation, soils and climate. For instance, vegetation influences the accumulation of SOM and nutrients in soil, and soils provide the plants with moisture and

nutrients. Additionally organic soils and vegetation mediate active layer thickness by insulating the soils, and ice lenses influence vegetation establishment via the frost heave of soils (Walker et al., 2004).

2.3.1 Diapirism

A diapir may develop when soil water pools in a concave depression at the base of the active layer under the barren frost boil center and low-density, ice-rich soil develops. SOC may accumulate in this ice-rich concavity above the permafrost table (Shilts, 1978; Cannone et al., 2004; Walker et al., 2004; Boike et al., 2008) as cryoturbation buries SOM or meltwater leaches dissolved organic matter from the surface through the soil profile (Tye et al., 2005; Schaeffer et al., 2013). When the overlying high-density soil in the active layer dries following snow melt and becomes more brittle, this soil sinks and the low-density viscous soil material in the lower active layer flows towards the soil surface by vertical heave, manifesting as a diapiric injection (Swanson et al., 1999).

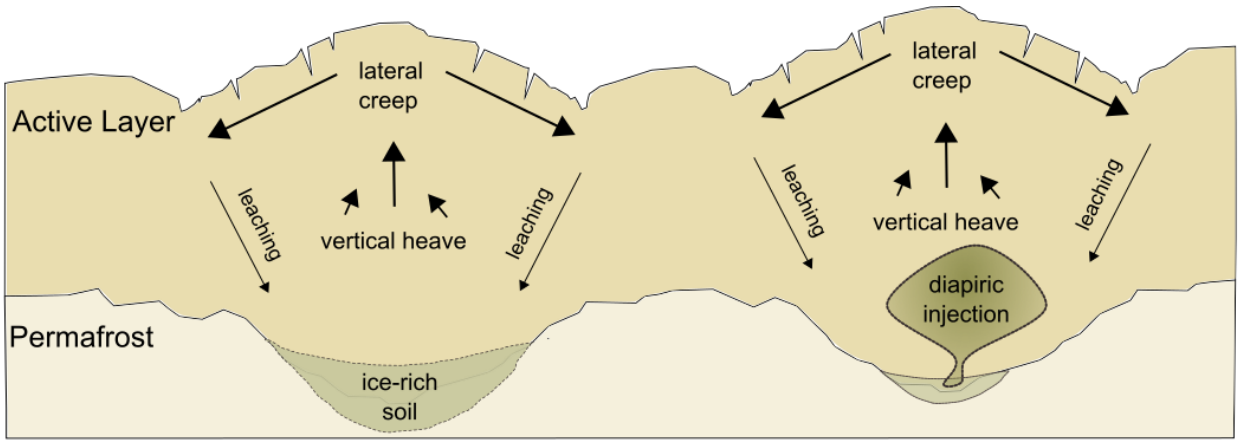

Figure 2.3 A conceptual diagram of soil movement regimes and diapir formation in frost boils. Solid arrows indicate the direction of soil movement of the major (thick line) cryoturbation mechanisms that occur during annual freeze/thaw cycles and result in frost boil formation. The profile of the permafrost table is inversely related to the surface in frost boils such that the permafrost table is deepest in the center and shallowest at the edges and a concave bowl develops below the frost boil center. The processes of leaching and accumulation of ice-rich soil in the concave bowl of the permafrost table over successive years (frost boil on left) can create a diapiric injection (frost boil on right). Adapted by Hardy (2016) from Walker et al. (2004).

2.3.2 Soil organic carbon accumulation in frost boils

The amount of SOC in High Arctic soils may be highly underestimated as cryoturbation redistributes SOC to depth (Bockheim, 2007; Horwath et al., 2008; Horwath Burnham and Sletten, 2010). Horwath et al. (2008) found that the active layer of non-sorted stripes in Greenland contained approximately 9.3 kg SOC m^{-2} and 62% was found below 25 cm. The majority of the SOC was found in the sandy margins and fine textured discontinuous horizons buried at depth below the barren ridges of the non-sorted stripes (Horwath et al., 2008). Similarily, Ugolini et al. (2006) and Michaelson et al. (2008) found SOC accumulations at depth in frost boils. SOC in the subsurface horizons of sorted circles at Devon Island, NU was about double the amount found in surrounding horizons. Soil carbon enrichment was thought to be a result of illuviation of dissolved organic carbon (DOC), and biological activity such as plant root or microbial additions (Ugolini et al., 2006). Michaelson et al. (2008) speculated that cryoturbation was an important process for redistributing SOC to depth in high and low Arctic frost boils in Canada and northern Alaska, citing an example where the SOC concentration of the subsurface horizon was 8 kg m^{-2} greater than that in the frost boil center. While these studies provide evidence that cryoturbation is an important process for sequestering carbon across the Arctic, little is known about the potential importance of these processes in structuring SOC distributions in high Arctic polar deserts.

2.3.3 Influence of climate change on frost boils

The polar regions are warming more rapidly than the global average (Jobbagy and Jackson, 2000; Schuur et al., 2008; Tarnocai et al., 2009; IPCC, 2013; Hugelius et al., 2014; Schuur et al., 2015) and are projected to have increased winter precipitation (IPCC, 2013, 2014). Widespread permafrost thaw and increased active layer thickness is expected across most of the Arctic (Walker et al., 2004; Davidson and Janssens, 2006; Jeffries et al., 2012; IPCC, 2013). These warmer and

potentially wetter conditions are favorable for increased cryoturbation and frost boil development (Callaghan et al., 2005). Historical warming has been linked to periods of SOC accumulation and storage in the Arctic due to increased cryoturbation (Bockheim, 2007; Horwath et al., 2008). It is also likely that increased precipitation and melting permafrost will also facilitate greater diapirism in polar desert frost boils due to accumulation of ice-rich water at the permafrost table and slumping of brittle surface soils as they dry throughout the growing season (Swanson et al., 1999). Walker et al. (2004) speculated influence of climate change on frost boil formation may be region specific, and due to the complex interactions involved in frost boil formation there is no consensus on how climate change will influence SOM storage and dynamics in frost boils.

At the most fundamental level, the arctic soil carbon pool is a balance of C inputs to the soil primarily from the net primary productivity (NPP) of plants, and outputs to the atmosphere as soil C is decomposed by microorganisms (Davidson and Janssens, 2006; Lützow and Kögel-Knabner, 2009). Arctic soils are not unique, in that the C inputs into arctic soils are primarily above ground plant litter and belowground inputs from root exudates and root turnover (Ping et al., 2015). The reason arctic soils tend to accumulate C, and this is where they begin to diverge from other soils, is that the cold and moist environment slow the decomposition of SOM (Davidson and Janssens, 2006; Ping et al., 2008, 2015). As all biological and chemical reactions are sensitive to temperature (Davidson and Janssens, 2006; Lützow and Kögel-Knabner, 2009), we need to understand how the rates of NPP and SOC decomposition will respond to increased temperature but also need to understand the other complex physical and biological interactions controlling C cycling in these environments.

High Arctic plant communities dominated by deciduous shrubs such as *S. arctica* can respond rapidly to environmental changes (Walker et al., 2006; Hudson et al., 2011). Globally, the

high and low Arctic appear to be greening as shrubs respond to a warmer climate (Beck and Goetz, 2011; Walker et al., 2012; Elmendorf et al., 2012; Myers-Smith et al., 2015), which may fundamentally change C cycling in these environments. For example, twenty years of warming in moist tundra soils resulted in no net change in total soil organic carbon however, warming changed the distribution of SOC despite with significantly increased SOC storage and microbial community activity at depth in the mineral soil (Sistla et al., 2013). Increased shrub growth directly influenced quantity, quality and distribution of plant-derived C inputs into the soil and indirectly influenced C cycling by changing soil moisture and temperature regimes (Sistla et al., 2013). While patterned ground features provide safe sites for plant establishment and strongly facilitate the expansion of woody vegetation in low Arctic ecosystems (Frost et al., 2013), shrub expansion in the coldest high Arctic sites has not been as widespread (Elmendorf et al., 2012). Cold and dry sites such as polar deserts often experience short-term increases in shrub cover in response to experimental warming though these changes are typically not sustained. Over the long-term, these sites tend to have increased abundance of graminoid species, increased canopy height of vascular plants, decreased mosses and lichens, and less exposed bare ground (Elmendorf et al., 2012). Given the observed changes to plant communities in response to experimental warming it is likely that polar desert ecosystems will also see an increase in plant-derived C inputs above and below-ground.

The temperature sensitivity of SOC decomposition, based on theoretical kinetics, is a function of substrate complexity, climate and the availability of substrate for decomposition (Davidson and Janssens, 2006; Lützow and Kögel-Knabner, 2009). Substrates originating in low temperature climates are expected to be more sensitive to temperature changes than those originating in warmer climates (Davidson and Janssens, 2006; Lützow and Kögel-Knabner, 2009). It is thought that the carbon stored in these soils both in the active layer and frozen in permafrost

are less processed by microorganisms compared to more southern soil, and thus are typically more readily decomposable (vulnerable), should the environmental conditions allow (Ping et al., 2015). Thus given the rapid warming observed in parts of the Arctic (IPCC, 2014), this implies that SOC stocks in High Arctic environments are some of the most vulnerable to climate change.

However, there is significant uncertainty in soil responses to climate change in the Arctic (Lamb et al., 2011). Considering only the temperature sensitivity of SOC decomposition is too simplistic because other environmental constraints can modify substrate availability and decomposition. Paré and Bedard-Haughn (2013b) observed differences in C and N cycling between landscape positions due to differences in soil moisture, thermal conditions, and the quantity and quality of SOM. Landscape positions with higher soil moisture and larger stores of labile organic matter had increased gross mineralization, N_2O and CO_2 emissions (Paré and Bedard-Haughn, 2013b), though they also suggest that it is possible these losses may be offset by enhanced plant growth contributing more labile inputs from plants to the soil environment. Differences in C and N cycling has also been observed between cryoturbated and non-cryoturbated soil horizons. In high Arctic polar deserts, Brummell et al. (2015) observed lower microbial C respiration in frost boils with diapir Bhy soil horizons compared to frost boils lacking these subsurface horizons. In other Arctic communities, organic soil horizons buried via cryoturbation in the active layer are less susceptible to decomposition compared to surface horizons (Gillespie et al., 2014).

Factors such as flooding, drought, and frozen soil limit substrate availability by inhibiting diffusion, and slowing or suppressing microbial activity (Davidson and Janssens, 2006). So while the decomposition of SOC in Arctic soils is expected to be sensitive to a warming climate, the presence of frozen and saturated soils has the potential to suspend or slow SOC decomposition.

Further complicating matters, the environmental factors are also temperature sensitive (Davidson and Janssens, 2006). For instance, increased temperatures promote deeper active layers (Walker et al., 2004; Jeffries et al., 2012). Thawing permafrost removes the most important environmental constraint on SOM decomposition in cryosols as SOM that was previously inaccessible to the microbial community will become available for decomposition (Davidson and Janssens, 2006). It is evident that understanding how SOM dynamics will respond to climate change relies on more than the temperature sensitivity of SOM but the influence climate change will have on the environmental constraints (Davidson and Janssens, 2006).

Climate change has the potential to both directly and indirectly influence these complex interactions in polar desert cryosols in both additive and contrasting directions. For instance, increased temperatures may directly promote changes such as increased microbial activity, thaw depth and plant growth. However, there are also indirect pathways influencing how different components of the ecosystem might respond to climate change (Walker et al., 2004). Vegetation growth may also be promoted by increased nutrient availability derived from microbial activity. However, thaw depth can also be indirectly influenced by vegetation, contrary to the increased thaw depth expected from warming, as increased plant growth can insulate the soil and prevent further thaw (Walker et al., 2004). Finally, there can be substantial lags between the relatively rapid vegetation responses to warming and soil responses (Lamb et al., 2011).

In summary, Arctic soils contain higher than expected soil organic matter (SOM) due to cryoturbation processes redistributing SOC to depth in permafrost affected soils (Bockheim and Tarnocai, 1998; Walker et al., 2004). Deep in the soil profile, SOM is physically protected from decomposition under frozen anaerobic conditions (Walker et al., 2004; Davidson and Janssens, 2006). In High Arctic polar deserts cryoturbation is often associated with frost boils, thus the

distribution and dynamics of SOM in frost boils is an important aspect of understanding how these soils might respond to climate warming. Due to the complex interactions involved in frost boil formation clear predictions on how climate change will influence SOM storage and dynamics cannot be made.

2.4 Measuring soil organic pools in polar desert soils

There are two main challenges that limit our ability to assess the carbon pools in remote regions. First, the logistical constraints of conducting Arctic fieldwork include a short field season to collect soil samples and the high cost of freighting samples to an analytical laboratory. Second, given the complex interactions between soil, vegetation and water in periglacial environments (Walker et al., 2004), a large number of samples are required to capture the fine-scale variability in SOC distribution (Banerjee et al., 2011).

Soil organic carbon content (SOCC; kg m^{-2}) is traditionally calculated as follows (Tarnocai et al., 2009):

$$SOCC = C \times BD \times T \times (1 - CF) \times 10 \qquad \text{(Eq. 2.1)}$$

where C is the % OC, BD is measured soil bulk density (g cm^{-3}), T is the soil layer thickness and CF is the percent of coarse fragments by weight (%). Soil organic carbon is typically determined by dry combustion using an elemental analyzer (Skjemstad and Baldock, 2007) or a chemical oxidation using the Walkley and Black (1934) method. To determine only organic carbon, soils are often treated acid prior to analysis to removed carbonates/inorganic C. Loss on ignition was often used in early studies as a quick predictor of SOM content in soils, however this method is imprecise (Skjemstad and Baldock, 2007).

2.4.1 Novel application of visible and near-infrared diffuse reflectance spectrophotometers to assess soil organic carbon

For over 20 years, diffuse reflectance spectroscopy techniques have been proposed as alternatives to traditional wet chemistry methods for estimating soil properties (e.g. Janik et al., 1998). Laboratory based visible and near-infrared (vis-NIR) diffuse reflectance spectroscopy (DRS) is well established as a rapid, cost-effective and non-destructive method to predict soil organic carbon (SOC) and other soil properties (Viscarra Rossel et al., 2006, 2008; Morgan et al., 2009; refer to reviews by Bellon-Maurel and McBratney, 2011 and Soriano-Disla et al., 2014). Given the availability of appropriate calibration models, a single scan of a soil takes less than a minute, requires no consumable reagents, and can be used to predict multiple soil properties. In contrast, field portable vis-NIR DRS methods are less well established. There is some concern that fields measurements may result in a loss of prediction accuracy because reflectance is sensitive to changes in soil moisture, texture and bulk density (Morgan et al., 2009; Bellon-Maurel and McBratney, 2011); however, field portable instruments allow users to assess the spatial variability of soil properties across their field sites and to depth in the soil profile at a resolution that would otherwise be unfeasible using traditional methods. Thus, the loss of prediction accuracy may be insignificant compared to the benefits associated with the ability of field-portable instruments to characterize the spatial variability of SOC (Viscarra Rossel et al., 2006; Bellon-Maurel and McBratney, 2011).

Spectroscopy techniques are well suited to agricultural and environmental sciences as vis, NIR and mid-infrared (MIR) spectroscopy techniques are sensitive to inorganic and organic phases of soil making them ideal for measuring many soil properties. In the MIR range (wavelengths 2,500 – 25,000 nm), some soil properties can be attributed to specific fundamental bands. In

contrast, soil properties are not as easy to distinguish in the vis-NIR range as soil properties tend to be associated with weak overtones and overlapping combinations of bands in the NIR (700 – 2,500 nm) range and electronic transitions of the electromagnetic spectrum in the vis (400- 700 nm) range (Viscarra Rossel et al., 2006). Thus, practical field application of vis-NIR spectroscopy requires the development of multivariate calibration models that relate the weak overtones and bands of soil spectra to laboratory measured SOC.

2.4.2 vis-NIR DRS approaches to field condition and in situ soils

While methods for estimating soil properties from field condition soils are not as well established as laboratory DRS methods done on dried and ground soil samples, a variety of approaches for estimating SOC have been tested on laboratory simulated in situ and actual in situ field conditions. In a review assessing vis, NIR and mid-infrared (MIR) spectroscopy of soil properties, Soriano-Disla et al. (2014) found that for the majority of soil properties (with the exception of extractable P) median R^2 of in situ calibration models was slightly lower than comparable laboratory based studies using dried and sieved samples (Table 2.2).

Laboratory simulated in situ methods include testing laboratory moistened soils (Stenberg et al., 2010; Nocita et al., 2013) and field moist soils (Chang et al., 2005; Morgan et al., 2009) to assess the influence of variable soil moisture on SOC prediction accuracy. Soil moisture can also influence the potential smearing of the soil profile when using probe-based field portable instruments, especially in the presence of heavy clays. Morgan et al., (2009) simulated the smearing of a soil profile using soil cores in the laboratory and found that calibration model prediction accuracies are generally not affected by smearing of the soil profile (Morgan et al. 2009). Though smearing is not an issue, soil moisture is an important factor to consider when developing calibration models for field application as increased moisture content can both decrease

(Chang et al., 2005; Morgan et al., 2009) or increase (Stenberg et al., 2010; Nocita et al., 2013) prediction accuracies of calibration models. Calibration models can minimize the influence of variable soil moisture by including diverse samples from the region of study (Chang et al. 2005) and samples with a similar range and variability of moisture conditions (Nocita et al. 2013) to the site being predicted. The same recommendation holds true for other soil properties that are known to influence prediction accuracies such as variable soil texture and bulk density (Morgan et al., 2009; Bellon-Maurel and McBratney, 2011).

Table 2.2. Median R^2 values for soil variables predicted using vis-NIR and NIR in situ and laboratory (dried and sieved soils) methods (Soriano-Disla et al., 2014).

	Median R^2	
Soil property	Laboratory	In situ[†]
Extractable P	0.52	0.72
Total organic C	0.85	0.80
Soil H_2O Content	0.86	0.82
Total C	0.90	0.88
Total N	0.86	0.84

[†]Based on at least three prediction models in the literature

Field-based in-situ methods have most commonly been used in agricultural studies and applications in natural environments are limited. There are three primary approaches to in situ spectroscopy: 1) on-the-go in situ methods and 2) static in situ methods and 3) modified field portable static in situ methods. On-the-go methods typically involve a shank type attachment that is mounted behind a vehicle, soil spectra are taken continuously as the vehicle drags the shank across the field site (Mouazen et al., 2007; Christy, 2008; Kweon and Maxton, 2013). Similar to

the on-the-go method, conventional static in situ methods typically involve a spectrophotometer attachment mounted on a vehicle. In this method a probe type attachment that is inserted into a vertical pilot hole and spectral samples are collected in increments along the soil profile (Kweon et al., 2008). These first two methods are best suited to agricultural sites with vehicle access.

Finally, field portable static in situ methods consist of hand-held field portable devices that facilitate rapid sampling of soil cores or samples in the field (Kusumo et al., 2008; Wenjun et al., 2014), and modified hand-held devices (Ben-Dor et al., 2008) or field-portable probe based spectrophotometer attachments (Guy et al., 2015) that allow the user to collect soil spectra down the profile of a pilot hole much like the truck mounted versions. These field-portable spectrophotometers are particularly useful for remote field locations where vehicle access is limited.

2.4.3 Calibration models

2.4.3.1 Statistical Approaches

Multivariate calibration models are required to relate soil spectra to soil properties measured in the laboratory. Calibration models to predict SOC have been developed using various methods including but not limited to multivariate adaptive regression splines, multiple linear regression, support vector machines, random forest, boosted regression trees, wavelet analyses, artificial neural networks, principal components regression and partial least squares regression (Viscarra Rossel and Behrens, 2010; Soriano-Disla et al., 2014). Discussion of all these statistical approaches is beyond the scope of this literature review therefore we will focus on the two most common multivariate calibration approaches: principle component analysis (PCA) and partial least squares regression (PLSR) (Chang et al., 2001; Viscarra Rossel et al., 2006; Soriano-Disla et al., 2014).

Principle components analysis and PLSR are multivariate methods that break down all the information from our predictor variables (soil spectra) into a set of latent variables or factors that best explain the variation in our data (Mevik and Wehrens, 2007). In PCA, the latent factors aim to explain the maximum variation in our response variable (soil property). In contrast, latent factors in PLSR attempt to capture the maximum variation in the response and predictor variables. The advantage of PLSR, is its ability many the many intercorrelated predictor variables and noise that makes up our soil spectrum (Viscarra Rossel et al., 2006). Accounting for the variation in our spectra is important for vis-NIR data that has many overlapping and weak bands, making it typically more suitable for the prediction of soil properties from very heterogeneous soil samples.

2.4.3.2 Calibration Datasets

Calibration models should contain enough samples to cover the range of variation expected in the samples to be predicted. Depending on the study, calibration models can be developed from small local calibration datasets, larger soil spectral libraries or a combination of both. Small local calibration models tend to be the most accurate for single field vis-NIR studies because the calibration models are developed from soils located on-site; however, these local models require sufficient samples to cover the range of variability found at the site, are relatively expensive and used alone have a very narrow range of useful applications (Sankey et al., 2008; Guerrero et al., 2014). Soil spectral libraries for laboratory-based vis-NIR have been developed for regional to global scale applications (Brown et al., 2006; Sankey et al., 2008; Guerrero et al., 2010; Wetterlind and Stenberg, 2010). Calibration models based on regional or global soil databases tend to be more economical as they contain a broader range of soils, but are often not accurate for the prediction of new sites (Sankey et al., 2008). One of the challenges with calibration models for in situ studies, is the lack of spectral libraries containing field condition soils thus often limiting in-situ studies to

small scale field sites. Several studies have found that spiking, or augmenting, global (Brown 2007; Sankey et al. 2008), national (Wetterlind and Stenberg 2010; Guerrero et al. 2014) or regional calibration models with a few local samples yielded improved SOC predictions (Sankey et al. 2008).

3. SPIKING REGIONAL VIS-NIR CALIBRATION MODELS WITH LOCAL SAMPLES TO PREDICT SOIL ORGANIC CARBON IN TWO HIGH ARCTIC POLAR DESERTS USING A VIS-NIR PROBE

3.1 Preface

A version of Chapter 3 has been published [Guy, A. L., S. D. Siciliano, and E. G. Lamb. 2015. Spiking regional vis-NIR calibration models with local samples to predict soil organic carbon in two High Arctic polar deserts using a vis-NIR probe. Can. J. Soil Sci. 95: 237-249.]. I was the primary author of this manuscript and was responsible for all major areas of concept formation, data collection, data analysis, and manuscript preparation. The unpublished regional data used for model development were collected by Aaron Betts under the supervision of SD Siciliano. SD Siciliano and EG Lamb were involved as supervisors throughout this project from the early stages of concept formation and data analysis to the manuscript composition and edits.

3.2 Abstract

In situ visible and near-infrared (vis-NIR) spectroscopy is a potential solution to the logistic constraints limiting the accuracy and spatial resolution of soil organic carbon (SOC) estimates for Arctic regions. The objective of our study was to develop a calibration model based on field-condition soils for in situ applications to predict SOC in High Arctic polar desert soils from vis-NIR spectra. Soils (n =240) for calibration models were collected from three regional Canadian Arctic sites in 2010 and two local target sites in 2013. Local and regional calibration models were developed using partial least squares regression (PLSR). We assessed whether spiking or spiking and extra-weighting, regional models with calibration samples from local sites improved prediction of the local sites. The local model yielded successful prediction of target sites (R^2 0.91) whereas unspiked regional models had poor prediction accuracy (R^2 = 0.07 to 0.36; n =4). Spiking regional models with as few as 12 local samples greatly improved the SOC prediction of target sites; the best spiked models had R^2 between 0.69 and 0.86. Extra-weighting spiking subsets in regional models yielded limited improvements in prediction performance. These results suggest that regional vis-NIR calibration models can be successfully used to predict SOC in High Arctic polar desert soils. The in situ application of these calibration models using field-portable instruments in remote areas, relative to traditional laboratory methods, can achieve higher sample sizes and the ability to characterize the spatial variability of SOC.

3.3 Introduction

Northern circumpolar soils store approximately 50% of total estimated global soil organic carbon (SOC) (Tarnocai et al., 2009), yet the SOC stores of many regions are not well understood, limiting the accuracy of large-scale Arctic SOC estimates (Campeau et al., 2014). Arctic regions are warming more rapidly than those of lower latitudes (IPCC, 2007) thus understanding the size

and distribution of the SOC pools in these regions is foundational to understanding how these soils will respond to a changing climate (Paré and Bedard-Haughn, 2013a; b). There are two main challenges that limit our ability to assess the carbon pools in these regions. First, the logistical constraints of conducting Arctic fieldwork include a short field season to collect soil samples and the high cost of freighting samples to an analytical laboratory. Second, given the complex interactions between soil, vegetation and water in periglacial environments (Walker et al., 2004), a large number of samples are required to capture the fine-scale variability in SOC distribution (Banerjee et al., 2011).

Visible and near-infrared (vis-NIR) diffuse reflectance spectroscopy is an efficient, non-destructive and less expensive alternative to traditional laboratory methods for estimating soil properties (Viscarra Rossel et al., 2006, 2008). Calibration models based on laboratory collected spectra on ground and dried samples yield good prediction results for SOC and other soil properties (refer to reviews Bellon-Maurel and McBratney, 2011; Soriano-Disla et al., 2014). For field condition soils, a variety of approaches for estimating SOC have been tested including using moist samples (Chang et al., 2005; Stenberg, 2010; Nocita et al., 2013), simulated in situ methods (Morgan et al., 2009), static in situ methods (Ben-Dor et al., 2008; Kusumo et al., 2008; Kweon et al., 2009; Wenjun et al., 2014) and on-the-go in situ methods (Mouazen et al., 2007; Christy, 2008; Kweon and Maxton, 2013). Particularly useful in a remote field environment is the novel static in situ method developed by Ben-Dor et al. (2008) where a spectrometer with a probe attachment is used to collect soil spectra down the profile of a drilled hole. In that study soil organic matter was successfully estimated using a partial least squares regression (PLSR) calibration model; development of calibration models for in situ studies can be challenging due to uncertainties associated with the variable soil moisture and scanning conditions of field condition soils.

Calibration model prediction accuracies for probe-based methods are generally not affected by smearing of the soil profile (Morgan et al., 2009). Calibration models are, however, affected by variability in soil moisture as increased moisture content can both decrease (Chang et al., 2005; Morgan et al., 2009) or increase (Viscarra Rossel et al., 2009; Stenberg, 2010; Nocita et al., 2013) prediction accuracies. Acceptable prediction accuracies can be obtained from field moist samples if the calibration model contains diverse samples from the region (Chang et al., 2005) and a similar range of moisture (Nocita et al., 2013) to the site being predicted.

Practical field application of vis-NIR spectroscopy requires the development of local or regional multivariate calibration models that relate the in situ spectra to laboratory measured SOC. Calibration models should contain enough samples to cover the range of variation expected in the samples to be predicted (Viscarra Rossel et al., 2009). Local calibrations based on field-site data tend to be the most accurate; however, they are limited in their application for remote sites and can be expensive as they require many local samples (Sankey et al., 2008; Guerrero et al., 2014). Calibration models based on regional or global soil databases tend to be more economical as they contain a broader range of soils, but are often not sufficiently accurate for the prediction of new sites (Sankey et al., 2008). Several studies have found that spiking, or augmenting, global (Brown, 2007; Sankey et al., 2008), national (Wetterlind and Stenberg, 2010; Guerrero et al., 2014) or regional calibration models with a few local samples yielded improved SOC predictions (Sankey et al., 2008). In some cases, the best spiked models had better SOC predictions than local models (Brown, 2007; Sankey et al., 2008). While the majority of studies focus on laboratory processed samples, Viscarra Rossel et al. (2009) successfully increased the prediction accuracy of clay content from in situ soil spectra by adding field condition samples to a national soils calibration dataset. To the best of our knowledge there have been no vis-NIR spectroscopy studies done on

arctic soils for in situ application, though Rinnan and Rinnan (2007) conducted a laboratory based study focussed on predicting several microbiological and chemical properties of highly organic arctic soils.

Given the logistical constraints of Arctic fieldwork, in situ vis-NIR technology has the potential to rapidly assess SOC content across arctic field sites at a level of detail that otherwise would not be possible. The main objective of our study was to develop a calibration model based on field condition soils for in situ applications to predict SOC of High Artic polar desert soils using vis-NIR spectra. In order to do this we assessed: i) the predictive ability of regional and local models, ii) if spiking regional models with calibration samples from local sites yields improved prediction of the local sites, and iii) if increasing the weight of local samples relative to the regional samples improved prediction of the local sites.

3.4 Materials and Methods

3.4.1 Soil samples

3.4.1.1 Regional samples

A regional soil dataset (n = 199) was collected in 2010 from three sites located on Ellesmere Island, NU (Aaron Betts, unpublished). The sites included two polar desert locations, Patterson River on the north-central coast and Okse Bay located on south-western coast, and a polar desert oasis at Alexandra Fiord (Lowland) on the east central side of Ellesmere Island (Fig. 3.1). The number of samples and distribution of SOC values at each site are displayed in Table 3.1.

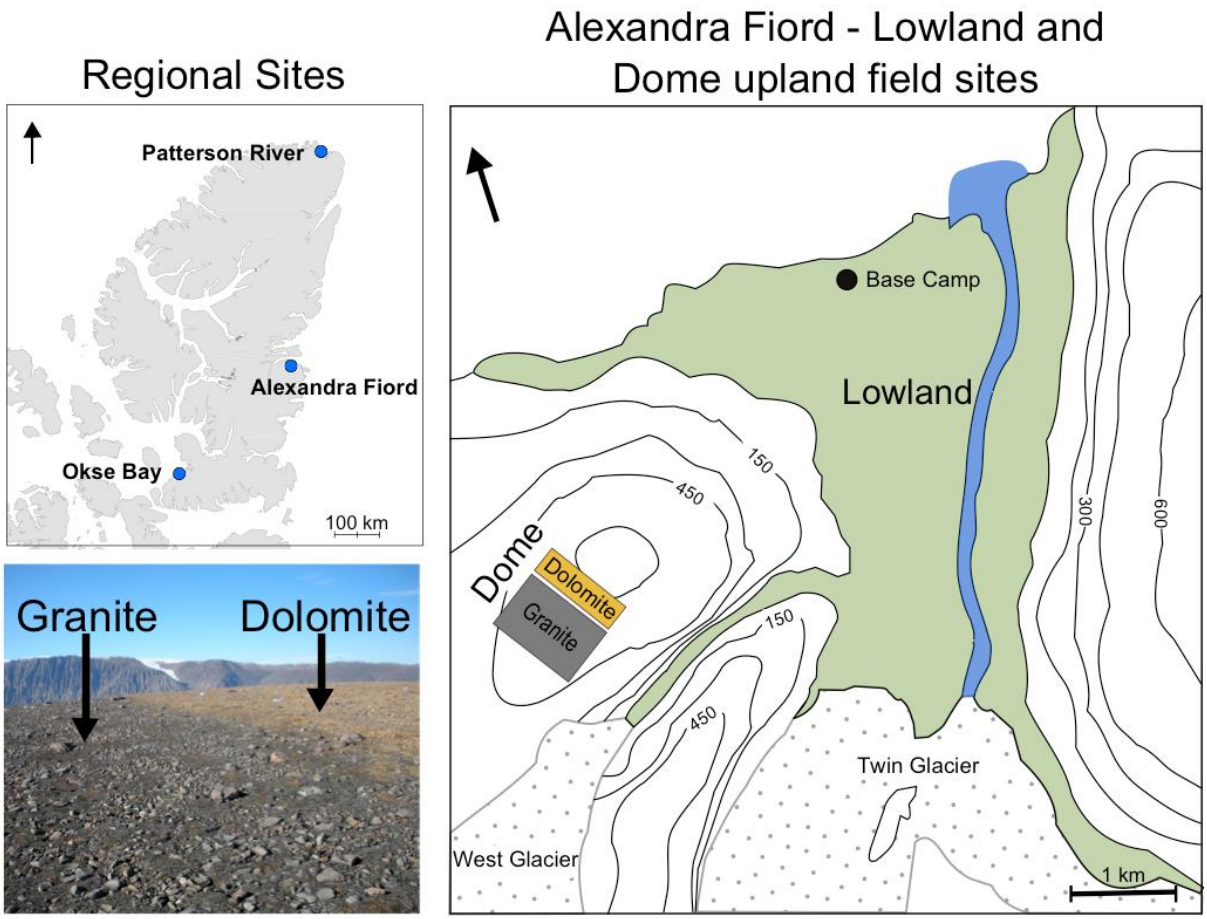

Fig. 3.1 Sites and sampling locations (clockwise from top-left): map of regional site locations on Ellesmere Island, map of local target sites (Granite and Dolomite) located at Dome near Alexandra Fiord Lowland, and image of local target sites (Granite and Dolomite).

3.4.1.2 Local target samples

The two adjacent polar desert target sites (Dolomite and Granite) are located on an upland plateau called Dome near the Lowland site and were sampled in July and August of 2013. Despite the close proximity and similar environmental conditions, the sites are derived from different parent materials and have very distinct soils (Fig. 3.1). The granitic parent material site soils are grey in color with a pH of 6.3 to 7.2 while the dolomitic site has light yellow to orange surface soils and a pH of 8.0 to 9.0 (Stewart et al., 2012). Throughout this study the target sites will be

referred to separately as Dolomite and Granite and together as Dome. The distribution of organic carbon values for Dolomite (n=21) and Granite (n=20) sites are displayed in Table 3.1.

Table 3.1. Characteristics and soil organic carbon data (g SOC kg^{-1} dry soil) of three regional sites used to develop the regional calibration models and the two Dome target sites.

	Regional Sites			Local Target Sites (Dome)	
	Alexandra Fiord Lowland	Okse Bay	Patterson River	Granite	Dolomite
Coordinates	78° 53' N 75° 55' W	77° 07' N 87° 56' W	82° 36' N 63° 25' W	78° 52' N 75° 54' W	
n	75	52	72	20	21
Minimum	4.3	3.0	5.8	3.0	8.8
Mean	77.7	22.5	41.4	4.7	22.1
Maximum	486.6	137.3	291.7	8.7	43.7
St. Dev	105.4	28.0	61.7	1.3	9.4

3.4.2 Spectral acquisition and laboratory analysis

Soil samples were collected in the field, transported and stored frozen until analysis. Due to the extremely remote field locations and coarse texture of our soils we were unable to collect the intact cores or samples that would be required for simulated in situ calibration models. Thus, soil spectra were collected on thawed field moist soil samples in the laboratory using a bench top set-up for a field portable visible and near-infrared (vis-NIR) spectrophotometer with a soil probe attachment (Veris Technologies, Salina, KS). The instrument records spectra between 350 and 2225 nm using two internal spectrometers: (1) Ocean Optics and (2) Hamamatsu. Spectra were output as spectral absorbance with 8-nm resolution.

Since the purpose of the calibration models is to predict organic carbon on in situ field samples, soils were not sieved and samples often included coarse soil fractions and small rocks. For each of the 240 soils analyzed, approximately 2 to 4 g of soil were packed into the sample

holder. One spectrum was acquired for each soil sample, with the exception of 12 soils collected from Alexandra Fiord in 2010 (Dryas n = 10, Willow n = 1), and Okse Bay (n = 1) and four soils collected from Alexandra Fiord in 2013 (Dolomite), which each had multiple spectra (2 to 10) averaged per soil. Following spectrum collection, those same soils were air-dried, ground using a mortar and pestle, sieved (850 µm) and pre-treated to remove carbonates. Soil organic carbon was determined for each sample by dry combustion of a ~ 0.25-g subsample using a LECO C632 carbon analyzer.

3.4.3 Spectral data management

The spectrophotometer spectra were trimmed to eliminate scan insensitive regions (<440 nm and >2200 nm) and the region influenced by the grating between the two spectrometers (950-1150 nm) (Kweon and Maxton, 2013). Samples from each site were divided into a calibration dataset (n=75%) for model development and a validation set (n=25%) to internally validate the models for a more representative estimation of the model performance than obtained by cross-validation (Varmuza and Filzmoser, 2009; Soriano-Disla et al., 2014); samples were randomly divided with the condition that organic carbon values of the test set fell within the range of the calibration dataset values. One regional sample was identified as an outlier and was removed from subsequent analysis as it had a very unusual spectrum likely due to an instrument error.

We conducted a principal component analysis (PCA) of the remaining spectral samples to examine the spectral diversity and similarities between the regional and target sites. Eight regional samples, primarily from the Lowland polar oasis, with high organic carbon content (>20% OC dry weight) were excluded from the dataset as organic rich soils were not expected in our target sites and the focus of this study was mineral soils.

3.4.4 Spectral preprocessing

Preprocessing transformations are used to prepare spectral data for modeling. The most common transformations often include smoothing to reduce random noise and/or the use of derivatives to extract important information (Vasques et al., 2008; Varmuza and Filzmoser, 2009). The choice of pre-treatment often depends on the data, though the Savitzky-Golay transformations (Savitzky and Golay, 1964) are commonly used. The effect of spectral pre-treatment on model performance was evaluated by applying various Savitzky-Golay smoothing and 1st derivative transformations separately and in combination to regional and local samples. We varied the polynomial order from 1st to 3rd polynomial orders and search window size from 3 to 9 for both transformations. All preprocessing was conducted using the *prospectr* package in R (Stevens and Lopez, 2013; R Core Development Team, 2015). The preprocessing transformation chosen for our models was 2nd order polynomial Savitzky-Golay smoothing with 9 smoothing points followed by Savitzky-Golay 1st derivative, 3rd order polynomial with 7 smoothing points.

3.4.5 Calibration models

Local and regional calibration models predicting soil organic carbon from soil spectra were developed using partial least squares regression (PLSR). Partial least squares regression (Wold et al., 2001; Bjørsvik and Martens, 2008) is a multivariate calibration method that can handle the many intercorrelated predictor (X) variables that make up a soil spectrum. Similar to PCA, PLSR decomposes all the information from our predictors into a set of latent variables or factors (Mevik and Wehrens, 2007). Unlike PCA, where factors aim to explain the maximum variation in the response variable (Y), PLSR factors capture the variance in the predictor (X) and response (Y) variables (Mevik and Wehrens, 2007), making it more suitable for predictions. We developed PLSR calibration models in R with the autopls package (Schmidtlein et al., 2012; R Core

Development Team, 2015) using log transformed SOC, and mean-centered and transformed vis-NIR soil spectra (Appendix A).

3.4.5.1 Local model

A local model (LM) was developed using only Dome calibration samples (Table 3.2) and validated using the Dome validation dataset. Calibration statistics were calculated separately for the Dolomite, Granite and Dome datasets.

Table 3.2. Soil organic carbon (g SOC kg^{-1} dry soil) characteristics of the calibration datasets used to develop the local model and four regional models.

	LM†	RM2‡	RM2‡	RM3‡	RM4‡
n	31	141	91	89	102
Min	3.0	3.0	3.0	3.0	4.3
Median	8.8	15.0	15.0	13.5	19.8
Mean	13.2	34.2	37.1	26.0	38.8
Max	43.7	198.3	198.3	191.8	198.3
St. Dev	10.5	40.8	43.7	32.2	44.1

† LM, local model developed using Dome samples

ɣ RM, regional model where RM1 includes all regional sites and RMs 2-4 each excluded one of the three sites: Patterson River (RM2), Lowland (RM3) and Okse Bay (RM4).

3.4.5.2 Regional models

We tested three methods for developing regional models of different combinations of regional sites for the prediction of target site SOC from vis-NIR spectra. Unspiked regional models based only on regional data were compared to models spiked with varying numbers of samples from the target sites and extra-weighted models where additional copies of the spiking subsets were added.

i) Unspiked Models

Four regional calibration models were developed to assess the influence of the different sites on model performance. Regional Model 1 (RM1) included all sites and Regional Models 2-4 each excluded one of the three sites: Patterson River (RM2), Lowland (RM3) and Okse Bay (RM4) (Table 3.2). The models were cross-validated using 10 randomly selected segments with each sample being left out of the calibration data set once. The optimum number of latent factors was determined by the first local minima of errors during the cross-validation procedure (Schmidtlein et al., 2012). Each RM was internally validated and independently validated by predicting its validation and the Dome target site datasets, respectively (Fig. F-i).

ii) Spiked Models

The regional models were spiked with three spiking subsets types (Dolomite, Granite and Dome) of various sizes (Fig. 3.2-ii) to evaluate the influence different numbers of spiking sites have on target site predictions and to determine the number of target samples required to improve predictions. Guerrero et al. (2014) found that choosing spiking subset sets based on spectral diversity yielded better model improvements than choosing samples representative of the range of SOC values. Thus, we selected spiking subsets using the Kernard-Stone algorithm, which deterministically selects samples evenly distributed across the first 3 components of a soil spectra PCA (Sila and Terhoeven-Urselmans, 2013). We used 25% of the target site dataset as prediction dataset and 75% to select spiking subsets (SSx). Spiking subset size (x) ranged from 1 to 15 samples for Dolomite and Granite, and even increments of 2 to 30 samples for Dome (with an equal number of samples from each target site). The number

of latent factors was set to the same number as the corresponding unspiked model. Each spiked RM was used to predict the prediction dataset associated with its SSx. For Dome spiked models, calibration statistics were calculated separately for Dolomite, Granite and Dome target sites. Due to the extremely remote location of target sites sample size was limited, thus the prediction datasets to validate the models are smaller than those typically used (Bellon-Maurel and McBratney, 2011).

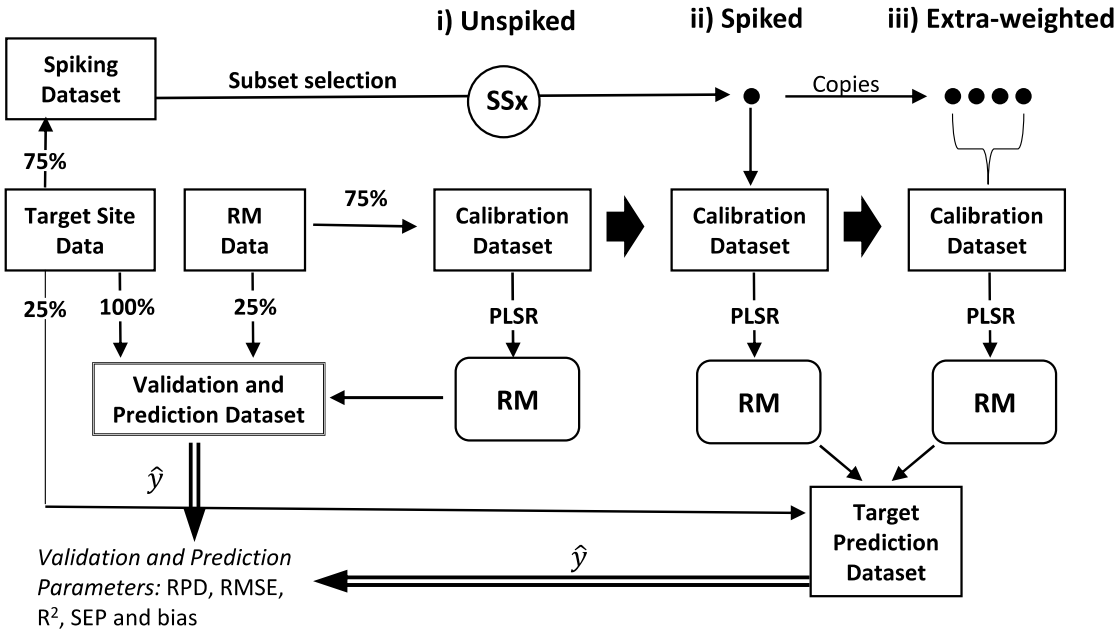

Fig. 3.2. Approach to developing in situ partial least squares regression (PLSR) calibration models using i) the unspiked regional model (RM) calibration dataset, ii) the RM calibration dataset spiked with spiking subsets (SSx; where x is the size of the spiking subset) and iii) the RM calibration dataset spiked and extra-weighted with additional copies of the spiking subsets (SS4 and SS12). Model performance parameters are calculated based on the predictions (ŷ) of the validation and prediction datasets.

iii) Spiked and Extra-weighted Models

The regional models were spiked and extra-weighted with additional copies of the Dolomite, Granite and Dome spiking subsets (SS4 and SS12) (Fig. 3.2-iii) to evaluate whether extra-weighting of samples could be used to improve calibration models in

lieu of adding additional target site samples. Spiking, predictions and calculation of calibration statistics proceeded as per the spiked models.

3.4.6 Calibration statistics

Model performance was evaluated based on five calibration statistics including coefficients of determination (R^2), root mean square error (RMSE; Eq. 3.1), ratio of prediction to deviation (RPD; Eq. 3.2), bias (Eq. 3.4) and bias corrected standard error of prediction (SEP_{-b}; Eq. 3.5). SOC predictions were back transformed before calculating the calibration statistics with the exception of R^2 that was calculated in log transformed space. No single calibration statistic can fully evaluate the performance of a model and therefore we have provided all the commonly presented statistics. We used R^2 values to measure the strength of the relationship between the observed and predicted SOC values, RMSE of validation (RMSEV) and prediction (RMSEP) are measures of model accuracy, and RPD standardizes the error allowing comparisons between models.

$$RMSE = \sqrt{\sum_{i=1}^{n} \frac{(\hat{y}_i - y_i)^2}{n}} \quad \text{(Eq. 3.1)}$$

$$RPD = SD/RMSE \quad \text{(Eq. 3.2)}$$

where $\hat{y}_i$ is the predicted value and y_i the measured value; n is the number of samples and SD is the standard deviation of the validation or prediction datasets.

The final two calibration statistics, bias and SEP_{-b} , are included as recommended by Davies and Fearn (2006) and Bellon-Maurel et al. (2010) to give a more detailed look at the error (RMSE) associated with the predictions. Bias is the average difference between measured and predicted values, an indication of whether SOC values tend to be over or under predicted. The

difference between RMSE and SEP gives a measure of how the relative amount of bias changes between models (Eq. 3).

$$RMSE^2 = {SEP_{-b}}^2 + bias^2 \quad \text{(Eq. 3.3)}$$

where:

$$bias = (\sum_{i=1}^{n} \hat{y}_i - y_i)/n \quad \text{(Eq. 3.4)}$$

$$SEP_{-b} = \sqrt{\left(\sum_{i=1}^{n} (\hat{y}_i - y_i - bias)^2\right)/(n-1)} \quad \text{(Eq. 3.5)}$$

Categorizing models based on a single calibration statistic is a straightforward way to identify good models before inspecting the full suite of calibration statistics used ensure overall model performance. Several studies have attempted to categorize calibration statistics, mainly R^2 and RPD values, using thresholds (Chang et al., 2001; Lee et al., 2009; Soriano-Disla et al., 2014). Both of these calibration statistics have undergone some scrutiny due to their dependence on the range and distribution of the data (see Davies and Fearn, 2006; Bellon-Maurel et al., 2010), and should be interpreted with respect to other calibration statics. Proposed thresholds for R^2 values are generally consistent (Chang et al., 2001; Lee et al., 2009; Wenjun et al., 2014; Soriano-Disla et al., 2014); whereas there is no consensus on the more subjective RPD thresholds (Bellon-Maurel et al., 2010). With this in mind, our models were evaluated based on the R^2 thresholds used by Soriano-Disla et al. (2014): excellent (>0.95), successful (0.90-0.95), moderately successful (0.80-0.90), moderately useful or approximately quantitative (0.70-0.80), possible to discuss trends (0.50-0.70), unreliable (<0.50).

3.5 Results

3.5.1 Regional sites

Regional and local target sites differ from one another based on their spectral signatures (Fig. 3.3). The first two components of the principal component analysis explained 79.5% of the variation in the soil spectra with the third component explaining an additional 7.3%. Patterson River was spectrally distinct from the other sites; samples clustered primarily in the bottom left quadrant of the principal component analysis space and the cluster did not overlap with the other sites. Okse Bay and Lowland samples were more dispersed in the principal component analysis space and exhibited significant overlap with each other with the exception of some high SOC Lowland sites that were dispersed in the bottom right quadrant of the principal component analysis plot. Local target sites clustered separately, were more tightly clustered than the regional sites and had very little overlap with the Lowland and Okse Bay sites.

3.5.2 Unspiked calibration models

The local model yielded successful predictions of the Dome (Dolomite + Granite) target site validation data with large R^2 and RPD values and low RMSEV and bias (Table 3.3). Validation of the unspiked regional models using a randomly selected subset (25%) of the regional model dataset yielded moderately successful predictions for RM4 and approximately quantitative predictions for RM1-3 (Table 3); however, when these models were independently validated using the Dome target site the results were very unreliable (Table 3.3, Fig. 3.4). Compared to local model predictions, the R^2 values of unspiked regional models were 60 to 92% lower, RPD values were 75 to 87% lower and RMSE values were 242 to 575% higher.

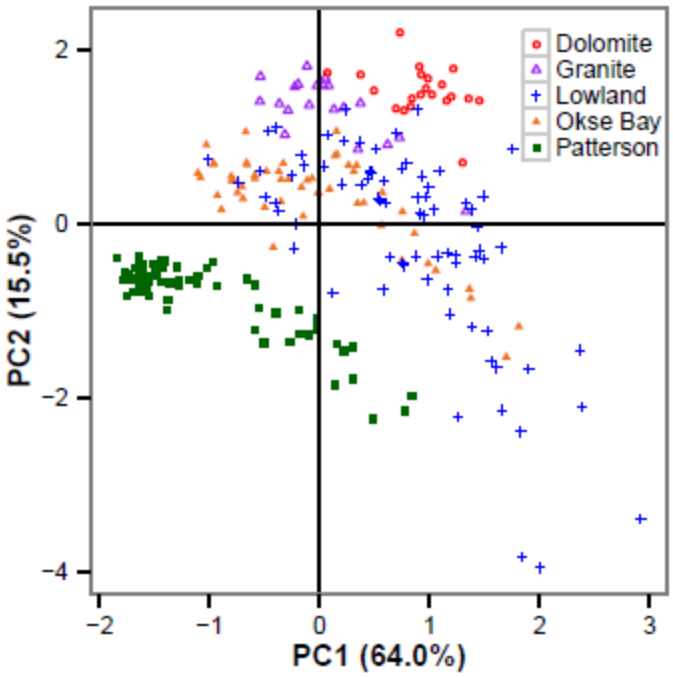

Fig. 3.3. Projection of regional and target sites on the first two principal components of a principal component analysis based on site visible and near-infrared spectra. Values in brackets indicate that amount of variation in the spectra captured by each axis.

Table 3.3. Model prediction performance parameters of validation and combined Dome target site prediction obtained from the four regional calibration models RM1, RM2, RM3 and RM4, and the prediction of the target site test sets by the local calibration model (LM). The parameters include the coefficient of determination (R^2), root mean square error of validation (RMSEV, g kg^{-1}) and root mean square error of prediction (RMSEP, g kg^{-1}), bias and the ratio of performance to deviation (RPD).

		Validation				Prediction			
Model	Latent Factors	R^2	RMSEV	BIAS	RPD	R^2	RMSEP	BIAS	RPD
LM	2					0.91	3.6†	-0.7	3.66
RM1	6	0.79	18.7	-3.4	2.02	0.25	12.5	-6.1	0.89
RM2	7	0.78	17.6	-1.1	2.16	0.25	12.3	-4.0	0.90
RM3	5	0.78	19.2	-6.5	1.68	0.07	15.2	4.0	0.73
RM4	4	0.81	21.1	-4.0	1.97	0.36	24.3	13.7	0.46

†RMSEV

The prediction accuracy of the regional models differed in magnitude and direction depending on the target site being predicted, indicating that the regional sites included in the regional models influence the prediction of the individual target sites differently (Fig. 3.4). For ease of interpretation, only Dome predictions (Fig. 3.4) and prediction parameters (Table 3.3, Fig. 3.5) for unspiked regional models are shown. The individual prediction parameters for Granite and Dolomite target site predictions by unspiked regional models are available in Figs. A.1-A.4. Generally, there was lower error (RMSEP = 8.8 ± 7.0 g SOC kg^{-1}) and better model fit (R^2 = 0.56 ± 0.02) associated with Granite site predictions compared to Dolomite site predictions (RMSEP = 15.6 ± 3.8, R^2 = -0.06 ± 0.25). RPD values were generally higher for dolomitic predictions compared to granitic predictions though this was primarily due to a much lower standard deviation for granitic samples compared to dolomitic samples (Figs. A.1-A.4).

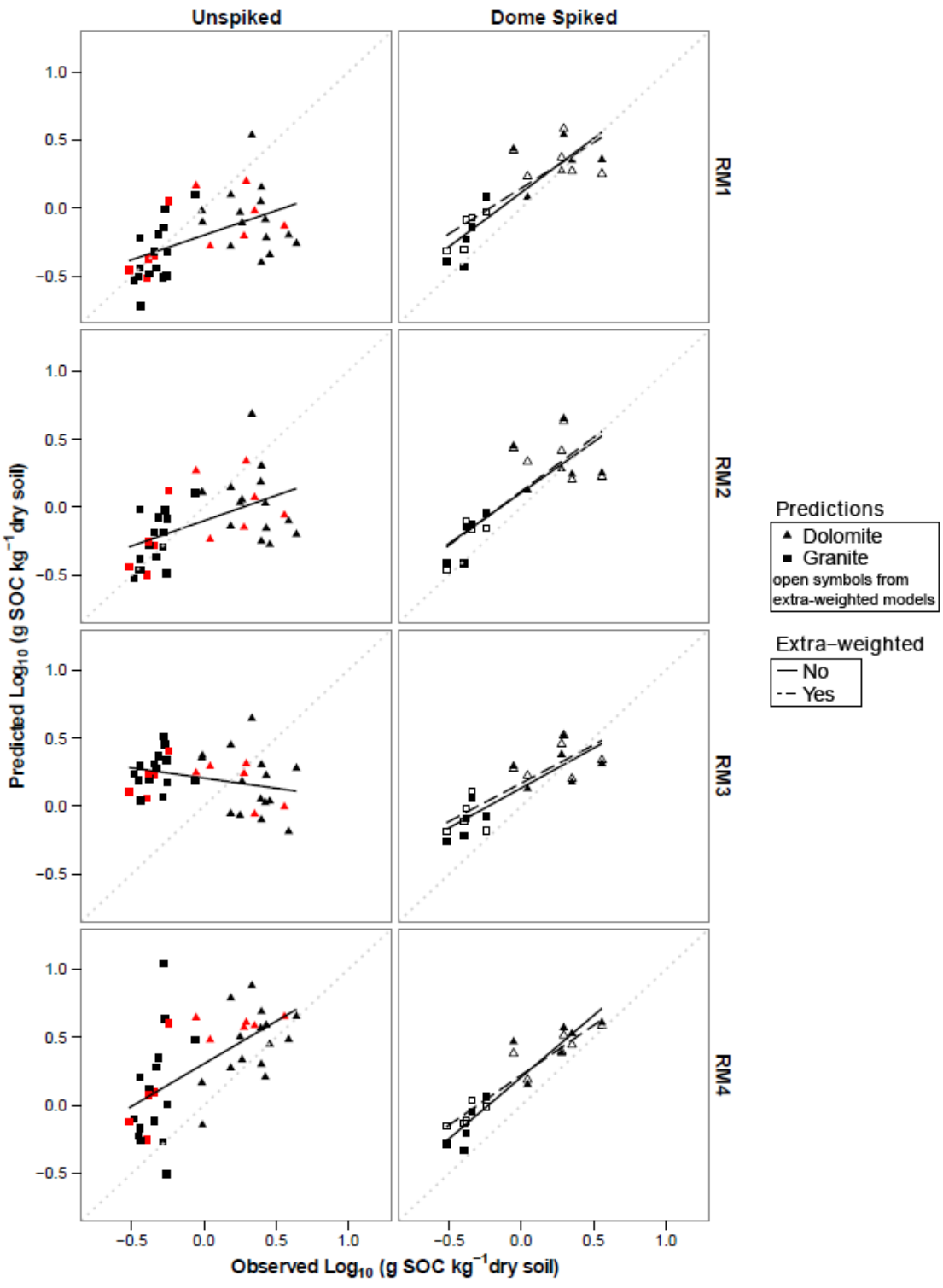

Fig. 3.4. Soil organic carbon predictions of four regional calibration models (RM1, RM2, RM3 and RM4) where all Dome target sites are predicted using unspiked models, and the Dome target test sites are predicted using models spiked or spiked and extra-weighted with four copies of the Dome spiking subset. The light grey dotted line is a 1:1 line, solid and dashed lines are linear regression lines, and the sites highlighted in red represent the target site test sets predicted by the spiked model.

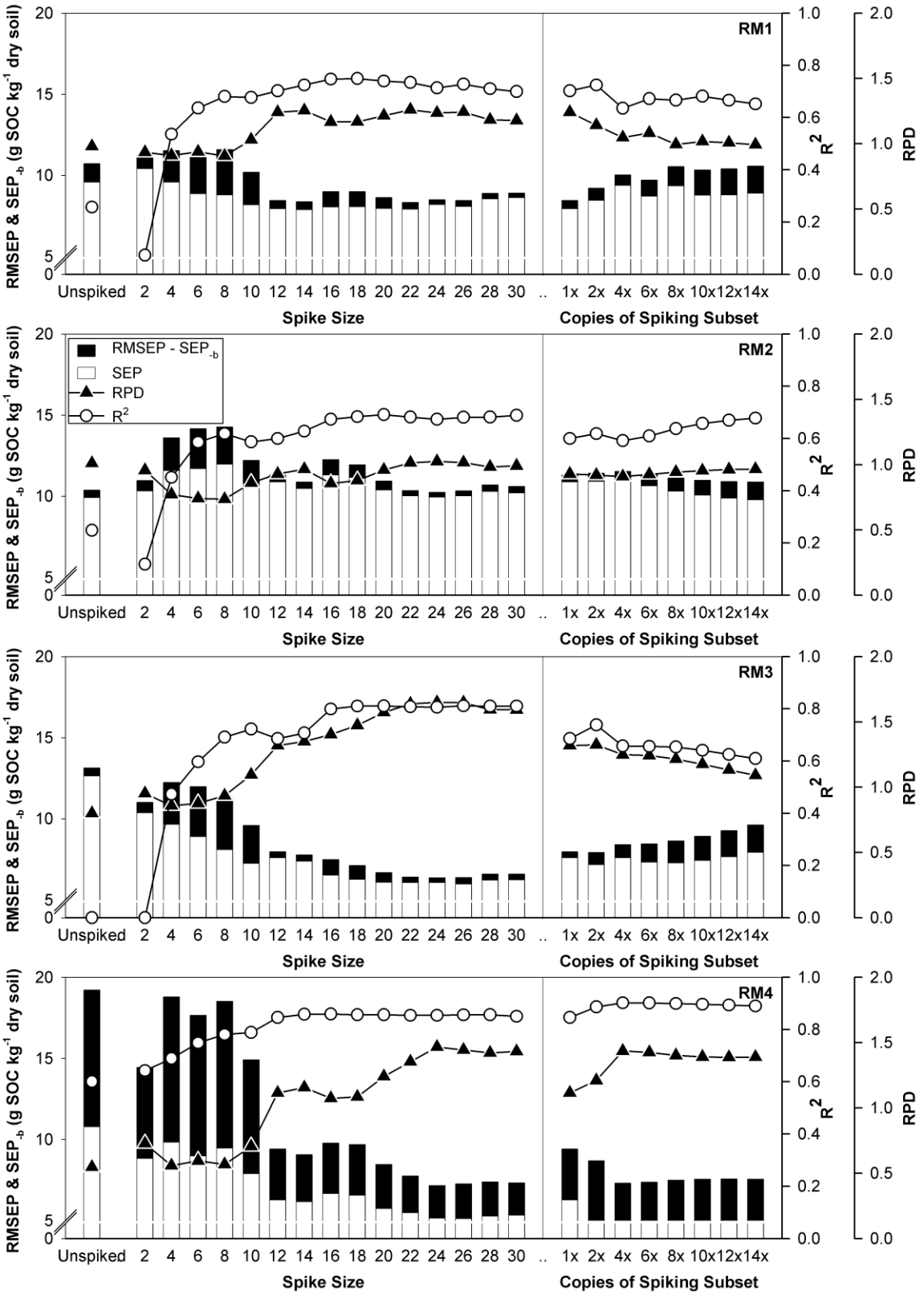

Fig 3.5. Model performance parameters of unspiked regional models, regional models spiked with Dome spiking subsets, and regional models spiked with additional copies of the Dome spiking subset (SS12) predicting the Dome target test set.

When all regional sites were included (RM1), or Patterson River sites were excluded (RM2) prediction performance was greatest (Table 3; Fig. 3.4). Given that Patterson River spectra were most dissimilar to the target sites (Fig. 3.3), we expected that removing these samples would improve the calibration model. However, excluding these spectra only slightly decreased error and bias; a small change that could be attributed to an additional latent factor in the model since the error and bias associated with Granite sites actually increased slightly (Fig. A.3). Excluding sites from Okse Bay (RM4) resulted in the poorest model overall (Table 3.3) with the largest bias and error for both Dolomite (Fig. A.2) and Granite (Fig. A.4) target sites. When the Alexandra Fiord Lowland sites were excluded from the regional model (RM3), RMSEP for dolomitic sites decreased from 17.3 g SOC kg^{-1} (RM1) to 15.4 g SOC kg^{-1}. In contrast, RMSEP for granitic sites increased from 2.2 g SOC kg^{-1} (RM1) to 14.9 g SOC kg^{-1}. This suggests that the spectra from the Lowland site contain important features that explain the variation in SOC for the granitic sites but also contain features that confound the ability to predict dolomitic sites.

3.5.3 Spiking

Spiking regional models improved Dome target site predictions (Fig. 3.4) and increased the prediction accuracy relative to the unspiked models (Fig. 3.5). For ease of interpretation, only Dome predictions (Fig. 3.4) and prediction parameters (Fig. 3.5) for regional models spiked with Dome spiking subsets are shown. Based on the R^2 criteria, the best spiked models were moderately useful (RM1; $R^2 = 0.75$) to moderately successful (RM3; $R^2 = 0.81$, RM4; $R^2 = 0.86$) in predicting the target sites; whereas the best RM2 ($R^2 = 0.69$) model was only suitable to discuss trends. Generally the best models had higher RPD values, less bias and lower RMSEP values relative to the unspiked models though RMSEP values were still greater than that of the local model (Fig. 3.5). Improved prediction performance of spiked regional models (Fig. 3.4) reflected in the

improved R^2 values (Fig. 3.5) may partially be attributed to the increased ability of spiked models to distinguish between the Dolomite and Granite target sites. However, for the majority of these models prediction parameters also improved within one or both of the individual Dolomite and Granite target sites. The prediction parameters for Granite and Dolomite target site predictions for regional models spiked with Dome spiking subsets, as well as Dolomite or Granite spiking subsets are available in Figs. A.1-A.4.

Spiking regional models with as few as twelve samples improved those models (Fig. 3.5). Though model fit (R^2) improved with as few as 4 samples, RMSE only had consistent improvements when spiked with Dome subsets of 12 or more samples (Fig. 3.5). Spiking regional models with ten or fewer samples often decreased prediction accuracy or provided little improvement in overall model performance (Fig. 3.5). Small spiking subsets likely increase the amount of model bias and act as outliers.

The accuracy of the Dolomite and Granite target site predictions differed depending on the spiking subset used to spike the regional models (Fig. 3.6, Figs. A.1-A.4). Spiking regional models with Dome spiking subsets yielded slightly better mean RMSEP of Dolomitic sites relative to the same sized spiking subsets containing only Dolomitic sites (Fig. 3.6A). The mean RMSEP of Dolomitic sites in response to spiking subset size for both Dolomite and Dome spiking subsets closely matches the trends presented for Dome sites predicted by Dome spiked regional models (Fig. 3.6A). In contrast, the mean RMSEP of Granitic sites in response to spiking subset size differed between Granite and Dome spiking subsets. Overall, predictions of granitic sites were better when models were spiked with granitic subsets relative to those spiked with the same sized Dome subsets (Fig. 3.6B). Similar to Dolomite predictions, mean RMSEP of Granite sites from Dome spiked models got worse or improved only slightly with small spiking subsets and only

consistently improved with subset sizes of 12 or more samples, whereas mean RMSEP from Granite spiked models decreased even with small spiking subset sizes (Fig. 3.6B).

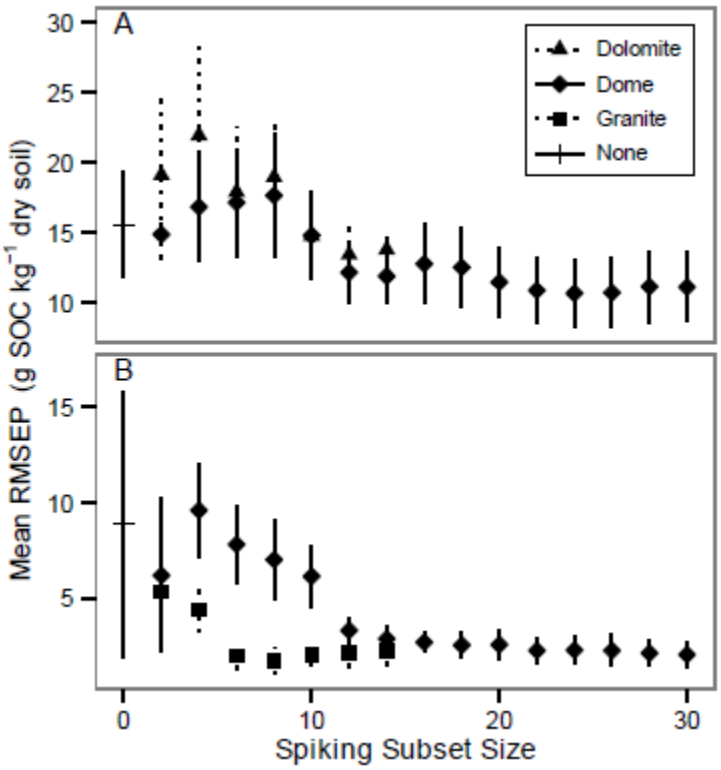

Fig. 3.6. Mean root mean square error of prediction (RMSEP) of the four regional models spiked with Dolomite, Granite or Dome spiking subsets predicting A) Dolomite and B) Granite test sets. Symbols refer to the type of spiking subset and error bars represent the standard deviation.

Regional model performance generally improved when spiked; however, the regional models responded differently to the spiking subsets (Fig. 3.6). For example, RM1 and RM2 spiked with small Dome and Granite spiking subsets had decreased model performance for the prediction of granitic sites. Most RM1 and RM2 models improved slightly with Granite spiking subsets sizes greater than 6 samples though more pronounced improvements to RM1 and RM2 prediction accuracy occurred when the models were spiked with Dome subsets with more than 20 or 12 samples, respectively (Fig. A.4). In contrast, RM3 and RM4 regional models model performance

improved with the addition of Granite or Dome spiking subsets even at very small subset sizes with the largest improvements occurring for subsets between 6 and 8 samples (Fig. A.4).

3.5.4 Extra-weighting

Spiking subsets of four (SS4) and twelve (SS12) samples showed similar trends when extra-weighted. SS12 was chosen as it was the first subset size where the mean RMSEP for all subsets was lower than the mean RMSE of the unspiked regional models (Fig. 3.6). The results presented here are for Dome predictions based on regional models spiked and extra-weighted with additional copies of the Dome spiking subset (SS12) (Fig. 3.4). Extra-weighting spiking subsets resulted in either small improvements or decreased prediction accuracy depending on regional model (Fig. 3.4). Model performance decreased for RM1 and RM3 with increased Bias and RMSEP, and decreased R^2 and RPD values with increasing copies of the spiking subset. RM2 had only slightly improved RMSEP, R^2 and RPD with increasing copies of the spiking subset. All performance parameters improved slightly when RM4 was spiked with two to four additional copies of the Dome SS12, however there was no additional benefit to increasing copy number. While granite predictions benefitted very little from extra-weighting, there were a select number of cases where extra-weighting improved dolomite predictions (Fig. A.2). RMSEP improved when RM4 was spiked and extra-weighted with Dolomite and Dome spiking subsets, and when RM3 was spiked and extra-weighted with the Dolomite spiking subset.

3.6 Discussion

This is the first study to assess the performance of calibration models for the prediction of soil organic carbon (SOC) in Arctic soils using vis-NIR spectroscopy. We attained successful to moderately successful SOC predictions of Arctic polar desert soils using the local calibration model (Table 3) and our best spiked regional models (Fig. 3.5), respectively. Typically, calibration

models for in situ applications have lower prediction accuracy relative to laboratory methods. In a comprehensive review of visible, NIR and mid-infrared (MIR) spectroscopy, the median R^2 of thirty-three studies using vis-NIR for the prediction of SOC was 0.83; median R^2 values were 0.80 for in situ methods and 0.85 for laboratory methods (Soriano-Disla et al., 2014). However, in this study and two studies using similar technology (Ben-Dor et al., 2008; Kweon et al., 2009), in situ calibration models surprisingly yielded better prediction performance than the median laboratory vis-NIR methods (Soriano-Disla et al., 2014).

Our local calibration model had only slightly lower prediction performance compared to the regional models developed by Ben-Dor et al. (2008) for the prediction of soil organic matter (SOM) with R^2 values of 0.92 and 0.94 and RMSEV of 3 g kg^{-1} and 2.1 g kg^{-1} for validation and prediction data sets, respectively. Our best spiked regional models had comparable prediction accuracy (R^2 = 0.69 to 0.86; RMSEP= 6.4 to 10.0 g kg^{-1}) to local calibration models (R^2 = 0.69 to 0.89; RMSEP= 0.8% to 1.27%) developed by Kweon et al. (2009). This suggests that the loss of prediction accuracy for in-situ methods relative to laboratory methods is insignificant compared to the higher sample sizes and the ability to characterize the spatial variability of SOC achievable with field-portable instruments (Viscarra Rossel et al., 2006; Bellon-Maurel and McBratney, 2011).

3.6.1 Does a regional model spiked with samples from target sites provide better predictions than an unspiked regional model?

Spiking regional models with as few as twelve local samples improved the prediction performance of all regional models. The improved R^2, RMSEP, bias and RPD are consistent with other studies combining large soil spectral libraries with local samples (Brown, 2007; Sankey et al., 2008; Wetterlind and Stenberg, 2010; Guerrero et al., 2014). It is evident that only a few local

samples provided adequate information on the variation of target site soils to predict SOC with moderately successful accuracy. This approach has major logistical benefits as it minimizes sampling effort at each target site and avoids the cost of constructing local calibrations.

Soil organic carbon predictions for the two new polar desert sites (Dome) based on unspiked regional models were very poor. This result suggests our unspiked regional calibration models did not cover the range of soil characteristics found at our target sites (Viscarra Rossel et al., 2008). This may simply be attributed to the small size of our regional models, however, several studies have shown that, even with calibration models based on diverse soils, inaccurate predictions can occur when those models are used to predict independent samples (Christy, 2008; Wetterlind and Stenberg, 2010; Bellon-Maurel and McBratney, 2011; Guerrero et al., 2014). Large initial calibration models can yield good prediction of soil properties, however spiking has the potential to further improve predictions (Sankey et al., 2008; Guerrero et al., 2010).

To achieve the best prediction accuracy, local target sites should be considered separately. We found that the prediction accuracies of regional models differed depending on the target site being predicted, and that the magnitude of improvement in response to spiking also differed. This was consistent with several other studies investigating multiple target sites (Brown, 2007; Wetterlind and Stenberg, 2010; Guerrero et al., 2014). Prediction accuracies of Granite sites were consistently better than those of Dolomitic sites in both unspiked and spiked regional models (Fig. 3.6). This indicates that the variation in soil properties at the Granite sites are better represented by the regional models compared to Dolomite sites. Given that Granite samples were more similar in spectral signature to Lowland and Okse Bay samples (Fig. 3.3) and had a narrower range of SOC content (Table 3.1), this was unsurprising. Despite improved Dolomite predictions in spiked

models, the variation in Dolomite soil properties may still be underrepresented in the spiked calibration models.

When choosing the size of spiking subsets, it is important to consider the proportion of spiking samples relative to the size of the regional calibration dataset. We found that spiking too few samples added variation to the calibration models that acted as outliers rather than contributing relevant information. In this study, spiking with as few as twelve local samples was sufficient to improve prediction accuracy of both target sites for four similar sized regional models. Guerrero et al., (2010, 2014) found that the same spiking size will improve smaller models more than medium or large models. Larger calibration datasets may thus require larger spiking subsets or extra-weighting of spiking subsets to improve prediction performance.

3.6.2 Does increasing the weight of local samples relative to the regional samples improve prediction of local sites?

Extra-weighting spiking subsets resulted in no consistent improvement to regional model predictions. Depending on the model, extra-weighting provided only small improvements and in some cases decreased prediction accuracy because, with the exception of RM4, bias increased when additional copies of the spiking subset were added (Fig. 3.5). For small spiking subsets, Guerrero et al. (2014) recommended extra-weighting as an effective way to improve the prediction performance of regional models. The limited improvement in our study may be due to the small regional models. Guerrero et al. (2014) observed larger model performance improvements when local samples were extra-weighted in medium and large calibration models. Sankey et al. (2008) also observed limited improvement in SOC predictions despite increasing the weight of local samples in large global calibrations. It is important to note that we found cases where Dolomite predictions improved when the RM3 and RM4 models were spiked with additional copies of the

Dome and Dolomite subsets (Fig. A.2). This indicates that extra-weighted spiking subsets may improve predictions if the target sites are very different from the sites included in the initial calibration, or the initial calibrations are proportionally very large compared to the spiking subset size.

3.7 Conclusions

Measures of soil organic carbon in High Artic polar desert soils were successfully to moderately successfully predicted using vis-NIR calibration models developed for in situ application. Spiking small regional models with as few as twelve local samples improved the SOC prediction of target sites, while extra-weighting spiking subsets in regional models yielded limited improvements in prediction performance. To obtain the best predictions, we recommend target sites should be dealt with separately. Additionally, the size of the regional calibration dataset should be considered when determining the minimum spiking size required.

In situ vis-NIR technology has the potential to efficiently and cost-effectively assess SOC content across arctic field sites at a level of detail that otherwise would not be possible. While in situ vis-NIR methods typically have lower prediction accuracies compared to laboratory vis-NIR methods, in this study we were able develop calibration models using field condition soils to predict SOC with reasonable accuracy using a local model and regional models spiked with local samples. Though more studies are required to validate the field methodology of in situ probe-based spectroscopy, the benefit of field-portable in situ instruments may out-weigh any potential cost in prediction accuracy. Spiking existing datasets with local samples also represents rapid and economical approach to minimize sampling effort at target sites and avoid costly-local models.

4. *SALIX ARCTICA* CHANGES ROOT DISTRIBUTION AND NUTRIENT UPTAKE IN RESPONSE TO SUBSURFACE NUTRIENTS IN HIGH ARCTIC DESERTS

4.1 Preface

A version of Chapter 4 has been published [Muller, A. L., S. P Hardy, S. D. Mamet, M. Ota, E. G. Lamb, S. D. Siciliano. 2017. *Salix arctica* changes root distribution and nutrient uptake in response to subsurface nutrients in High Arctic deserts. Ecology 98(8): 2158–2169.]. This manuscript was reformatted for inclusion in this dissertation. SP Hardy and myself were the primary authors of this manuscript and were responsible for all major areas of concept formation, data collection, data analysis, and manuscript preparation.

I was responsible for (1) assessing how common diapir horizons are in a polar desert landscape using visible near-infrared reflectance (vis-NIR), (2) collecting and conducting the preliminary analysis and interpretation of root biomass, and subsurface SOC distribution, and (3) conducting the vegetation surveys and data analysis.

SP Hardy was responsible for (1) developing the initial concept for the vegetation data analysis which was used in her thesis, (2) quantifying the natural abundance of N held in diapirs using $\delta^{15}N$, and (3) determine if *S. arctica* is exploiting the nitrogen in these horizons using an enriched $\delta^{15}N$ tracer. An earlier concept of this manuscript was published in SP Hardy's thesis [Hardy, S.P. 2016. Fertility of frost boils and the effect of diapirism on plant nitrogen uptake in a

polar desert ecosystem of the Canadian High Arctic. M.Sc. thesis, Dept. Soil Science, Univ. of Saskatchewan, Saskatoon, SK].

SD Mamet contributed to the analysis and interpretation of the root biomass and subsurface SOC data. This included kriging the subsurface SOC in ArcGIS, creating Fig. 4.1 and the analysis of the root biomass data in SAS. SD Mamet also aided in the manuscript preparation, edits and reformatting for publication. M Ota contributed the gross mineralization and nitrification rate data (Appendix B; Table B.3). In addition to the co-authors, Anne Bjorkman, James Cahill, Paul Grogan, and 3 anonymous provided helpful comments on this paper. SD Siciliano and EG Lamb were involved as supervisors throughout this project from the early stages of concept formation and data analysis to the manuscript composition and edits.

4.2 Abstract

Moisture is critical for plant success in polar deserts but not by the obvious pathway of reduced water stress. We hypothesized that an indirect, nutrient-linked, pathway resulting from unique water/frozen soil interactions in polar deserts creates nutrient-rich patches critical for plant growth. These nutrient-rich patches (diapirs) form deep in High Arctic polar deserts soils from water accumulating at the permafrost freezing front and ultimately rising into the upper soil horizons through cryoturbated convective landforms (frost boils). To determine if diapirs provide an enhanced source of plant-available N for *Salix arctica* (Arctic willow), we characterized soil, root, stem, and leaf ^{15}N natural abundance across 24 diapir and non-diapir frost boils in a High Arctic granitic semi-desert. When diapir horizons were available, *S. arctica* increased its subsurface (i.e., diapir) N uptake and plant root biomass doubled within-diapir. Plant uptake of enriched ^{15}N injected into organic rich soil patches was 2.5 fold greater in diapir than in non-diapir frost boils. *S. arctica* % cover was often higher (mean of 7.3 ± 1.0 SE) on diapiric frost boils, compared to frost boils without diapirs (4.4 ± 0.7), potentially reflecting the additional 20% nitrogen available in the subsurface of diapiric frost boils. Selective N acquisition from diapirs is a mechanism by which soil moisture indirectly enhances plant growth. Our work suggests that diapirs may be one mechanism contributing to Arctic greening by shrub expansion.

4.3 Introduction

Moisture and nutrient supply is limiting in arctic polar desert plant communities. Though we know both are important for plant community development, we lack a comprehensive understanding of the mechanisms by which moisture interacts with soil nutrients in periglacial environments to influence vegetation. In High Arctic deserts, increased soil moisture has been linked to plant community development but not to individual plant water status or

evapotranspiration, suggesting the importance of indirect moisture mechanisms (Gold and Bliss, 1995). We know that surficial moisture can indirectly increase nitrogen availability in polar desert plant communities by stimulating biological soil crust nitrogen fixation (Gold and Bliss, 1995; Dickson, 2000), and subsurface water can provide substantial N and P to plants in arctic ecosystems underlain by permafrost (Chapin et al., 1988). Since polar desert surface soils dry relatively quickly, limiting N fixation rates (Dickson, 2000), we postulated that the unique subsurface water interactions with frozen soil in High Arctic frost boils may provide an indirect moisture pathway to supply nutrients, specifically N, to plants.

In High Arctic deserts, the dominant subsurface water/soil interactions occur in frost boils—small (<3 m diameter) patches of barren or sparsely-vegetated soil formed by frost action (van Everdingen, 1998), common in many polar desert landscapes (Walker et al., 2004; Ugolini et al., 2006). Frost boils form as water migrates to a freezing front in the subsurface (i.e., the permafrost table), freezing and upheaving material with each successive thaw-freeze event (Appendix S2; Figs. S1 & S2). The churning convective action of annual freeze-thaw cycles upheaves frost boil centers and restricts plant establishment to the boil periphery (Cannone et al., 2004; Walker et al., 2008; Michaelson et al., 2012). A diapir (upward intrusion of low density material) may develop when moisture pools in a concave depression below the frost boil center and low-density, ice-rich soil develops at the base of the active layer (maximum depth of annual soil thaw). As overlying high-density material in the active layer sinks, low-density ice-rich material flows towards the soil surface by vertical heave (Swanson et al., 1999). A nutrient-rich soil horizon (Bhy) may form as cryoturbation buries SOM or meltwater leaches dissolved organic matter from the surface through the soil profile (Tye et al., 2005; Schaeffer et al., 2013), accumulating in the ice-rich concavity above the permafrost table (Cannone et al., 2004; Walker

et al., 2004; Boike et al., 2008) (Fig. 2.3). Any condition that facilitates greater accumulation of water at the base of the active layer (e.g., increased soil moisture and/or active layer deepening) or raises the permafrost table (e.g., insulation from dried organic material) may manifest the subsurface water effect of Gold and Bliss (1995) as a diapiric injection (Swanson et al., 1999).

Diapirs are subsurface nutrient-rich patches in an otherwise nutrient-poor polar desert environment, where the majority of High Arctic plants roots are restricted to the upper half of the active layer (Bell and Bliss, 1978; Iversen et al., 2015); thus it is unknown how arctic plant species may respond to diapirs. Many plants forage for nutrients by selectively proliferating roots into nutrient-rich patches (Hodge, 2004; Cahill and McNickle, 2011), but the possibility that High Arctic plant species preferentially utilize diapir horizons as an N source has not been investigated. Plants in polar deserts typically produce smaller and shallower root systems relative to other tundra vegetation types (Bell and Bliss, 1978; Iversen et al., 2015). Nevertheless, some polar desert plants such as *Dryas integrifolia* and *Saxifraga oppositifolia* can grow roots down to the permafrost layer (~ 40 cm) in High Arctic cryoturbated soils (Lamb et al., 2016). Preferential root foraging into this poorly understood pool of deep soil N might be critical to meeting the nutrient requirements of High Arctic plant species. Recent shrub proliferation in some areas has been linked to increased frequency of frost boils (Frost et al., 2013; Frost and Epstein, 2014). This proliferation may be facilitated by nutrient-rich diapir horizons resulting from increased active layer thaw depth (Swanson et al., 1999), which may become more common in a warmer, wetter arctic (Christensen et al., 2007; Zhang et al., 2012). With N availability a key constraint on arctic plant responses to projected warming (Hartley et al., 1999; Shaver et al., 2000), understanding interactions between diapirs and plant roots is central to understanding plant community responses to warming.

We hypothesized that a ubiquitous shrub in polar deserts, *Salix arctica* (Arctic willow) (Bliss and Matveyeva, 1992), may selectively forage for nitrogen in diapiric frost boils. We outlined several research objectives to test this: (1) assess how common diapir horizons are in a polar desert landscape using visible near-infrared reflectance (vis-NIR), (2) quantify the natural abundance of N held in these diapirs using $\delta^{15}N$, and (3) determine if *S. arctica* is exploiting the nitrogen in these horizons using an enriched $\delta^{15}N$ tracer, root biomass, and vegetation surveys. This study reports, for the first time, a comprehensive in-situ field investigation of how diapir horizons influence plant-soil nitrogen dynamics in these vast barren landscapes.

4.4 Materials and Methods

4.4.1 Field site

The field site is located on a mountain plateau five km southwest of Alexandra Fiord, Ellesmere Island, NU (78°51′N, 75°54′W). Plant communities here were previously described by Bliss et al. (1994). The site is differentiated into two distinctive soil types derived either from granitic or dolomitic parent material. The granitic area (650 m.a.s.l) is located on a gentle gradient (2 to 5°), immediately upslope of the dolomitic material (500 m.a.s.l) to the east, and downslope of a glacier (750 m.a.s.l.) to the northwest. Soil pH ranges from 5.5 on granitic material to 7.9 on the dolomitic material (Bliss et al., 1994). Poorly to well-developed frost boils are common across the site (Appendix C; Fig. C.1). Soils are Regosolic Turbic Cryosols with limited horizon development, low organic matter, and low plant-available N and P (Brummell et al., 2012). Thin cryptogamic bryophyte crusts (e.g., *Pogonatum denatum*), lichens (e.g., *Catallaria subnegans* and *Cladonia* spp.), and cyanobacteria (e.g., *Nostoc commune*) are common on moist surfaces (Bliss et al., 1994).

4.4.2 Diapir horizon abundance

Non-destructive detection of diapir horizons in polar deserts is challenging because there are no diagnostic surface features on frost boils indicative of a subsurface soil organic matter enriched diapiric Bhy horizon. To detect the presence of these Bhy horizons in frost boils, we used a custom field portable visible and near-infrared (vis-NIR) spectrophotometer (Veris Technologies, Salina, KS) equipped with a soil probe attachment and light source. vis-NIR is an efficient and non-destructive method to examine the spatial distribution of soil properties (Bellon-Maurel and McBratney, 2011; Soriano-Disla et al., 2014). Using this vis-NIR model we conducted an in situ survey of the depth distributions of soil organic carbon (SOC) in frost boils that would be indicative of a diapir Bhy horizon. The vis-NIR operates with two internal spectrometers (Ocean Optics and Hamamatsu) to record spectra between 350 and 2225 nm and outputs the spectral absorbance with 8-nm resolution. Practical field application of vis-NIR spectroscopy requires multivariate calibration models that relate the in situ spectra to laboratory measured SOC. Calibration models for SOC based on laboratory processed and in situ soils (refer to reviews Bellon-Maurel and McBratney, 2011; Soriano-Disla et al., 2014), as well as simulated in situ and field condition soils have yielded accurate prediction results (Morgan et al., 2009; Chapter 3 cited as Guy et al., 2015). Further, laboratory based and in situ models have been applied to successfully predict soil properties from spectra taken in situ (Viscarra Rossel et al., 2009).

In July-August 2013, we established 12 sampling blocks on granitic and five blocks on dolomitic parent material. These sampling blocks varied in size from 0.5 to 1.75 ha. Blocks delineated areas of differing topography to ensure we sampled frost boil features over the full range of slope, water availability, and microclimate on the landscape (Appendix C; Figs. C.2 & C.3). Within each block, frost boils were sampled using two randomly positioned perpendicular

transects (3–4 m in width and 17–50 m in length) that approximately intersected the block midpoint. An additional 55 frost boils were sampled opportunistically for a total of 560 frost boils.

In each direction from the power source located at block midpoint, along each arm of the perpendicular transects, the first five to eight frost boils encountered were sampled with the vis-NIR spectrophotometer. No more than 8 frost boils were sampled along each arm, though the number of frost boils sampled varied depending on frost boil size and distance between frost boils. The vis-NIR spectrophotometer probe was inserted into a 3.3 cm diameter pilot hole in the center of each frost boil and we collected spectra of the soil at two cm increments from the soil surface to ~ 35 cm or to the top of the permafrost layer, which is approximately 30-35 cm deep in July (Brummell et al., 2012). Soil spectra were analyzed in the field for SOC using a preliminary partial least squares regression model (Bjørsvik and Martens, 2008) relating SOC to soil spectra from field condition soil samples (n = 199) from Alexandra Fiord polar oasis, Patterson River and Okse Bay, Ellesmere Island, NU. This model was later updated using local samples per the methodology described in Guy et al. (2015) and final models are summarized below. Briefly, models were developed separately for dolomite and granite parent materials by optimizing the regional Ellesmere Island (n = 199) and local Dome (n = 41) samples included in the calibration model to reduce error and model bias. In the field, we visually inspected the SOC profiles of each frost boil and classified frost boils as diapir frost boils if they had a subsurface increase of at least 0.2 log % SOC - indicative of the diapir Bhy horizon, and non-diapir in the absence of any SOC peak.

4.4.3 Natural nitrogen abundance and distribution among frost boils

The flow of N through the soil and into the plant root upon uptake can be traced using naturally occurring $\delta^{15}N$ signatures and external additions of ^{15}N-enriched isotopic labels (Dawson et al., 2002; Bedard-Haughn et al., 2003). For the natural abundance $\delta^{15}N$ method, the fractionation

of ^{15}N through various abiotic and biotic processes results in characteristic ranges of ^{15}N:^{14}N ratios for different N sources. Thus, the $\delta^{15}N$ signature of a soil can be used to characterize whether, for instance, the soil N is primarily derived via N-fixation, plant litter, mycorrhizal interactions, or mineralization by microbes (Hobbie and Hobbie, 2006; Makarov, 2009; Craine et al., 2015). Further, the natural $\delta^{15}N$ signature of a plant can provide some insight as to where the plant might be sourcing N from the soil (Bedard-Haughn et al., 2003).

To examine the natural abundance of nitrogen we sampled 24 non-diapir and diapir frost boils where we collected both *S. arctica* plant tissues and soil samples from soil pits. These sites were also used to investigate the subsurface distribution of SOC and root biomass, described in the section below. We collected leaf and aboveground stem tissue, and gently excavated the attached belowground stem/root tissue from three individual *S. arctica* plants located on each frost boil. Small soil samples were taken from a soil pit face at 5 cm depth increments from 0-35 cm. We used maximums and minimums from SOC concentration profiles of each frost boil (predicted from the vis-NIR data) to select three soil samples from each pit representing three different SOC sources found in frost boils: 1) surface SOC, 2) high concentrations of subsurface SOC, and 3) low concentrations of subsurface SOC.

Soil and vegetation samples were analyzed for $\delta^{15}N$, total N concentration, and total C concentration on a thermal conversion/elemental analyzer isotope ratio mass spectrometer (TC/EA-IRMS ThermoFinnigan Delta Plus). The N isotopic composition was expressed as $\delta^{15}N$ in parts per thousand (‰) (Chalk et al., 2015). Prior to isotopic analysis, vegetation samples were dried at 40°C for 24 hours and soil samples were separated from bulk root material and air dried (Brearley, 2009). Dried samples were ground using a ball mill, and 2-4 mg of vegetation sample

and 60-80 mg of soil sample packed into tin capsules. We determined gravimetric soil moisture content (θ_d) by drying 1 g of soil at 100°C for 24 h.

4.4.4 Diapir horizons as a potential nitrogen source for plants

4.4.4.1 Vegetation aboveground cover

To examine how vegetation cover and frost boil geomorphology varied across the polar desert landscape and between non-diapir and diapir frost boils, we recorded general visual descriptions of frost boils and inter-boil areas in each block (i.e., frost boil and inter-boil size, orientation, and surface connectivity). We surveyed relative abundance of plant species on 52 frost boils across the 12 granitic blocks by visual cover estimates (Mueller-Dombois and Ellenberg, 1974). Vegetation cover was assessed in a 0.75 x 0.75 m plot containing a grid of nine contiguous 0.25 x 0.25 m (0.0625 m^2) subplots. The grid was randomly positioned on the vegetated edge and extended to the frost boil center. We recorded the cover of vascular plants, lichens and bryophytes, and physical descriptors such as rock, gravel, litter, and bare ground in each subplot.

4.4.4.2 Distribution of subsurface SOC and root biomass

To visualize the fine-scale distribution of SOC and root biomass on frost boils, we sampled 12 diapir and 12 non-diapir frost boils across our sampling blocks using the vis-NIR spectrophotometer and soil cores. Within each frost boil, the vis-NIR probe was inserted into the center of each of the nine vegetation subplots and soil spectra collected in 2 cm depth increments from the surface to permafrost depth ($n \approx 18$/subplot). To determine root biomass we excavated a soil pit at the center of each frost boil and collected two 100 cm^3 soil cores using 5.3 x 5.0 cm soil sampling rings at each of the 0-10, 10-20, and 20-30 cm depth increments. We manually picked all roots from each soil core and determined wet root biomass; the roots were not dried as they will be processed by molecular methods for another study. We did not differentiate between live and

dead roots as we were not confident in our ability to do so accurately. While dead roots can comprise <5% to >85% of belowground biomass in Arctic systems (Iversen et al., 2015), the depth distribution of dead roots is similar, yet more uniform, compared to that of live roots (Dennis, 1977). Thus, we expected the combined distribution of live and dead roots to closely reflect the distribution of live roots. Eleven missing samples were not processed.

4.4.4.3 Soil to plant nitrogen tracers

Nutrient source mixing, fractionations between mycorrhizae and the plant, or internal fractionations within the plant can limit the inferences possible from natural abundance methods (Evans, 2001; Robinson, 2001; Kalcsits et al., 2014). To overcome this, we used ^{15}N-enriched tracers to track soil-to-plant nitrogen flow from nutrient-rich soil patches to plant above- and belowground biomass (Templer et al., 2012). Three blocks on each of the dolomitic and granitic parent material were selected for the enriched isotope study. In each block, one non-diapir and one diapir frost boil (n=12) were injected with ^{15}N-labelled ammonium nitrate solution ($^{15}NH_4{}^{15}NO_3$, 98 at.% ^{15}N) immediately following snowmelt (between 12–19 July 2013). Snowmelt was delayed by ca. 1 to 2 weeks in 2013 due to low spring temperatures, and unusually high winter snowpack and saturated soils. A 648 cm^2 injection grid with 72 injection points spaced 3 cm apart was placed at the centre of each frost boil. At each injection point, we injected 1 ml of the labeled N solution into the soil to a frost boil specific depth using a syringe with a 30 cm needle. The injection depth for each frost boil corresponded to the depth of maximum SOC in the diapir Bhy horizon and highest subsurface SOC at a similar depth in non-diapir frost boils, as detected by the vis-NIR spectrophotometer (Table 4.1). Injection depths were similar between diapir and non-diapir frost boils to ensure any plant uptake of the labelled solution was due to the inherent differences in the biology (rooting depth and microbial activity) and soil properties (bulk density, porosity, and/or

water content) between the frost boils, and not related to the injection depth. A total of 105 mg of $^{15}NH_4{}^{15}NO_3$ was added to each grid, equalling 238 g N m^{-2}. The amount of $^{15}NH_4{}^{15}NO_3$ added equalled 16.5% of K_2SO_4 extractable NH_4-N and NO_3-N in the soil solution (Grogan et al., 2004) and was calculated from measurements 0 to 30 cm above permafrost at Dome site (Brummell et al., 2012). Given the small total N pool in polar deserts (Brummell et al., 2012) and the assumption that this additional tracer is behaving like native nitrogen, adding this sizable fraction of tracer to the available pool should minimize any dilution effects caused by differences in N pool sizes between diapir and non-diapir frost boils. After a four-week incubation period, leaf, aboveground stem, and belowground stem/root tissue were collected from the three *S. arctica* plants closest to the injection grid (n=9) on each frost boil. To assess ^{15}N mixing and N cycling rate differences we destructively sampled 32 other frost boils with and without diapirs at the depth of maximum SOC (for methodology see Appendix B; Table B.3).

Vegetation samples were prepared for isotopic analysis as described above, with the exception that root tissue was rinsed prior to drying with calcium-rich water to remove any enriched label adhered to outer tissue. Enriched values were expressed as atomic percentages of ^{15}N (at.% ^{15}N)

4.4.5 Data analyses

4.4.5.1 Diapir horizon abundance

Spectral samples collected from dolomitic and granitic sites were re-analyzed separately for carbon using partial least squares regression (PLSR) models that were optimized to predict SOC at those sites as described in (Guy et al., 2015). As recommended by Guerrero et al. (2010, 2014), we tested which samples from regional and local arctic sites to include in the models and whether weighting samples from our local field sites improved model predictions (Guy et al.,

2015). The final model for granitic sites contained 89 regional arctic samples and 15 samples from the granitic site (R^2= 0.75, RMSE = 0.11% SOC). The final model for dolomitic sites contained 102 regional arctic samples, 15 samples from granitic sites, and 15 samples from dolomitic sites, which were given 15 times more weight in the calibration model (R^2=0.74, RMSE= 0.85% SOC). Classification of diapir and non-diapir frost boils was revised to include any subsurface carbon peak greater than could be explained by random variation in the PLSR model predictions. We calculated the prevalence of diapirs as the proportion of frost boils with diapir Bhy horizons to the total number of frost boils sampled to a minimum depth of 15 cm (n=560). We used Pearson's chi-squared tests to test whether the presence of diapir horizons (Diapir = "Y" or "N") differed among the experimental blocks, between dolomitic (n=5) and granitic (n=12) substrates, and among vegetation groups (described below).

Table 4.1 ^{15}N enriched solution injection depth into non-diapir (n=6) and diapir (n=6) frost boils in dolomitic and granitic sampling blocks.

Desert	Block	Depth of Injection (cm)	
		Non Diapir†	Diapir‡
Dolomite	D2	13.5	13.5
	D3	23.5	25.5
	D5	21.5	21.5
Granite	G1	20.0	27.5
	G2	20.0	20.0
	G4	27.5	20.0

† Highest subsurface SOC at a depth similar to diapir Bhy horizon found in diapir frost boil
‡ Depth of maximum SOC in the diapir Bhy horizon

4.4.5.2 Natural nitrogen abundance and distribution among frost boils

Statistical analyses were performed using SAS/STAT® software (Version 9.4, SAS Institute, Cary, NC, USA). Soil parameters total C, total N, θ_d, and $\delta^{15}N$ were analyzed for normality using Shapiro-Wilk's test; non-normally distributed data were transformed using Box-Cox transformations. Mixed effects models were implemented using the MIXED procedure in a randomized complete block design with SOC source ("surface", "high", or "low"), frost boil type ("non-diapir" or "diapir"), and their interaction as fixed factors and block as a random effect. Effects were considered statistically significant at $P < 0.05$ and Fisher's Least Significant Difference (LSD) method was used to compare means when a significant effect was found.

We used mixed effects models to compare vegetative cover and average soil properties between two groups of blocks that varied in the surface cover of vegetation (explained below and described in the results) and frost boil types using the 12 non-diapir and 12 diapir frost boils in the granitic polar desert. Models were fit using the lme4 package in R version 3.2.2 (Bates et al., 2015; R Core Development Team, 2016). Parameters including soil properties (total C, total N, and θ_d) and vegetation cover (as above) were modeled with surface cover group ("I" or "II"), frost boil type ("non-diapir" or "diapir"), and their interaction as fixed factors and block as a random effect. The grouping of frost boils is described below, but briefly, Group I frost boils had greater bryophyte cover, compared with Group II frost boils which had more bare ground and lichen cover.

4.4.5.3 Diapir horizons as a potential nitrogen source for plants

4.4.5.3.1 Vegetation aboveground cover

We examined variation in surface cover across the site using Ward's minimum variance clustering and principal component analysis (PCA) of the average block cover of vascular plants,

lichens, bryophytes, litter, bare ground, rock, and gravel. We chord-distance transformed the surface cover data prior to analyses, and the optimum number of clusters was selected from silhouette width graphs (Borcard et al., 2011). We then used analysis of variance (ANOVA) to test for surface cover differences among surface cover groups. Models were fit using the aov function in R with surface cover on frost boils (n = 52) as the response variable and surface cover group as the main effect. Clustering and PCA analysis were run using the *vegan* package for R version 3.2.2 (Oksanen et al., 2016; R Core Development Team, 2016).

4.4.5.3.2 Distribution of subsurface SOC and root biomass

We visually examined the fine-scale distribution of SOC within frost boils for conspicuous peaks in SOC. Due to the heterogeneous lateral and vertical distribution of SOC distinct subsurface peaks/pockets of SOC become masked when looking at the average of all non-diapir/diapir pairs; thus one representative non-diapir/diapir frost boil pair was chosen to illustrate the subsurface SOC distribution detected by vis-NIR spectroscopy. Kriging interpolation among sampling points was used to produce subsurface soil organic carbon (SOC) profiles using ArcMap (ESRI Inc., Redlands, CA). Root biomass was log transformed to meet assumptions of normality and mixed effects models were implemented using the MIXED procedure in a randomized complete block design with depth increment ("0 to 10", "10 to 20", or "20 to 30"), frost boil type ("non-diapir" or "diapir"), and their interaction as fixed factors and block as a random effect (SAS/STAT® Version 9.4; SAS Institute, Cary, NC, USA).

4.4.5.3.3 Soil to plant nitrogen tracers

To determine the source of nitrogen uptake by *S. arctica* from individual SOC sources within non-diapir and diapir frost boils, simple linear regression was performed between the natural abundance of soil $\delta^{15}N$ of SOC sources and leaf $\delta^{15}N$ separately within frost boil types

using PROC REG (SAS/STAT® Version 9.4; SAS Institute, Cary, NC, USA). Regression slopes were tested for significance using Student's *t* tests.

Enriched isotope at.%^{15}N in vegetation was analyzed as a generalized linear mixed model in a randomized complete block design treatment design using the GLIMMIX procedure and applying a gamma distribution using the LINK function. Vegetation tissue ("leaf", "aboveground stem", and "belowground stem/root"), frost boil type, and their interaction were tested as fixed factors and block as a random effect. The LSD method was used to compare means when a significant effect was found.

4.5 Results

4.5.1 How common are diapirs in polar desert frost boils?

We detected peaks of subsurface soil organic carbon indicative of the diapir Bhy horizon in 174 of 560 (31%) frost boils sampled across dolomite and granitic sites (Appendix C; Fig. C.3). Diapirs were equally abundant on dolomitic and granitic substrates, ($df = 1$, $n = 560$, $\chi^2 = 1.48$, $p = 0.22$), but varied among sampling blocks ($df = 16$, $n = 560$, $\chi^2 = 37.93$, $p < 0.01$).

Due to logistical constraints (i.e., very late snowmelt), we were unable to complete detailed vegetation work in the dolomitic polar desert and all vegetation data reflects data from the granitic polar desert. Diapirs were more abundant in blocks with greater bryophyte cover. We grouped experimental blocks into two groups based on surface cover representing contrasting vegetation cover and frost boil geomorphology (Appendix B; Table B.1). We detected diapir horizons within 36% of Group I frost boils (greater bryophyte cover), compared with 16% of group II (more bare ground and lichen cover) ($df = 1$, $n = 345$, $\chi^2 = 13.93$, $p < 0.01$). Group I had well-heaved frost boils and well-connected medium to large rocky inter-boil areas. In contrast, Group II frost boils

were poorly sorted with weakly connected small to medium rocky inter-boil areas. Percent cover of *S. arctica* did not differ between these groups ($F_{1,50} = 1.5$, $p = 0.23$).

4.5.2 Is nitrogen more abundant in diapiric frost boils?

Total soil C and N concentrations differed between diapir and non-diapir frost boils, with 6.9% higher average soil C and 11.3 to 20.4% greater soil N in diapir frost boils, though the differences based on our selected sampled were not significant ($P > 0.05$) (Table 4.3). The concentration of total soil C ($p = 0.03$), but not total N ($p = 0.06$), differed between soil SOC sources with the highest C at the frost boil surface followed by the diapir Bhy horizon, which we termed as a high organic carbon layer (Table 4.3). Low soil nutrient levels emphasized the harshness of polar desert landscapes: C and N within frost boils averaged 2.9 ± 0.2 g and 0.26 ± 0.02 g N kg^{-1} dry soil, respectively. Additionally, there were no differences in gravimetric soil moisture content (θ_d) between frost boil types and SOC sources, although soils with low SOC sources consistently had higher soil moisture (Table 4.3).

4.5.3 Are there more *Salix arctica* shrubs on diapiric frost boils?

On the granitic site, there was 50% greater *S. arctica* cover ($p < 0.01$) and double the leaf litter ($p < 0.02$) on diapirs compared to non-diapirs for Group II (high lichen cover) frost boils (Table 4.2). Group I (high bryophyte cover) frost boils also had more *S. arctica* and litter cover on diapiric relative to non-diapir boils, but these differences were much less pronounced ($p > 0.05$) than for Group II frost boils. *S. arctica* was the dominant vascular species in both surface cover groups with 7–8% cover relative to 15 other species including *Dryas integrifolia* and *Cassiope tetragona* each with < 1% average cover (Appendix B; Table B.1).

Table 4.2 Plant and soil characteristics of non-diapir (n=12) and diapir (n=12) frost boils on granitic parent material. Values are means ± SE of each frost boil type within surface cover groups.

Frost boil type	Surface cover group†	Total plant‡	*S. arctica*§ (% cover)	Litter§	Soil total N¶ (g kg^{-1})	Soil total C¶	θ_d¶ (kg kg^{-1})
Non-diapir	I	66.6 ± 4.0	7.8 ± 0.9	13.6 ± 1.2	0.25 ± 0.01	3.0 ± 0.7	0.096 ± 0.004
	II	67.8 ± 5.1	4.4 ± 0.7	8.1 ± 0.9	0.22 ± 0.01	2.3 ± 0.1	0.094 ± 0.008
Diapir	I	52.2 ±5.4	8.5 ± 2.0	17.8 ± 3.6	0.28 ± 0.05	3.1 ± 0.6	0.094 ± 0.008
	II	51.0 ± 4.5	7.3 ± 1.0	16.8 ± 4.0	0.27 ± 0.05	2.6 ± 0.5	0.100 ± 0.009
Summary of frost boil type							
Non-diapir		61.8 ± 1.8	6.7 ± 0.8	11.8 ± 1.1	0.24 ± 0.01	2.8 ± 0.5	0.096 ± 0.003
Diapir		62.2 ± 3.9	8.1 ± 1.4	17.5 ± 2.7	0.27 ± 0.04	3.0 ± 0.4	0.095 ± 0.006
Summary statistics of mixed effects models with frost boil type as a main effect							
Frost Boil Type		$F_{[1,11]}$=0.01, p=0.19	$F_{[1,11]}$=1.13, p=0.31	$F_{[1,11]}$=3.79, p=0.08	$F_{[1,11]}$=0.52, p=0.49	$F_{[1,11]}$=0.04, p=0.85	$F_{[1,11]}$=0.04, p=0.85

†Surface cover groups based on similarities in surface cover features according to Table B.1.
‡Total plant refers to vascular plant, bryophyte, and lichen cover.
§Mean ± standard error were calculated based on mean % surface cover on frost boils.
¶Mean soil property values for frost boils were calculated from four different depths. θ_d = gravimetric soil moisture content.

Table 4.3 Soil characteristics of frost boils on granitic parent material according to soil organic carbon (SOC) layers. Values are means ± SE of soil cores from SOC sources within non-diapir (*n*=12) and diapir (*n*=12) frost boils.

Frost boil type	SOC source †	Total soil C (g kg^{-1})	Total soil N	θ_d (kg kg^{-1})
Non-diapir	Surface‡	3.1 ± 0.5	0.27 ± 0.03	0.090 ± 0.008
	High§	3.0 ± 0.7	0.25 ± 0.03	0.095 ± 0.005
	Low‖	2.6 ± 0.4	0.23 ± 0.01	0.104 ± 0.007
Diapir	Surface‡	4.5 ± 1.1	0.37 ± 0.08	0.093 ± 0.006
	High/Bhy§	3.2 ± 0.8	0.30 ± 0.07	0.089 ± 0.007
	Low‖	2.3 ± 0.3	0.23 ± 0.02	0.098 ± 0.005

†SOC sources selected from the frost boil SOC profile predicted using vis-NIR spectrophotometry.
‡Surface SOC sampled from 0 to 5 cm depth and represents inputs primarily from litter fall and N_2 fixation by organisms in the soil crust.
§Represents the highest subsurface SOC source in a non-diapir frost boil or a max SOC of a Bhy horizon in a diapir frost boil.
‖Low SOC represents the lowest SOC source in the soil profile.

4.5.4. Are roots associated with the diapiric Bhy horizon?

Deep (20-30 cm) root biomass was greater in diapir compared with non-diapir frost boils, with 131 ± 35 (SE) mg root 100 cm^{-3} soil in diapirs compared to 58 ± 14 mg root 100 cm^{-3} soil in non-diapir frost boils ($P < 0.05$) (Fig. 4.1), though there were only relatively small differences in total plant cover (Table 4.2). Overall root biomass did not differ between non-diapir and diapir frost boils ($t_{124} = 1.377$, p = 0.171) and the majority of roots were found in the shallow soil layers within all frost boils. The upper soil depths had similar root biomass between diapir and non-diapir frost boils. In the top 10 cm, there were 206 ± 42 mg root 100 cm^{-3} soil for diapirs and 213 ± 16 mg root 100 cm^{-3} soil in non-diapir frost boils. These root distributions corresponded closely with the organic carbon distribution that often peaked 20 to 30 cm below ground in diapir frost boils and varied between 0 and 10 g SOC kg^{-1} dry soil (non-diapir: adjR^2 = 0.103, $F_{1,65}$ = 8.575, p = 0.004; diapir: adjR^2 = 0.069, $F_{1,55}$ = 5.127, p = 0.028*;* Fig. 4.1). Non-diapir frost boils often had more uniformly distributed SOC, with no discernible SOC peak.

4.5.5 Are plant and diapiric Bhy nitrogen signatures linked?

Natural ^{15}N abundance differed among (p < 0.01) soil organic carbon sources but not between frost boil types. Surface and high organic carbon sources tended to be $\delta^{15}N$ depleted and low organic carbon sources were $\delta^{15}N$ enriched in diapir frost boils relative to non-diapir frost boils, although these differences were not significant statistically (Appendix C; Fig. C.4). In diapir frost boils, natural abundance $\delta^{15}N$ of *S. arctica* foliage was correlated with soil $\delta^{15}N$ in the diapir Bhy ($P < 0.05$, $r^2 = 0.62$) and low SOC horizons *(*$P < 0.05$, $r^2 = 0.59$) (Fig. 4.2), despite greater total N at the soil surface compared to the Bhy diapir horizon (Table 4.3). In contrast, non-diapir frost boil plant $\delta^{15}N$ was linked to surface soil $\delta^{15}N$ ($P < 0.05$, $r^2 = 0.45$) but not to deeper SOC horizons (Appendix B; Table B.2).

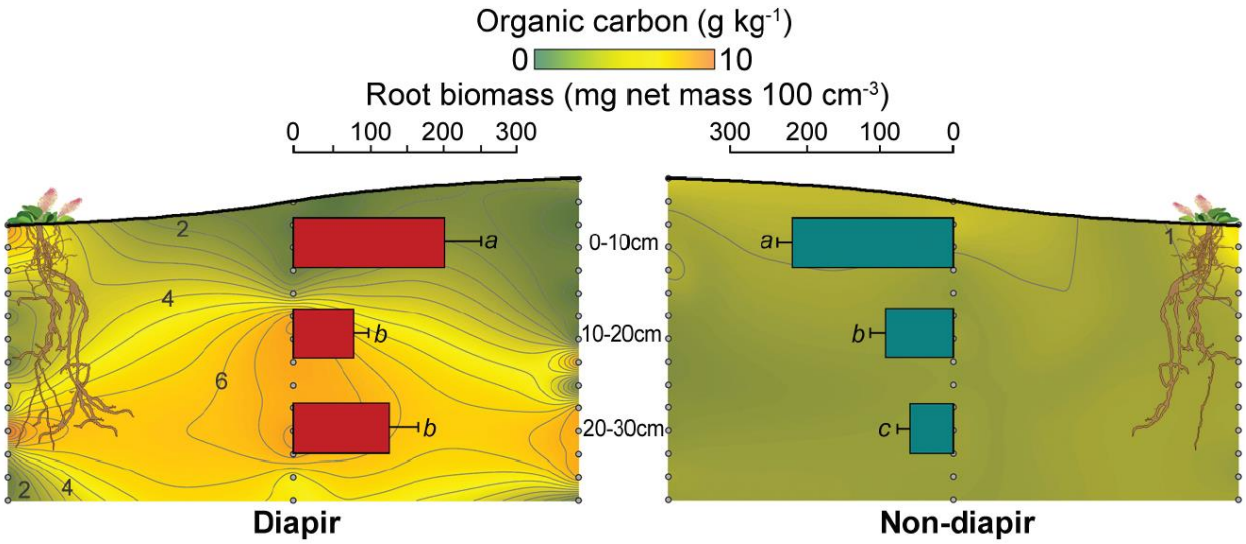

Fig. 4.1 Mean root biomass (mg wet mass 100 cm^{-3}) ± standard error at three depths in diapir (red) and non-diapir (blue) frost boils. Kriging interpolation was used to produce subsurface organic carbon (OC) profiles along a half cross-section of each frost boil. Contours represent concentrations of organic carbon at 0.5 g SOC kg^{-1} dry soil intervals. Elevated OC values indicate diapir presence. *Salix* roots are artistic rendering to complement root biomass patterns (inset bar graphs). Letters represent significant differences between biomass means (LSD, $p < 0.05$).

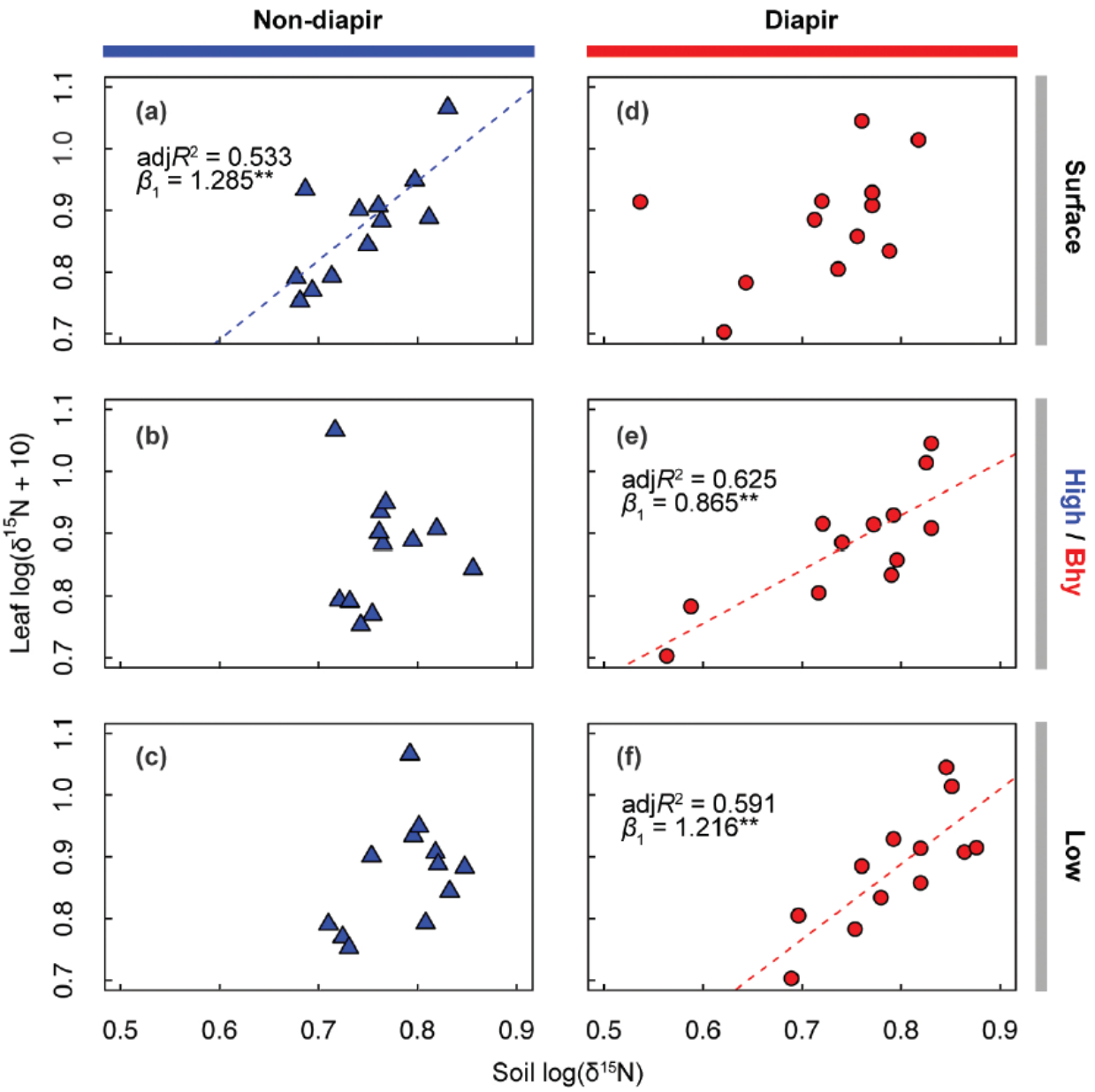

Fig. 4.2 Natural abundance $\delta^{15}N$ in *S. arctica* leaves is linked to soil $\delta^{15}N$ in polar desert soil horizons. Carbon sources in soil horizons were classified as: (a,d) ground surface, (b,e) high (blue) or Bhy (red), or (c,f) low in non-diapir (left in blue triangles) and diapir (right in red circles) frost boils. Adjusted R^2 and slope (β_1) values are reported for significant regressions ($p < 0.05$) and non-significant regressions are indicated by the absence of a line.

4.5.6 Do plants selectively take up nitrogen from the diapir Bhy horizon?

When ^{15}N-enriched nitrogen was injected into the Bhy horizon (or high subsurface SOC horizon in a non-diapir frost boil), the concentration of ^{15}N in *S. arctica* tissue was substantially more in plants grown on diapir frost boils compared to non-diapir frost boils (Fig. 4.3). At the end of the growing season, average plant at.%^{15}N was 2.5 times higher (2.7 ± 0.7 at.%^{15}N) on diapirs compared to 1.1 ± 0.1 at.%^{15}N on non-diapir frost boils. *S. arctica* had the highest concentration of ^{15}N in leaf tissue for both frost boil types, suggesting that ^{15}N is actively transferred from the roots to support new leaf growth. We did not clip all of the biomass from each frost boil to avoid killing the slowly growing plants, and thus could not estimate total recovery of injected ^{15}N by plants. We did however, destructively sample other diapirs to assess ^{15}N mixing and N cycling rate differences between frost boils with and without diapirs at the depth of maximum SOC. There were no significant differences in gross mineralization ($P > 0.06$) or gross nitrification ($P > 0.07$) rates between diapir and non-diapir frost boils for July 12-22 (start date of injection experiment) (Appendix B; Table B.3).

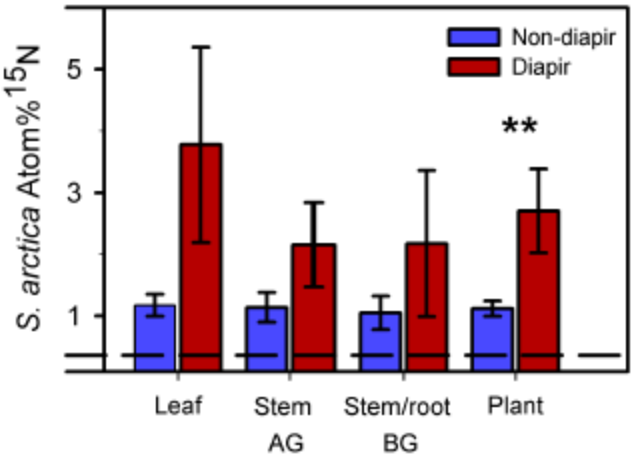

Fig. 4.3 Mean concentration of enriched isotope at.%^{15}N ± SE of different *Salix arctica* tissues growing on frost boils with enriched nitrogen injected into diapir (red) or non-diapir (blue) soil horizons. The black dashed line indicates the natural abundance level of plant at.%^{15}N of 0.366. There was a significant difference between plant tissue means of non-diapir and diapir frost boils ($P < 0.01$; indicated by **).

4.6 Discussion

In the early 1990's, Gold and Bliss (1995) made an unusual finding: moisture was important in the polar deserts of Devon Island, NU, but not through the obvious mechanism of improving plant water status. Here, we have provided a potential mechanism to answer the question posed by Gold and Bliss over two decades ago. Subsurface water in polar deserts is important because of its role in diapir formation, and diapirs are an important nutrient source for the dominant polar desert plant, *S. arctica*, contributing to increased *S. arctica* cover.

4.6.1 Plant response to diapir nutrient patches

Despite having relatively little change in above ground vascular plant cover, polar desert plants had greater root biomass within diapir horizons and actively took up labeled N from these nutrient patches (more ^{15}N was used from diapirs relative to non-diapir frost boils with no Bhy horizon). In the absence of diapir horizons, the δ^{15}N signature of plants suggests that they primarily

relied on N sources at the soil surface. Thus, it appears that diapir horizons provide a unique and previously unknown source of N for polar desert plants.

Increased N availability in diapirs is important because like many plants, *Salix* spp. respond strongly to increased N by increasing cover, leaf density, leaf N concentration, and photosynthetic rate (Baddeley et al., 1994; Arens et al., 2008; Leffler and Welker, 2013). Plants commonly forage for nutrients from spatially and temporally variable patches (McNickle et al., 2009; Cahill and McNickle, 2011) by deploying fine roots and mycorrhizal hyphae, or increasing uptake rates (Hodge, 2004; Sullivan et al., 2007). Although root elongation is slow in polar desert plants, many High Arctic species root to depths of 15 to 40 cm (Iversen et al., 2015; Lamb et al., 2016), well within the depth range of diapir horizons (10 to 35 cm). The 2.5-fold increase in at.%^{15}N and greater root biomass within diapir horizons demonstrates that *S. arctica* is able to actively access these N-rich patches.

4.6.2 Why might plants prefer diapiric soil organic matter?

Based on our enrichment experiment, ^{15}N acquired from the diapir horizon concentrated in leaves prior to leaf senescence in mid-August. There was between 11 to 20% more nitrogen present in diapir frost boils compared to non-diapir frost boils. Though not *statistically* significant, we argue diapir N may represent an *ecologically* significant nutrient source for *S. arctica*. Despite higher N concentration in the surface soil, the δ^{15}N signature of *S. arctica* indicates preference for diapir nutrients which may be due to the higher concentration of N in diapirs as well as the timing of N release relative to plant demand. N_2-fixation rates by biological soil crusts in polar deserts can be 1.5 to 2-fold higher than in low-latitude arctic systems (Stewart et al., 2011b), with the majority of available N at the soil surface accumulating within a few days of snowmelt (Dickson, 2000; Schmidt and Lipson, 2004; Buckeridge and Grogan, 2010). Early season N uptake is used

for leaf production (Tolvanen and Henry, 2001), however, a high proportion of this early season N may be lost through leaching (Tye et al., 2005; Yano et al., 2010; Schaeffer et al., 2013) and microbial processes (Ma et al., 2007; Brummell et al., 2014). Due to these limitations in surface N availability, *S. arctica* may rely on subsurface N patches to satisfy midseason demands such as photosynthetic system maintenance, stem growth and/or leaf storage (Maessen et al., 1983; Baddeley et al., 1994; Campioli et al., 2012), which peak in early to late July (Tolvanen and Henry, 2001; Arndal et al., 2009).

The positive correlation between the natural abundance $\delta^{15}N$ of *S. arctica* and $\delta^{15}N$ signature of low SOC sources in diapir frost boils suggests that plants may also place substantial amounts of active root biomass outside of diapir horizons. While these low SOC areas of the soil profile contained less total N than the surface and diapir horizons, these soils were often deeper in the active layer and consistently had higher moisture within frost boils. Moisture can limit *S. arctica* growth in polar deserts (Gold and Bliss, 1995), though it is thought to be less important than N limitation (Robinson et al., 1998; Leffler and Welker, 2013). The foraging responses of plants to moisture patches is not well understood (Cahill and McNickle, 2011), however, our observation suggests *S. arctica* may actively forage for moisture as well as N in these deserts.

4.6.3 Distribution and availability of nitrogen in diapirs

Diapirs were a common feature of frost boils in these two polar deserts and were strongly linked to geomorphological features. In wetter and more active landscapes, diapirs were twice as abundant relative to drier, more static landscapes. Excavations of frost boils indicate that the diapir Bhy horizon typically forms below the center of the frost boil as a spatially variable plume several decimetres in thickness (Swanson et al., 1999; Ugolini et al., 2006). Our non-destructive survey of a large number (n = 560) of frost boils at this site supports these estimates with observed Bhy

thickness between 5 to 15 cm and the carbon peak typically occurring between 10 and 30 cm from the soil surface. Compared to other subsurface high-N sources (usually ≤ 5 cm in thickness), diapir horizons were relatively fertile patches in the soil profile. Thus, although average N was similar between diapir and non-diapir frost boils, the size, location, and concentration of N-rich patches differed, and plants actively responded to this difference.

Our $\delta^{15}N$ natural abundance data suggest that the $\delta^{15}N$ signature of the diapir Bhy nutrient patch is intermediate between the $\delta^{15}N$ signatures of the surface and low SOC subsurface mineral soils, suggesting that it could be a mixture of these two materials (Robinson, 2001). Soil surface N derived from litter decomposition and N_2-fixation by bryophyte-cyanobacterial associations (Stewart et al., 2011b) likely leaches through the soil profile (Tye et al., 2005; Schaeffer et al., 2013) and accumulates above the permafrost table in a concavity below the frost boil center (Cannone et al., 2004; Walker et al., 2004; Boike et al., 2008). As the active layer thaws, subsurface soil and permafrost N mixes with this surface leachate to form a slurry; given the right density differential the slurry is then ejected into the upper soil horizons to form a diapir. This sequence results in a wide $\delta^{15}N$ range within the diapir Bhy because surface N is ^{15}N-depleted (Högberg et al., 1996; Rhoades et al., 2008; Stewart et al., 2011a), whereas N released from SOM decomposition and N mineralization have $\delta^{15}N$-enriched signatures. Once ejected into the upper soil horizons, $\delta^{15}N$ will continue to enrich with SOM mineralization (Biasi et al., 2005; Mackelprang et al., 2011; Mueller et al., 2015). This variability in the diapir $\delta^{15}N$ signature is likely the reason for the lack of statistically significant differences in the soil $\delta^{15}N$ despite clear differences in the links between plant and soil $\delta^{15}N$.

4.6.4 Diapirism and Arctic greening: are the two linked?

Conditions favourable for frost boil development are expected to increase across the Arctic (Callaghan et al., 2005; Walker et al., 2008; Klaus et al., 2013) and increased moisture and temperature will likely increase the magnitude of diapir formation (Swanson et al., 1999). While there is significant uncertainty in soil responses to climate change in the Arctic (Lamb et al., 2011), high Arctic plant communities dominated by deciduous shrubs such as *S. arctica* can respond rapidly to environmental changes (Walker et al., 2006; Hudson et al., 2011). Globally, the high and low Arctic appear to be greening as shrubs respond to a warmer climate (Beck and Goetz, 2011; Walker et al., 2012; Myers-Smith et al., 2015). Diapirism is not limited to polar deserts but can also occur, and may be more common, in other regions of continuous permafrost (Swanson et al., 1999). Here, we have described a mechanism by which diapirs increase nutrient supply to a dominant shrub species. How common this mechanism is across other Arctic landscapes and species is unknown. Yet our work suggests that diapirs may be one mechanism facilitating the greening of Arctic vegetation, and may partially contribute to recent trends of increased plant cover across the Arctic.

5. SOIL ORGANIC CARBON IN TWO HIGH ARCTIC POLAR SEMI-DESERTS USING A VIS-NIR PROBE

5.1 Preface

In Chapter 3, we demonstrated that vis-NIR models based on field condition soils are suitable for the prediction of SOC in High Arctic barren environments and in Chapter 4 we used a field portable vis-NIR spectrophotometer to detect subsurface enrichments of SOC indicative of diapir Bhy horizons in the center of frost boils. Moreover, on a broad scale the frequency of these enrichments were linked to broad differences in vegetation community and a nitrogen tracing study demonstrated that the dominant deciduous shrub *Salix arctica* is able to access N from subsurface sources when these patches are present. In this chapter, we characterize the quantity and distribution SOC in the frost boils of two High Arctic polar semi-deserts.

5.2 Abstract

High Arctic soil organic carbon (SOC) is an important component in the global C cycle, yet there is considerable uncertainty in the estimates for the polar deserts and semi-deserts that dominate these regions. We postulated that within some patterned ground features, such frost boils, subsurface patches of SOC resulting from diapirism were contributing to previously unaccounted for subsurface SOC pools. This study used a field portable visible and near-infrared spectrophotometer to look at the quantity, distribution, and spatial variation of SOC in 560 polar semi-deserts frost boils at two Canadian high Arctic sites. Specifically, we investigated how subsurface pockets of SOC in frost boils resulting from diapirism contribute to SOC storage in these environments. Our best estimate of SOC stored in the active layer of High Arctic polar semi-deserts is 8.14 ± 0.45 Pg SOC. Though total soil organic carbon content did not differ between the dolomite and granite polar semi-deserts, SOC was clearly being stored differently. The dolomitic site had greater SOC content below 10 cm ($p = 0.01$) reflecting more common occurrence of subsurface SOC patches (46% of frost boils) compared to the granitic site (29.5%; $P < 0.01$). When subsurface patches of SOC were detected in frost boils they contained nearly double the SOCC of frost boils without subsurface patches, with 11.4 ± 6.3 kg SOC m^{-2} compared to 6.4 ± 3.6 kg SOC m^{-2} respectively ($p < 0.01$), and on average 40% of SOC was located within patch. Despite diapiric frost boils representing only 35% of all frost boils, these findings suggest that frost boils with diapiric patches represent an important, yet heterogenous, pool of SOC in polar semi-deserts.

5.3 Introduction

Barren environments dominate the High Arctic (705 000 km^2; CAVM Team, 2003; Walker et al., 2005), however these areas are underrepresented in the databases used to quantify Arctic soil organic carbon (SOC) pools (Ping et al., 2008; Tarnocai et al., 2009; Hugelius et al., 2014).

Given that northern circumpolar regions are warming more rapidly than the global average, it is imperative that we understand the size and distribution of these High Arctic SOC pools for global carbon-climate models (Schuur et al., 2008, 2015; IPCC, 2013). These cold dry barren environments are thought to contain little SOC relative to other ecosystems in the permafrost region due to limited soil development; nevertheless the large area covered by these environments makes these SOC stores globally important. High Arctic soils are estimated to contain 34 ± 16 Pg SOC in the top 0-3 m of soils, or 3% of the 1035 ± 150 Pg SOC found in permafrost regions (Hugelius et al., 2014). SOC estimates for these regions have a large degree of uncertainty (Ping et al., 2008; Hugelius et al., 2014), which can in part be attributed to the heterogeneous nature of these permafrost affected soils and the limited number of studies available with sufficient numbers of pedons to capture the fine-scale spatial variation required for upscaling SOC estimates (Banerjee et al., 2011; Mishra and Riley, 2012; Campeau et al., 2014).

In High Arctic semi-deserts, complex interactions between vegetation, water/ice and soil redistributes SOC in the soil profile of small (< 3 m) patterned ground features called frost boils (Washburn, 1956; Walker et al., 2004, 2008; Michaelson et al., 2012). Frost boils are common in these landscapes (Bliss et al., 1994; Lévesque, 1997; Anderson and Bliss, 1998; Ugolini et al., 2006), and are characterized by circular patterns of frost-heaved barren or sparsely vegetated mineral soil with vascular plant cover restricted to the margins of the boil (Cannone et al., 2004; Walker et al., 2004; Michaelson et al., 2012). Frost boils form from the convective churning action of cryoturbation that results, in part, from the annual freeze-thaw of water in the active layer migrating to the permafrost table, freezing and upheaving the fine to medium textured soils in the frost boil centers (Walker et al., 2004). The importance of cryoturbation for sequestering carbon in frost boil soils is well documented in the low Arctic tundra ecosystems (Bockheim and Tarnocai,

1998; Ping et al., 1998; Walker et al., 2004; Bockheim, 2007); however, few studies examine SOC storage in High Arctic frost boils (Ugolini et al., 2006; Michaelson et al., 2008; Horwath Burnham and Sletten, 2010). Critically in the context of global change models, Horwath Burnham and Sletten (2010) found that C pools in High Arctic barren environments are likely underestimated due to unaccounted lower active layer SOC pools. We postulated that subsurface enrichments of SOC in the center of frost boils resulting from diapirism were contributing to previously unaccounted for subsurface SOC pools (Muller et al., 2017; Chapter 4). A diapir may develop when soil water pools in a concave depression at the base of the active layer under the barren frost boil center and low-density, ice-rich soil develops. SOC may accumulate in this ice-rich concavity above the permafrost table (Shilts, 1978; Cannone et al., 2004; Walker et al., 2004; Boike et al., 2008) as cryoturbation buries SOM or meltwater leaches dissolved organic matter from the surface through the soil profile (Tye et al. 2005, Schaeffer et al. 2013). When the overlying high-density soil in the active layer dries (following snow melt) and becomes more brittle, this soil sinks and the low-density viscous soil material in the lower active layer flows towards the soil surface by vertical heave, manifesting as a diapiric injection (Swanson et al. 1999).

This study is the most comprehensive study to date of SOC distribution in High Arctic polar semi-deserts. Logistical constraints including the high cost of travel and freighting samples from remote field locations, and a short High Arctic field season to collect soil samples has limited the number of pedons used for large-scale carbon inventories. For example, inventories for the entire High Arctic region (Hugelius et al., 2014) and the North American barren vegetation complexes (Ping et al., 2008) are based on as few as 8 and 20 pedons respectively. Using a novel field portable vis-NIR spectrophotometer we collected over 13,000 soil spectra in situ on 560 frost boils to investigate the size and location of SOC pools in the shallow active layer of two polar

semi-deserts (see Chapters 3 and 4 cited as Guy et al., 2015; Muller et al., 2017). The study objectives were to 1) quantify the amount and distribution of SOC found in the active layer of the polar semi-desert study sites, and 2) examine spatial variation in SOC between and across polar semi-deserts, as well as within frost boils. Specifically, we were interested in characterizing the subsurface pockets of soils found in the center of frost boils resulting from diapirism, and determining their contribution to SOC storage in these polar semi-desert environments.

5.4 Materials and Methods

5.4.1 Field site

Alexandra Fiord Dome is an Arctic polar semi-desert located on an upland plateau on the east-central side of Ellesmere Island, Nunavut (78º51'N, 76º06'W). This location presents a unique opportunity to examine two adjacent polar semi-desert field sites on different parent materials. The lower dolomitic site is fairly level (500 m a.s.l) and transitions into the granitic site that gently slopes to the upper bound of granitic material approximately 650 m a.s.l. (Bliss et al. 1994). The dolomitic site is classified as B1 cryptogram, herb barren according to the Circumpolar Arctic Vegetation Map (CAVM), and contains lighter coloured soils with a pH of 8.0-9.0; whereas the granitic site is classified as a B3b noncarbonate mountain complex (granitic), and contains darker grey soils with a pH of 6.3-7.2 (Stewart et al., 2011). The dominant soils are Regosolic Turbic Cryosols on both sites (Stewart et al., 2011) and sorted circles are numerous (Bliss et al. 1994).

5.4.2 vis-NIR survey

5.4.2.1 Frost boil sample locations/ spectral data acquisition

We established twelve blocks on granitic and five blocks on dolomitic sites to account for differences in slope, water availability and micro-climate across the field sites. These sampling blocks delineated areas of relatively homogenous frost boil geomorphology and topography

(Muller et al., 2017). Blocks varied in size from 0.5 to 1.75 ha. Within each block, frost boils were sampled using two randomly positioned perpendicular transects (3–4 m in width and 17–50 m in length) that approximately intersected their midpoints. Sampling efforts were doubled in four of the five dolomitic blocks as late snow melt prevented sampling in the granitic site. These blocks were roughly divided in half and two pairs of perpendicular transects were surveyed.

In each direction from the transect midpoints, along each arm of the perpendicular transects, the first five to eight frost boils encountered were sampled with a field portable vis-NIR spectrophotometer (Veris Technologies, Salina, KS). The vis-NIR spectrophotometer probe was inserted into a 3.3 cm diameter pilot hole in the center of each frost boil and we collected spectra at two cm increments from the soil surface to 36.5 cm or to the top of the permafrost layer, which is approximately 30–35 cm deep in July (Brummell et al. 2012). Frost boils in dolomitic blocks (n = 214) were sampled July 9-14, 2013 and July 14- 24th, 2013 in granite blocks (n = 346); average sampling depth was shallower at the dolomitic site (29 cm) compared to the granitic site (35 cm). In addition to the block sampling, 55 frost boils were sampled opportunistically making a total of 560 frost boils included in the analysis.

5.4.2.2 Fine-scale distribution of subsurface SOC

We intensively sampled 24 frost boils to visualize the three-dimensional distribution of SOC. We used preliminary field analyses of the vis-NIR spectrophotometer data to identify 12 frost boils with subsurface carbon enrichments and 12 frost boils without enrichments in our granitic sampling blocks. At each fine-scale frost boil, soil organic carbon was assessed in a 0.75 x 0.75 m plot containing a grid of nine 0.25 x 0.25 m (0.0625 m^2) subplots. The grid was randomly positioned on the vegetated edge and extended towards the frost boil center. The vis-NIR probe

was inserted into the center of each of the nine subplots and similar to above, soil spectra were collected from the surface to permafrost depth (n ≈ 18 depth increments/subplot).

5.4.2.3 Spectral data management

Over 13,000 spectral soil samples were taken in the frost boil centers and the fine-scale sampling grids. Soil spectra were visually monitored throughout field sampling, and any anomalies such as improper soil contact, non-soil material such as rocks covering the scanning window, and software errors were noted. Briefly, spectra were smoothed using the Savitzky-Golay transformation in the prospectr package (Stevens and Lopez, 2013), and samples were scanned for outliers using the spectra.outliers function in the soil.spec package in R (Sila and Terhoeven-Urselmans, 2013; R Core Development Team, 2015). This function, based on multidimensional scaling (MDS), transforms the smoothed data using a first derivative Savitzky-Golay algorithm to remove measurement differences. Euclidean spectral similarity distances are then computed and arranged along MDS axes in Euclidean space. Ninety-four samples that were more than three standard deviations from the mean were flagged as potential outliers; however, only 56 samples were removed.

Spectral samples collected from dolomitic and granitic sites were analyzed separately for soil organic carbon using partial least squares regression (PLSR) models as described in Chapter 3 (Guy et al., 2015). The final model for granitic prediction contained 89 regional arctic samples spiked with 15 samples from the granitic site (R2= 0.75, RMSE = 0.11% SOC); the final model to predict dolomitic sites contained 102 regional arctic samples spiked with 15 samples from granitic sites and 15 samples from dolomitic sites which were extra-weighted (15 x) (R^2=0.74, RMSEP= 0.85% SOC). Samples were removed from analysis if their predicted value exceeded the range of these calibration models (n=92). Ten frost boils were eliminated from further analysis due to

insufficient sampling points resulting from shallow rocky soils, spectral outliers, prediction outliers, or sampling error.

5.4.3 Field sampling

We excavated soil pits on frost boils to determine bulk density and coarse fragments for soil organic carbon content calculations using two different approaches. For granitic frost boils with fine-scale vis-NIR sampling grids (n=24), we collected two 100 cm^3 soil cores at each of the 0–10, 10–20, and 20–30 cm depth increments. For other frost boils in the granitic (n=6) and dolomitic sites (n=10), smaller soil pits were excavated and two 100 cm^3 soil cores per pit were taken at two of the aforementioned depth increments. Twelve samples were dropped from analysis due to rocky soils, or damaged/missing samples.

5.4.4 Soil organic carbon content calculation

Soil organic carbon content (SOCC; kg m^{-2}) was calculated for polar semi-desert soils by combining the traditional methodology used for arctic soils (Tarnocai et al., 2009) and calculating area under the curve (Yeh and Kwan, 1978). This modified method allowed us to better incorporate our SOC measurements that were taken at 2 cm depth increments using vis-NIR spectroscopy. Traditionally, SOCC (kg m^{-2}) is calculated as follows:

$$SOCC = C \times BD \times T \times (1 - CF) \times 10 \qquad \text{(Eq. 6.1)}$$

where C is the % SOC, BD is measured soil bulk density (g cm^{-3}), T is the soil layer thickness and CF is the percent of coarse fragments by weight (%). For each SOC (% SOC) measurement, we first calculated SOC density kg m^{-3} (Phillips, 2011). For the soil surface, SOCC was calculated using traditional methods as above by multiplying the SOC density by the horizon thickness or depth of the first sampling point. For values below the first sampling point, spline

interpolation was used to calculate SOCC using the auc function in the MESS package in R (Ekstrøm, 2018).

5.4.4 Soil organic carbon mass calculation

Soil organic carbon mass (Pg SOC) was calculated by multiplying the calculated average SOCC by the 1.005 x 10^6 km^2 area designated as High Arctic polar semi-desert (Bliss and Matveyeva, 1992; Horwath Burnham and Sletten, 2010). Uncertainty intervals for our estimates were calculated based on the propagated standard error from the two polar semi-desert estimates, which reflects the variance between frost boils within each site and the number of frost boils sampled. This procedure assumes equal contribution of the granitic and dolomitic sites to the polar semi-desert estimate, and accuracy of the area mapped as polar semi-deserts (Hugelius et al., 2014).

5.4.5 Data analyses

5.4.5.1 SOC storage between polar semi-deserts

We used mixed effects models to test for differences in total SOCC and SOCC of different depth increments between the dolomite and granitic polar semi-desert sites. Differences between these sites were tested using the desert (Granite/Dolomite) variable. SOCC was log transformed to meet assumptions of normality. Models were fit with total frost boil SOCC (n=550) as the response variable, desert as the fixed effect and sampling blocks as a random effect. To test for differences in SOC storage with depth, SOCC was the response variable, desert, depth increment (0 to 10 cm, 10 to 20 cm, 20 to 30 cm and 30+ cm) and their interaction were fixed effects, and sampling blocks as a random effect. For this analysis, incomplete depth increments due to shallow or insufficient sampling (<3 data points) were removed from the analysis.

Mixed effects models were also used to evaluate differences in vis-NIR measured SOC (g kg-1), coarse fragments, and bulk density with depth between the dolomite and granitic polar semi-deserts. Five hundred and fifty frost boils were sampled for SOC across 5 dolomitic blocks (n=205) and 12 granitic blocks (n=345), resulting in 9320 vis-NIR measured SOC samples included in the analysis. SOC was log transformed to meet assumptions of normality. Models were fit with SOC (n= 9320) as the response variable, desert, depth and their interaction were fixed effects. Frost boils and sampling blocks were included as random effects. Forty frost boils were sampled for bulk density and coarse fragments across 4 dolomitic blocks (n=10) and 11 granitic blocks (n=30). Values for each depth increment (0 to 10 cm, 10 to 20 cm, 20 to 30 cm) were averaged by frost boil, then block prior to analysis. Models were fit with bulk density or coarse fragments as the response variable, desert, depth increment and their interaction were fixed effects, and sampling blocks as a random effect. All models were fit with the *lmer* function of the lmerTest package in R (Kuznetsova et al., 2016).

5.4.5.2 SOCC storage across polar semi-deserts

Differences between blocks were evaluated for each polar semi-desert separately to avoid induced spatial dependence due to parent material. Within each site we used analysis of variance (ANOVA) to test for differences in total frost boil SOCC between sampling blocks. Models were fit with the *lm* function in R with log transformed total frost boil SOCC as the response variable and sampling blocks as the main effect. Least squares means were used to test for differences between factor levels using the lsmeans package in R (Lenth, 2016). To evaluate at what scales SOCC is spatially correlated across each polar semi-desert, we plotted isotropic spherical variograms of total frost boil SOCC (kg m^{-2}). Variograms were fit using the fit.variogram function

of the gstat package in R (Pebesma, 2004; Legendre and Legendre, 2012). Frost boils with missing coordinates (n= 110) due to a GPS malfunction were excluded from the spatial analysis.

5.4.5.3 Detecting diapiric horizons in frost boil centers

To detect subsurface Bhy horizons, indicative of diapirism in frost boils, we categorized the 550 frost boils by the distribution of SOC concentration within the soil profile. When frost boils had a subsurface patch of soil with increased SOC relative to the surrounding soil matrix (a diapir Bhy horizon), we determined the degree of that soil enrichment (strength), depth and thickness of the patch within the soil profile. Subsurface patches with enriched SOC had at least two sample points enriched with more than 10 g kg^{-1} SOC compared to the overlying mineral soil. The upper and lower bounds of the patch delineate regions of the soil profile containing more than 5 g kg^{-1} SOC relative to the overlying mineral soil. The degree of soil enrichment reflects the strength of frost boil development. This was categorized as weak (10 to 20 g kg^{-1}), moderate (20-30 g kg^{-1}) or strong (>30 g kg^{-1}) based on the measured contrast between the maximum patch SOC and the minimum overlying soil matrix SOC. This differed from our previous assessment of diapir horizons which focussed only on the presence and absence of visually distinct sub-surface enrichments of SOC (Muller et al., 2017).

We used Pearson's chi-squared tests to test whether the frequency of presence of diapir horizons in frost boils differed among the experimental blocks and between dolomitic (n = 5) and granitic (n = 12) substrates.

5.4.5.5 Fine-scale distribution of SOC within frost boils

To visualize the fine-scale distribution of SOC, we sampled 24 frost boils, 12 expected to have diapirs based on preliminary analysis 12 expected not to have diapirs, across our granitic sampling blocks using the vis-NIR spectrophotometer. Three-dimensional (3D) kriging

interpolation among sampling points was used to produce subsurface soil organic carbon (SOC) plots using the gstat package in R (Pebesma, 2004). Sample variograms were plotted and the best fit variogram models for 3D kriging were selected for each frost boil. Initially, isotropic spherical models were fit to sample variograms with a cut-off distance of 60 cm and bin width of 4 cm to ensure spatial correlation between subplots was considered in the models. Parameters and model selections (exponential, linear or Gaussian) were adjusted to improve model fit.

5.5 Results

5.5.1 Soil organic carbon content in polar semi-deserts

5.5.1.1 How much SOC is stored in polar semi-deserts?

The amount of SOC stored in the 1.005×10^6 km^2 top 30 cm of the polar semi-deserts is estimated at 7.34 ± 0.42 Pg SOC. Our best estimate of total SOC storage in the active layer to a depth of ~37 cm is 8.14 ± 0.45 Pg SOC.

5.5.1.2 Does SOC storage differ between polar deserts?

Total soil organic carbon content in frost boils does not differ between the dolomite and granite polar semi-deserts, though a depth by desert interaction indicates that SOC is being stored differently (Table 5.1). Overall, the dolomitic site had greater SOCC at the 10 to 20 cm ($t_{(18)}$ = 3.03, p = 0.01) and 20 to 30 cm depth increments (Table 5.1; $t_{(20)}$ = 3.14, p = 0.01) than the respective granitic increments, but this was not evident in the 0 to 10 cm increment ($t_{(18)}$ = -0.60, p = 0.56). These SOCC values have large standard deviations ranging from roughly 60-95% of SOCC values, likely indicating there is spatial variation in total SOCC and SOCC at the various depths across both polar semi-deserts.

Table 5.1. Soil organic carbon content in the center of frost boils in the granitic and dolomite polar semi-deserts (kg SOC m^{-2})

Depth (cm)		Dolomite (n=205)	Granite (n=345)
		(kg SOC m^{-2})	
0 to 10	mean ± sd	2.59 ± 1.75	3.17 ± 2.97
	Range	0.42 to 10.34	0.19 - 18.02
10 to 20	mean ± sd	2.74 ± 1.93	2.09 ± 1.82
	Range	0.48 – 15.80	0.33 - 14.45
20 to 30	mean ± sd	2.17 ± 1.44	1.84 ± 1.33
	Range	0.05 – 7.81	0.40 - 9.60
30+	mean ± sd	1.02 ± 0.72	1.14 ± 1.00
	Range	0.04 - 3.32	0.07 - 8.77
Total	mean ± sd	8.00 ± 4.82	8.21 ± 5.62
	Range	1.67 – 26.33	1.75 - 35.71

Summary statistics of mixed effect models

Variable	Desert	Depth	Desert x Depth
Total SOCC	$F_{[1,14]} = 0.00$, $p = 0.99$	--	--
SOCC	$F_{[1,15]} = 1.14$, $p = 0.30$	$F_{[3,1495]} = 379.99$, $p < 0.01$	$F_{[3, 1495]} = 38.45$, $p < 0.01$

Differences in SOCC storage with depth is likely due to the depth by desert interactions in SOC g kg^{-1}, coarse fragments, and bulk density (Table 5.2). The dolomite blocks had on average 35% higher SOC in the mineral soil with an average of 26.3 ± 4.4 g SOC kg^{-1} dry soil compared to 18.4 ± 3.6 g SOC kg^{-1} in granitic blocks (Table 5.2). Generally, percent SOC in the dolomite site tends to increase slightly with depth, whereas in the granitic site SOC decreases with depth. Opposite trends are evident for coarse fragments and bulk density with these decreasing with depth in dolomitic site but increasing slightly with depth in the granitic site.

Table 5.2. Mean soil organic carbon, bulk density and coarse fragment values for dolomite and granite polar semi-deserts. Values are mean ± standard deviation and were averaged by frost boil, block, and then by desert.

Depth		Dolomite			Granite		
		Soil Organic Carbon †	Bulk Density‡	Coarse Fragments	Soil Organic Carbon	Bulk Density	Coarse Fragments
cm		g kg^{-1}	g cm^{-3}	% by weight	g kg^{-1}	g cm^{-3}	% by weight
0 to 10	mean	21.2 ± 8.7	1.72 ± 0.10	38.7 ± 9.1	22.9 ± 3.9	1.52 ± 0.13	24.9 ± 8.8
	range	5.7 to 31.9	1.61 to 1.81	28.5 to 45.6	17.8 to 28.7	1.28 to 1.72	13.4 to 45.1
10 to 20	mean	22.8 ± 9.2	1.42 ± 0.14	24.7 ± 9.5	16.5 ± 4.1	1.60 ± 0.18	24.8 ± 10.1
	range	6.2 to 33.3	1.26 to 1.59	15.4 to 37.3	11.9 to 25.6	1.36 to 1.97	13.5 to 48.6
20 to 30	mean	26.5 ± 2.1	1.21 ± 0.19	23.9 ± 1.0	15.5 ± 2.9	1.62 ± 0.15	27.0 ± 7.5
	range	25.7 to 30.0	1.00 to 1.34	22.1 to 23.9	11.5 to 20.9	1.43 to 1.88	16.0 to 37.8
Summary of Desert (0 to 30)	mean	26.3 ± 4.4	1.45 ± 0.13	28.4 ± 93	18.4 ± 3.6	1.56 ± 0.14	25.3 ± 7.1
	range	21.1 to 33.1	1.28 to 1.60	19.7 to 41.5	13.7 to 24.8	1.37 to 1.87	16.9 to 40.6

Summary statistics of mixed effects models

Variable	Desert	Depth	Desert x Depth
Soil Organic Carbon	$F_{[1, 16]} = 0.72$, $p = 0.41$	$F_{[3, 8804]} = 69.77$, $p < 0.01$	$F_{[3, 8804]} = 461.87$, $p < 0.01$
Coarse Fragments	$F_{[1,13]} = 0.84$, $p = 0.37$	$F_{[2,25]} = 4.60$, $p = 0.02$	$F_{[2,25]} = 4.81$, $p = 0.02$
Bulk Density	$F_{[1,15]} = 4.08$, $p = 0.06$	$F_{[2,27]} = 5.45$, $p = 0.01$	$F_{[2,27]} = 12.67$, $p < 0.01$

† Five hundred and fifty frost boils were sampled for SOC across 5 dolomitic blocks (n=205) and 12 granitic blocks (n=345).
‡ Forty frost boils were sampled for bulk density and coarse fragments across 4 dolomitic blocks (n=10) and 11 granitic blocks (n=30).

5.5.1.3 Does SOC storage differ across polar semi-deserts?

Total frost boil SOCC varied significantly between blocks in the granitic polar semi-desert ($F_{[11,333]} = 5.59$, $p < 0.01$), with block averages ranging from 4.6 to 12.3 kg SOC m^{-2}. Differences between dolomitic blocks were less pronounced ($F_{[4,200]} = 3.46$, $p = 0.01$), with only one block containing significantly less SOC than three of the four other dolomite blocks.

The experimental variograms fit with spherical models were used to examine at what distances SOCC was spatially correlated across the polar semi-deserts. In the dolomitic site, spatial autocorrelation was detected to distances of 16.5 m (Figure 5.1a). This range of spatial correlation is relevant to samples within the same sampling blocks as the perpendicular transects ranged from 17 m to 45 m in length whereas distances between transects of adjacent blocks often exceeded 20

m, the point at which there is no spatial correlation. The large nugget effect, accounting for 45% of the total sill, indicates that there is likely either fine scale variation in SOCC at scales smaller than the distance between frost boils or measurement error (Legendre and Legendre, 2012). The granitic site had a pure nugget effect which means there is no spatial autocorrelation detected between the frost boils sampled at these scales (Figure 5.1b).

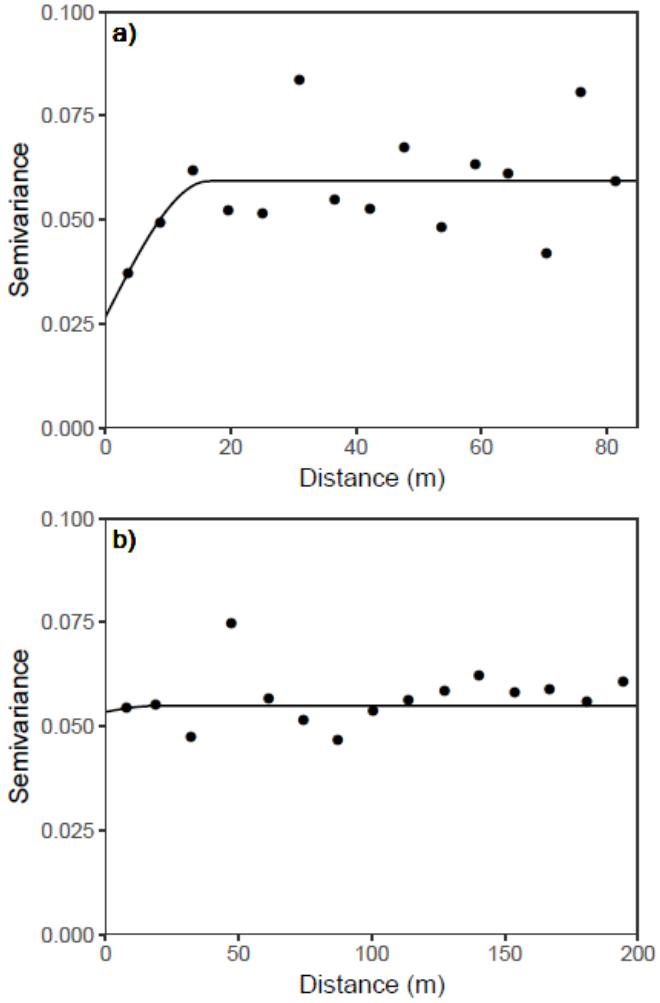

Fig. 5.1. Variograms of total frost boil soil organic carbon content (kg m^{-2}) in the a) dolomitic (n=96) and b) granitic (n = 344) polar semi-deserts

5.5.2 Soil organic carbon distribution and storage within frost boils

5.5.2.1 How common are subsurface SOC patches indicative of Diapir Bhy horizons?

Patches of subsurface mineral soil enriched with soil organic carbon relative to the surrounding soil matrix were detected on 35.8% of the frost boils sampled using vis-NIR (n=197). Subsurface patches of SOC were more common in the dolomitic compared to the granitic polar semi-desert (df = 1, n = 550, χ^2 = 15.02, P < 0.01); with 46% of frost boils containing subsurface enrichments in the dolomite site versus 29.5% in the granitic site. The number of subsurface patches detected varied among granitic sampling blocks (df = 11, n = 205, χ^2 = 34.01, P < 0.01), but not the dolomitic blocks (df = 4, n = 205, χ^2 = 6.01, P = 0.20).

When subsurface patches enriched in SOC were detected, the depth, thickness and degree of SOC enrichment, factors indicative of diapir development, were extremely variable between frost boils. Nearly half (45.2%) the patches detected in frost boils were located near the bottom of the active layer (Figure 5.2c; n= 89). Patches located in the middle (Figure 5.2e; n=66) and top (Figure 5.2d; n= 23) of the active layer were detected in 33.5% and 11.7% of frost boils, respectively. Frost boils with multiple subsurface peaks were identified on 9.6% of frost boils with patches detected (Figure 5.2f; n = 19). Average patch thickness varied depending on location ($F_{[3,193]}$ = 7.53, p < 0.01), with the thinnest patches occurring in the top subsurface soils (6.6 cm; range 2 to 20 cm). Patches in the mid-active layer (12.0 cm; range - 2 to 26 cm) and the supra permafrost region (9.5 cm; range - 1.5 to 23 cm) were on average slightly thicker. Of the frost boils with subsurface patches, 47.2% (n= 93) were strongly developed with greater than 30 g kg^{-1} SOC contrast with the overlying soil matrix, 24.4% (n=48) were moderately developed (20-30 g kg^{-1} SOC) and 28.4% (n=56) were weakly developed (10-20 kg^{-1} SOC).

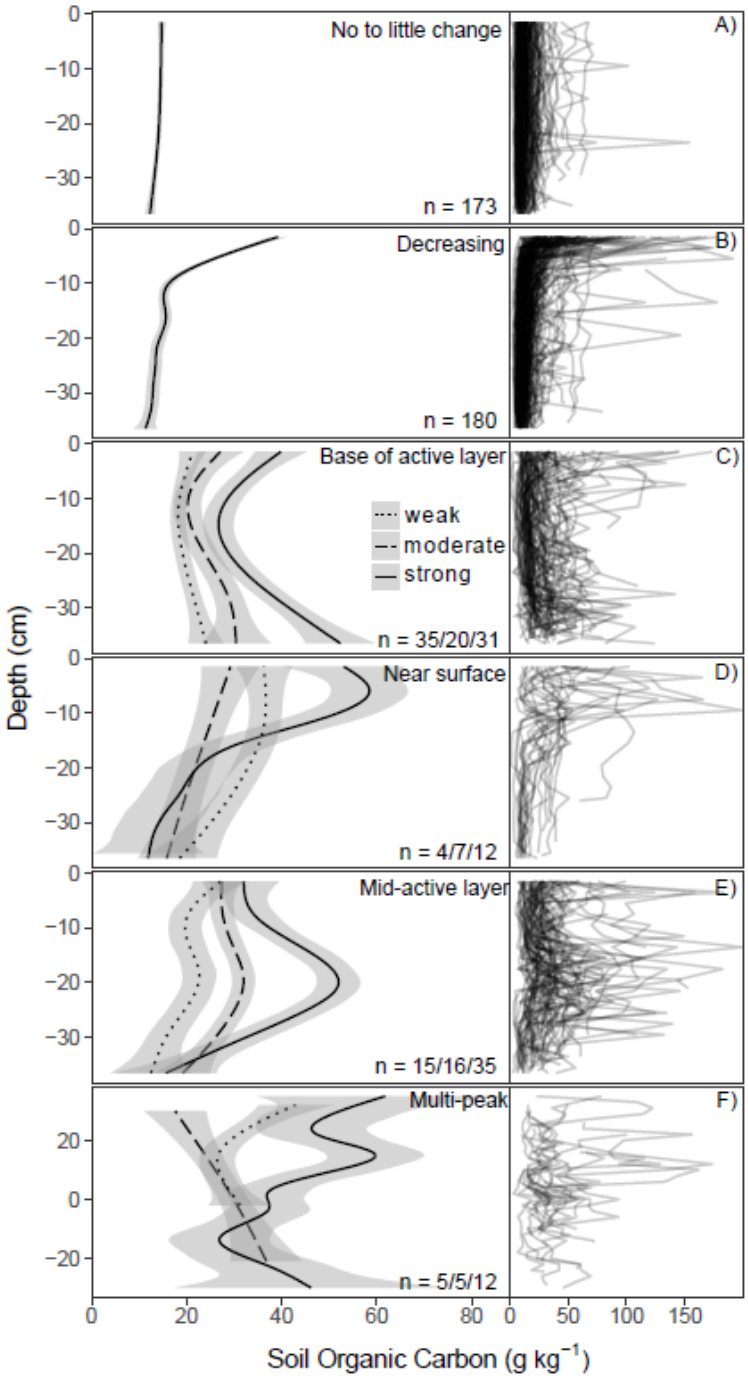

Fig. 5.2 Summarized (left panels) and raw (right panels) characteristic soil profiles of soil organic carbon (SOC; g kg-1) detected in the center of frost boils using vis-NIR spectroscopy (n=550). Frost boils without subsurface SOC patches had either A) little to no change, or B) decreasing SOC with depth. Subsurface SOC patches were detected C) at the base, D) near the top, E) in the middle, or F) at multiple depths within the active layer of frost boils. Lines represent average gam (generalized additive model) smoothed values with the 95% CI shaded in gray; line type shows the strength of frost boil development measured as weak (10 to 20 g kg^{-1}), moderate (20-30 g kg^{-1}) or strong (>30 g kg^{-1}) contrast between the maximum patch SOC and the minimum overlying soil matrix SOC. Multi-peak frost boils (f) are displayed with depth normalized to the dominant peak to better illustrate the soil profiles. For panels c-f, n = weak/moderate/strong.

5.5.2.2 What does a diapir/subsurface patch look like?

We visually assessed the distribution of SOC within the intensively sampled frost boils (n=24) using the vis-NIR fine-scale sampling grids. We found that the concentration of SOC is not only heterogeneous vertically, as we saw in the frost boil centers, but also laterally across the frost boils. Four representative frost boils were chosen to illustrate common patterns observed in subsurface SOC distribution (Figure 5.3). Variogram models used for kriging and 3D renderings of the kriged SOC values for all frost boils are found in Appendix 4.

Frost boils that had no subsurface patches of SOC enrichment detected in their centers either had little to no change in SOC with depth or had decreasing SOC with depth. Those frost boils that had little to no change in SOC at their centers typically had the least variation in SOC within the frost boil and the regions of highest SOC tended to be at the surface under the vegetated frost boil edges (Fig. 5.3A). In contrast, frost boils that had greater SOC at the soil surface often had subsurface patches enriched in SOC along the edge or elsewhere, though these patches were not detected in the centers (Fig. 5.3B).

When subsurface patches enriched with SOC were detected in the center of frost boils, the spatial distribution of SOC across the fine-scale grids does not generally reflect the center SOC profile. For example, frost boils 1018 and 1130 respectively had strong and moderate SOC enrichments located at the bottom of the active layer. However, 1018 only had subsurface enrichments evident along the margins of the frost boil (Fig. 5.3C), whereas, frost boil 1130 had a patch located at depth in the center (Fig. 5.3D).

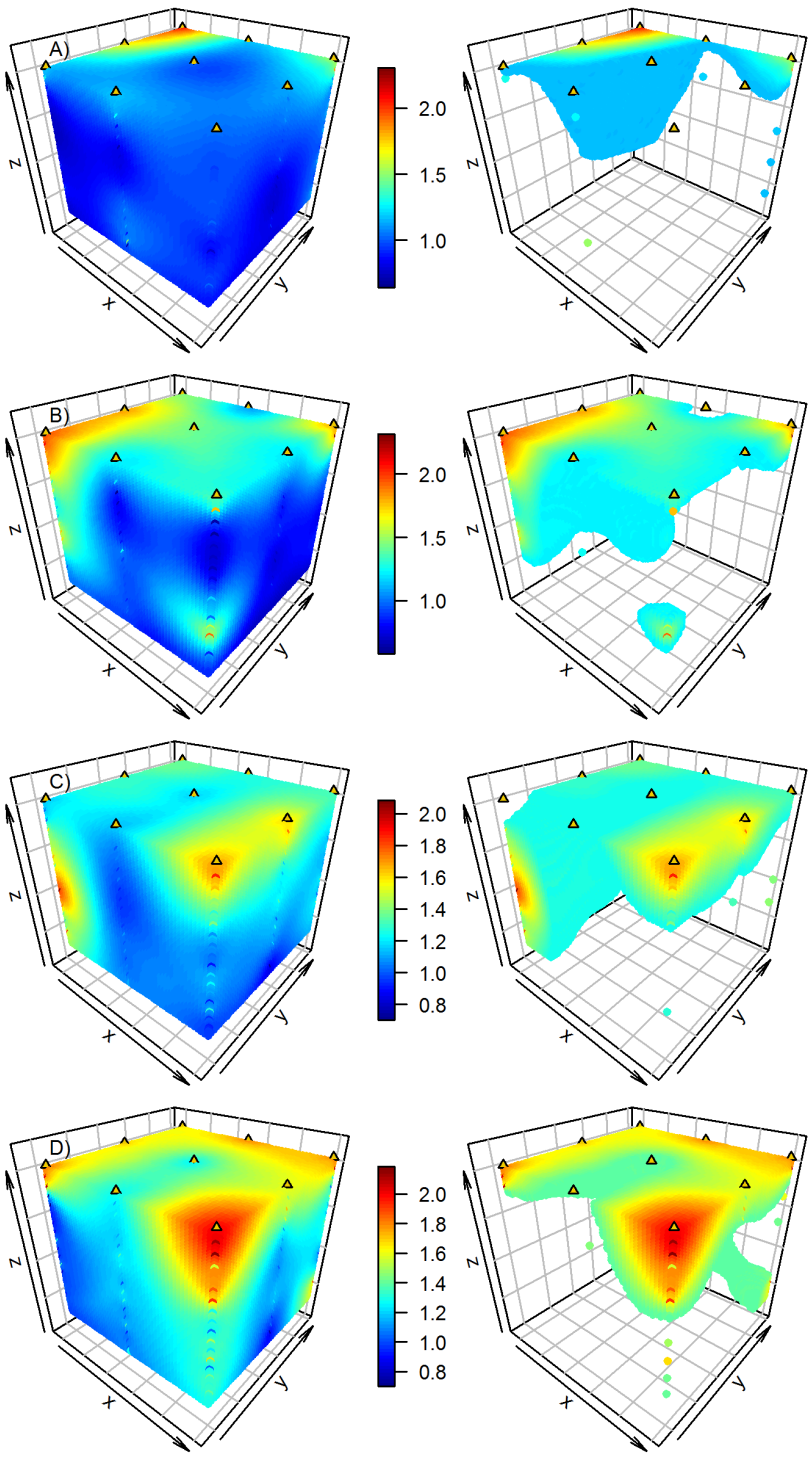

Fig. 5.3. Three dimensional renderings of log transformed SOC (g kg^{-1}) resulting from kriging interpolation between vis-NIR sampling locations for frost boils A) 593, B) 1103, C) 1018, and D) 1130. All kriged values (left panels), and values enriched with at least 10 g kg^{-1} SOC in the top quartile of the frost boil subsurface values (right panel) are displayed to highlight regions of greatest SOC. The x-axis extends from the edge of the frost boil toward the center and the y-axis is parallel to the edge. The vis-NIR sampling locations are represented by triangular points.

5.5.2.3 How much SOC is stored in subsurface patches?

Frost boils with subsurface patches of carbon contained nearly double the SOCC of frost boils without subsurface patches, with 11.4 ± 6.3 kg SOC m^{-2} in the active layer compared to 6.4 ± 3.6 kg SOC m^{-2} respectively ($F_{[1,547]} = 188.68$, $p < 0.01$). When frost boils contain subsurface patches, on average 40 % of the total SOC is found within the patch. Of the carbon contained in polar semi-desert frost boils approximately half the carbon is stored in frost boils containing subsurface patches, despite representing only 35% of all frost boils. Approximately 20% of carbon found in polar semi-desert frost boils is stored in subsurface patches.

5.6 Discussion

High Arctic barrens have been underrepresented in northern circumpolar carbon inventories resulting in carbon pool estimates with a large amount of uncertainty (Ping et al., 2008; Hugelius et al., 2014). Some studies suggest that soil carbon in the lower active layer of High Arctic barren environments represents a previously unaccounted for and poorly understood pool of carbon (Horwath et al., 2008; Horwath Burnham and Sletten, 2010). Here, we provided a comprehensive look at the spatial variability and quantity of SOC in High Arctic polar semi-deserts using a novel field portable vis-NIR spectrophotometer. This study highlights the contribution of subsurface enrichments of SOC in the center of frost boils resulting from diapirism to these previously unaccounted for subsurface SOC pools, and the implications these patches have plant-soil carbon feedbacks in a warming Arctic.

5.6.1 SOCC storage in polar semi-deserts

The entire High Arctic is estimated to contain 34 ± 16 Pg SOC with 10 ± 3 Pg SOC in the top 30 cm of soil (Hugelius et al., 2014). Our estimates suggest that High Arctic semi-deserts alone contain 7.34 ± 0.42 Pg SOC in the top 0-30 cm and 8.14 ± 0.45 Pg SOC in the shallow active layer.

These values are very similar to the Horwath Burnham and Sletten (2010) Greenland based estimate of 7.87 Pg SOC for the High Arctic polar semi-desert active layer. Our results support their assessment that these regions contain approximately 8 times more SOC than previously estimated by Bliss and Matveyeva (1992a) and the important role of cryoturbation processes for redistributing SOC to depth. They found that close to a third of that carbon is stored in the lower active layer (Horwath Burnham and Sletten, 2010). In this study, approximately 36 to 40% of SOC is stored below 20 cm in the granitic and dolomitic polar semi-deserts, and of the carbon contained in polar semi-desert frost boils, approximately 20% is stored in subsurface patches. Thus, subsurface enrichments of SOC in the center of frost boils resulting from diapirism contribute to this previously unaccounted for SOC pool – though not equally between polar semi-deserts.

Total frost boil soil organic carbon content did not differ between the dolomite and granite polar semi-deserts, despite the dolomite site having on average 35% higher soil organic carbon in the mineral soil. It is evident that SOC is being stored differently in these sites, as the dolomitic site had greater SOCC from 10 to 30 cm depth compared to the granitic site. This is likely due to the depth by desert interactions of SOC being driven by the presence of subsurface SOC patches. On average percent SOC in the dolomite semi-desert tends to increase slightly with depth, whereas in the granitic semi-desert SOC decreases with depth. Subsurface patches of SOC were more common in the dolomitic compared to the granitic polar semi-desert; with 46% of frost boils containing subsurface enrichments in the dolomite site versus 29.5% in the granitic site.

5.6.2 Diapirism and Arctic warming

While the total SOC stored in subsurface pockets were likely previously underestimated in global change models, these pools represent a relatively small proportion of the SOC stored in permafrost soils. Why then should we care about these small pools of carbon?

Diapirs provide a moisture mediated nutrient source to plants such as *Salix arctica* growing on the surface (Muller et al., 2017), and because diapirs provide a relatively stable pool of SOC they may play an important role in the plant-soil C feedbacks driving the polar semi-desert carbon balance. We know that the frequency of diapirs is linked moisture and frost boil development in the granitic polar semi-desert landscape (Muller et al., 2017). As the climate warms, the increased moisture and temperature conditions will become more favorable for frost boil development across the Arctic (Callaghan et al., 2005; Walker et al., 2008; Klaus et al., 2013). Thus, the magnitude of diapir formation will also likely increase (Swanson et al., 1999).

While there is significant uncertainty in the net change in soil SOC due to warming in the Arctic (Lamb et al., 2011; Sistla et al., 2013), changes in the distribution of SOCC below ground and overall increases in C stored in plant biomass have been observed in other Arctic ecosystems (Sistla et al., 2013). Some have suggested that a "biological awakening" or priming effect may occur where increased thaw depth and soil temperatures will allow plants to extend roots deeper, releasing C-rich labile root exudates and leachates at depth that will stimulate microbes (Sistla et al., 2013; Wild et al., 2014, 2016). We know that *S. arctica* is able to extend roots into diapir patches (Muller et al., 2017), likely releasing root exudates at depth. Yet, we see lower soil respiration rates on frost boils with diapir patches (Brummell et al., 2015), and C and N cycling rates are depressed (Ota et al., 2020). Soil organic matter in the High Arctic can be relatively recalcitrant (Paré and Bedard-Haughn, 2013a) and cryoturbated organic material in the subsoil have lower decomposition rates relative to organic surface soils in other Arctic ecosystems (Gillespie et al., 2014; Wild et al., 2016). The potential impacts of this biological awakening will have on diapirism and plant-soil C feedbacks influencing the SOC storage in the High Arctic remain uncertain.

6. SUMMARY AND CONCLUSIONS

6.1 Dissertation Overview

Evaluating soil organic carbon (SOC) pools in High Arctic polar deserts and semi-deserts is challenging due to unique frost-driven soil processes such as diapirism that re-distribute SOC in the active layer of these permafrost affected soils (Swanson et al., 1999; Bockheim, 2007). In this dissertation I endeavored to capture the fine-scale spatial variation of SOC in these heterogenous soils with the aim of investigating two main ideas. First, that subsurface patches of SOC resulting from diapirism in the active layer represent an Arctic carbon pool that has previously been underestimated, and second that these patches are an important nutrient source for plants, such as *Salix arctica*, growing in these moisture and nutrient limited environments.

My study of polar semi-desert SOC focussed on detecting the subsurface enrichments of SOC indicative of diapir Bhy horizons in the center of frost boils using a novel field portable visible near-infrared (vis-NIR) spectrophotometer and developing the partial least squares regression calibration models based on field condition soils to predict SOC from vis-NIR soil spectra for our in-situ applications. To date this is one of the most comprehensive studies to look at the spatial distribution of active layer SOC in polar semi-desert frost boils with 13,000 spectral soil samples on 560 frost boils across two High Arctic sites located on an upland plateau near Alexandra Fjord, NU. Understanding the size and distribution of subsurface patches enriched in SOC resulting from diapirism was critical in assessing the contribution of such patches to the overall polar semi-desert carbon pool and investigating their role as a nutrient source. In the

following sections, I broadly discuss overall findings of my thesis, and consider how these findings can inform future research into the vulnerability of subsurface patches of SOC and the above- and below-ground plant community responses to subsurface nutrient patches in a changing arctic climate.

6.2 Summary of Findings

I estimate that the amount of SOC stored in the active layer of High Arctic polar semi-deserts is at 8.14 ± 0.45 Pg SOC, which represent approximately 80% of the SOC estimated in the top 30 cm of soil for the entire High Arctic (Hugelius et al., 2014). Similar to the Horwath Burnham and Sletten (2010), this estimate is approximately 8 times more SOC than previously estimated by Bliss and Matveyeva (1992a) and highlights the important role of cryoturbation processes for redistributing SOC to depth. Patches of subsurface mineral soil enriched with soil organic carbon relative to the surrounding soil matrix were detected on 36% of the frost boils sampled and were more common in the dolomitic polar semi-desert.

I show that the frequency subsurface SOC enrichments indicative of diapir Bhy horizons are linked to broad differences in vegetation community in the granitic polar semi-desert and that the dominant deciduous shrub *S. arctica* is able to access N from subsurface sources when these patches are present. Diapir horizons were more commonly detected in the center of frost boils in areas with well-sorted frost boils and greater bryophyte cover indicative of higher moisture. In contrast, diapir horizons were less common in areas with poorly sorted frost boils, and more bare ground and lichen cover. The cover of *S. arctica* is often higher on diapiric frost boils compared to frost boils without diapirs. Though this trend is only significant in the areas with poorly developed frost boils, it likely reflects the increased soil nutrients and water available in the subsurface of diapiric frost boils.

When diapir horizons were present, *S. arctica* increased its subsurface (i.e., diapir) N uptake and plant root biomass doubled within the diaper relative to non-diapir soils at similar depths. Plant uptake of enriched ^{15}N injected into organic rich soil patches was 2.5 fold greater in diapir than in non-diapir frost boils, demonstrating that these changes in rooting patterns are directly tied to the uptake of limiting soil resources.

Lastly, I show that frost boils with subsurface patches of carbon contained nearly double the SOCC compared to frost boils without subsurface patches. When frost boils contain subsurface patches, on average 40% of the total SOC is found within the patch. Despite diapiric frost boils representing only 35% of all frost boils, approximately half the SOC in polar semi-deserts is stored in frost boils containing subsurface patches.

My study demonstrates that subsurface patches of SOC resulting from diapirism contribute to previously underestimated carbon pools in polar semi-deserts. Horwath Burnham and Sletten (2010) found that SOC pools in High Arctic barren environments are likely underestimated due to previously unaccounted for SOC pools in the lower active layer. In polar semi-deserts, they found close to a third of SOC is stored in the lower active layer. In this study, I found that approximately 36 to 40% of SOC is stored below 20 cm in the granitic and dolomitic polar semi-deserts, and ~20% of all SOC contained in polar semi-desert frost boils is stored in subsurface patches. Further, due to the heterogenous nature of these soils, previous SOC estimates for these regions have a large degree of uncertainty (Ping et al., 2008; Hugelius et al., 2014). Here, I provide the most comprehensive studies to date characterizing the fine-scale spatial variation of SOC in frost boils. Understanding this spatial variability is required for upscaling SOC estimates in these heterogenous soils (Banerjee et al., 2011; Mishra and Riley, 2012; Campeau et al., 2014) and reducing the uncertainty of current High Arctic SOC estimates in our global change models.

6.3 Future Research Directions

My work, combined with other recent studies of these soils, has demonstrated that diapiric patches are both an important store of soil carbon, and a point of strong biological activity (Brummell et al., 2015; Hardy, 2016; Muller et al., 2017; Ota et al., 2020). There are several avenues along which research into the role of diapiric patches in polar semi-deserts should be continued. First, there needs to be a focus on the abiotic and biotic factors contributing to the development of diapiric patches through time and, in the short term, study of the temporal variability of plant available nutrients during the growing season. Further, understanding how polar semi-desert plant species forage for nutrients from diapiric patches will contribute to our understanding of plant community assembly in polar semi-deserts and the response of polar semi-desert plants to the changing climate.

6.3.1 Temporal heterogeneity of subsurface patches

During my research, it has become apparent that not all subsurface patches associated with diapirism are created equal. Not only did I observe spatial variability in the frequency of frost boil diapir horizons across the polar semi-desert landscape, but there was also substantial variability in the depth, thickness and degree of SOC enrichment within these subsurface patches. Plants commonly forage for nutrients from patches that are both spatially and temporally variable (McNickle et al., 2009; Cahill and McNickle, 2011) by proliferating fine roots, increasing uptake rates and through associations with mycorrhizal hyphae (Hodge, 2004; Sullivan et al., 2007). While polar semi-desert plants are increasing root biomass at depth in response to spatially variable diapir patches, the temporal variability of these patches has yet to be investigated. There are two aspects to temporal variability that I think should be considered to better understand the stability of these resource patches. First, we fundamentally need to better understand how these diapiric

patches develop over time and second, we need to understand how plant available nutrients in the patches change throughout the growing season. Some plants such as *Cassiope tetragona, Luzula arctica* and *Luzula confusa,* with root longevities of 6 to 9 years (Bell and Bliss, 1978; Iversen et al., 2015), may be more sensitive to the seasonal changes in diapir nutrients. In contrast, S. *arctica* can be extremely long lived (Aiken et al., 2007) and, while we know *S. arctica* allocates a greater proportion of biomass belowground compared to other High Arctic species (Maessen et al., 1983), we do not know how long lived the roots are (Iversen et al., 2015). Thus, individual plants may be responding to diaper formation on decadal scales.

Morphologically, it is difficult to identify simple diapir forms in polar semi-desert soils as subsurface patches are likely the result of many diapiric intrusions superimposed (Phillips, 2011). The range of diapic patch forms detected in my study (Chapter 4; Fig 5.2) could potentially act as proxy for the stages of diapir development over time, as the patches detected ranged from weak SOM enrichment at the base of the active layer to strongly enriched patches in the middle of the active later. Additionally, examining how the labile and recalcitrant fractions of SOM in these frost boils change through the various stages of development could provide valuable insight into important geomorphic-plant-microbe interactions driving important patterns of N and C cycling in polar semi-deserts (Ota et al., 2020).

Our understanding of the seasonal changes in plant available nutrient in diapic patches is limited. The below ground growing season in arctic environments is 50% longer than that of above ground plant – revealing a 'hidden' season not previously accounted for (Blume-werry et al., 2016). This suggests that a full understanding plant-nutrient patch dynamics will require studies looking beyond the typical Arctic field season. Current studies focus on the brief peak of aboveground productivity and active layer depth. Studies examining root dynamics as the active

layer thaws early in the season may be particularly important. Further, examining the labile and recalcitrant fractions of SOM in diapic horizons is extremely important as the complexity of the organic substrates will determine how stable the nutrient source is through time. The chemical and physical variability of organic inputs to the soil can directly influence the amount of inorganic nutrients potentially released and the ease at which the microbial biomass can decompose the material and releases inorganic nutrients available for plant uptake (Hodge, 2004). The differential mobility of inorganic nutrients also contributes to the spatial and temporal heterogeneity of soil nutrients. For example, nitrate (NO_3^-) is extremely mobile and easily leached from the soil profile (Cain et al., 1999; Hodge, 2004), whereas phosphate ions strongly sorb to the surface of clay minerals and become immobile. The short-term dynamics of these nutrients as the active layer of polar semi-desert cryosols thaw in early spring are nearly unknown.

6.3.1 Below-ground plant community response to diapirs

One avenue that was not fully explored in this dissertation and warrants further investigation, is the plant community responses to the subsurface pockets of nutrients (diapir Bhy horizons) in frost boils. Given that frequency of diapirs is linked to broad scale differences in aboveground plant community and we know that *S. arctica* is able to access nutrients from diapirs when they are present (Muller et al., 2017, Chapter 4), I expected to see distinct differences in the cover of dominant vascular plant, *S. arctica*, non-vascular plants and litter between diapir and non-diapir frost boils. However, we did not observe consistent differences in these measures – likely because we did not fully consider the complexity of the plant community or the subsurface nutrient patches. From an ecological perspective, understanding which plant species can access and compete for nutrients in these subsurface patches will provide insight into plant-soil interactions influencing plant community assembly in polar semi-deserts. Additionally, understanding these

plant-soil interactions may be useful in explaining the current shifts of plant communities in response to long-term climate warming (Elmendorf et al., 2012) and help predict how polar semi-desert plants will respond to projected environmental change. Therefore, I think that it is critical that future studies focus on characterizing the belowground plant community in diapirs and frost boils generally using next-generation sequencing.

The distribution of above ground Arctic plant communities associated with patterned ground (Anderson and Bliss, 1998) and the responses of these communities to long–term climate warming are relatively better understood than their the below ground components (Elmendorf et al., 2012; Frost et al., 2013; Iversen et al., 2015; Blume-werry et al., 2016). The below ground plant community has been referred to as the "unseen iceberg" in tundra environments and though polar deserts and semi-deserts having a much smaller proportion of total plant biomass belowground compared to tundra environments (Iversen et al., 2015), similar uncertainties exist in these environments. The results of this study provide some of the first insights into the belowground ecology of polar semi-deserts and the ability plants to forage for patchy resources in these extreme environments. As the Arctic experiences rapid warming and drastic environmental changes as the glaciers melt, sea-ice recedes and permafrost degrades, we are likely to see major shifts in Arctic plant communities over the coming decades. Uncovering the 'unseen iceberg' in polar semi-deserts may be the answer to better understand how these communities will respond.

7.0 REFERENCES

Aiken, S.G., M.J. Dallwitz, L.L. Consaul, C.L. McJannet, R.L. Boles, et al. 2007. Flora of the Canadian Arctic Archipelago: descriptions, illustrations, identification, and information retrieval. http://nature.ca/aaflora/data (accessed 16 June 2020).

Amundson, R. 2001. The carbon budget in soils. Annu. Rev. Earth Planet. Sci. 29: 535–562. doi: 10.1146/annurev.earth.29.1.535.

Anderson, D.G., and L.C. Bliss. 1998. Association of plant distribution patterns and microenvironments on patterned ground in a polar desert, Devon Island, N.W.T., Canada. Arct. Alp. Res. 30(2): 97–107. http://www.jstor.org/stable/1552124.

Arens, S.J.T., P.F. Sullivan, and J.M. Welker. 2008. Nonlinear responses to nitrogen and strong interactions with nitrogen and phosphorus additions drastically alter the structure and function of a High Arctic ecosystem. J. Geophys. Res. Biogeosciences 113(G03S09). doi: 10.1029/2007JG000508.

Arndal, M.F., L. Illeris, A. Michelsen, K. Albert, M. Tamstorf, et al. 2009. Seasonal Variation in Gross Ecosystem Production, Plant Biomass, and Carbon and Nitrogen Pools in Five High Arctic Vegetation Types. Arctic, Antarct. Alp. Res. 41(2): 164–173. doi: 10.1657/1938-4246-41.2.164.

Baddeley, J.A., S.J. Woodin, and I.J. Alexander. 1994. Effects of increased nitrogen and phosphorus availability on the photosynthesis and nutrient relations of three arctic dwarf shrubs from Svalbard. Funct. Ecol. 8(6): 676–685.

Banerjee, S., A. Bedard-Haughn, B.C. Si, and S.D. Siciliano. 2011. Soil spatial dependence in three Arctic ecosystems. Soil Sci. Soc. Am. J. 75(2): 591. doi: 10.2136/sssaj2010.0220.

Bates, D., M. Maechler, B. Bolker, and S. Walker. 2015. Fitting linear mixed-effects models using lme4. J. Stat. Softw. 67: 1–48.

Batten, D.S., and J. Svoboda. 1994. Plant communities on the uplands in the vicinity of the Alexandra Fiord lowland. In: Svoboda, J. and Freedman, B., editors, Ecology of a polar oasis, Alexandra Fiord, Ellesmere Island, Canada. Captus University Press, North York, Ontario. p. 97–110

Beck, P.S.A., and S.J. Goetz. 2011. Satellite observations of high northern latitude vegetation productivity changes between 1982 and 2008: Ecological variability and regional differences. Environ. Res. Lett. 6: 045501. doi: 10.1088/1748-9326/7/2/029501.

Bedard-Haughn, A., J.W. Van Groenigen, and C. Van Kessel. 2003. Tracing 15N through landscapes: potential uses and precautions. J. Hydrol. 272(1–4): 175–190. doi: 10.1016/S0022-1694(02)00263-9.

Bell, K.L., and L.C. Bliss. 1978. Root growth in a polar semidesert environment. Can. J. Bot. 56(20): 2470–2490. doi: 10.1139/b78-299.

Bellon-Maurel, V., E. Fernandez-Ahumada, B. Palagos, J.-M. Roger, and A. McBratney. 2010. Critical review of chemometric indicators commonly used for assessing the quality of the prediction of soil attributes by NIR spectroscopy. TrAC Trends Anal. Chem. 29(9): 1073–1081. doi: 10.1016/j.trac.2010.05.006.

Bellon-Maurel, V., and A. McBratney. 2011. Near-infrared (NIR) and mid-infrared (MIR) spectroscopic techniques for assessing the amount of carbon stock in soils – Critical review and research perspectives. Soil Biol. Biochem. 43(7): 1398–1410. doi: 10.1016/j.soilbio.2011.02.019.

Ben-Dor, E., D. Heller, and A. Chudnovsky. 2008. A novel method of classifying soil profiles in the field using optical means. Soil Sci. Soc. Am. J. 72(4): 1113. doi: 10.2136/sssaj2006.0059.

Biasi, C., O. Rusalimova, H. Meyer, C. Kaiser, W. Wanek, et al. 2005. Temperature-dependent shift from labile to recalcitrant carbon sources of arctic heterotrophs. Rapid Commun. Mass Spectrom. 19(11): 1401–1408. doi: 10.1002/rcm.1911.

Bithell, S.L., L.T.T. Tran-Nguyen, M.N. Hearnden, and D.M. Hartley. 2014. DNA analysis of soil extracts can be used to investigate fine root depth distribution of trees. AoB Plants 7(0): plu091-. doi: 10.1093/aobpla/plu091.

Bjørsvik, H.-R., and H. Martens. 2008. Data analysis: calibration of NIR instruments by PLS regression. In: Burns, D.A. and Ciurczak, E.W., editors, A handbook of near-infrared analysis. 3rd ed. CRC Press, Boca Raton, FL

Bliss, L.C. 2000. Arctic tundra and polar desert biome. In: Barbour, M.G. and Billings, W.D., editors, North American terrestrial vegetation. 2nd ed. Cambridge University Press. p. 1–40

Bliss, L.C., and W.G. Gold. 1999. Vascular plant reproduction, establishment, and growth and the effects of cryptogamic crusts within a polar desert ecosystem, Devon Island, N.W.T., Canada. Can. J. Bot. 77(5): 623–636. doi: 10.1139/b99-031.

Bliss, L.C., G.H.R. Henry, J. Svoboda, and D.I. Bliss. 1994. Patterns of plant distribution within two polar desert landscapes. Arct. Alp. Res. 26(1): 46–55. doi: 10.2307/1551876.

Bliss, L.C., and N. V. Matveyeva. 1992. Circumpolar Arctic vegetation. In: Chapin III, F.S., Jefferies, R.L., Reynolds, J.F., Shaver, G.R., and Svoboda, J., editors, Arctic ecosystems in a changing climate: an ecophysiological perspective. Academic Press, San Diego, California, USA. p. 59–89

Bliss, N.B., and J. Maursetter. 2010. Soil organic carbon stocks in Alaska estimated with spatial and pedon data. Soil Sci. Soc. Am. J. 74(2): 565–579. doi: 10.2136/sssaj2008.0404.

Bliss, L.C., and J. Svoboda. 1984. Plant communities and plant production in the western Queen Elizabeth Islands. Holarct. Ecol. 7(3): 325–344.

Bliss, L.C., J. Svoboda, and D.I. Bliss. 1984. Polar deserts, their plant cover and plant production in the Canadian High Arctic. Holarct. Ecol. 7(3): 305–324.

Blume-werry, G., S.D. Wilson, J. Kreyling, and A. Milbau. 2016. The hidden season : growing

season is 50 % longer below than above ground along an arctic elevation gradient. New Phytol. 209: 978–986.

Bockheim, J.G. 2007. Importance of cryoturbation in redistributing organic carbon in permafrost-affected soils. Soil Sci. Soc. Am. J. 71(4): 1335–1342. doi: 10.2136/sssaj2006.0414N.

Bockheim, J.G., K.M. Hinkel, and F.E. Nelson. 2003. Predicting carbon storage in tundra soils of Arctic Alaska. Soil Sci. Soc. Am. J. 67(3): 948. doi: 10.2136/sssaj2003.0948.

Bockheim, J.G., and C. Tarnocai. 1998. Recognition of cryoturbation for classifying permafrost-affected soils. Geoderma 81(3–4): 281–293. doi: 10.1016/s0016-7061(97)00115-8.

Bohn, H. 1982. Estimate of organic carbon in world soils: II. Soil Sci. Soc. Am. J. 46: 1118–1119. doi: doi:10.2136/sssaj1982.03615995004600050050x.

Boike, J., O. Ippisch, P.P. Overduin, B. Hagedorn, and K. Roth. 2008. Water, heat and solute dynamics of a mud boil, Spitsbergen. Geomorphology 95(1–2): 61–73. doi: 10.1016/j.geomorph.2006.07.033.

Borcard, D., F. Gillet, and P. Legendre. 2011. Spatial analysis of ecological data. In: Gentleman, R., Hornik, K., and Parmigiani, G.G., editors, Numerical Ecology with R. Springer, New York, New York, USA. p. 227–292

Boulanger-Lapointe, N., E. Lévesque, S. Boudreau, G.H.R. Henry, and N.M. Schmidt. 2014. Population structure and dynamics of Arctic willow (Salix arctica) in the High Arctic. J. Biogeogr. 41(10): 1967–1978. doi: 10.1111/jbi.12350.

Brearley, F.Q. 2009. How does sample preparation affect the d15N values of terrestrial ecological materials? J. Plant Nutr. Soil Sci. 172(4): 461–463. doi: 10.1002/jpln.200900005.

Brown, D.J. 2007. Using a global VNIR soil-spectral library for local soil characterization and landscape modeling in a 2nd-order Uganda watershed. Geoderma 140(4): 444–453. doi: 10.1016/j.geoderma.2007.04.021.

Brown, D.J., K.D. Shepherd, M.G. Walsh, M. Dewayne Mays, and T.G. Reinsch. 2006. Global soil characterization with VNIR diffuse reflectance spectroscopy. Geoderma 132(3–4): 273–290. doi: 10.1016/j.geoderma.2005.04.025.

Brummell, M.E., R.E. Farrell, S.P. Hardy, and S.D. Siciliano. 2014. Greenhouse gas production and consumption in High Arctic deserts. Soil Biol. Biochem. 68: 158–165. doi: 10.1016/j.soilbio.2013.09.034.

Brummell, M.E., R.E. Farrell, and S.D. Siciliano. 2012. Greenhouse gas soil production and surface fluxes at a High Arctic polar oasis. Soil Biol. Biochem. 52: 1–12. doi: 10.1016/j.soilbio.2012.03.019.

Brummell, M.E., A. Guy, and S.D. Siciliano. 2015. Does diapirism influence greenhouse gas production on patterned ground in the High Arctic? Soil Sci. Soc. Am. J. 79(0): 889–895. doi: 10.2136/sssaj2015.01.0026.

Buckeridge, K.M., and P. Grogan. 2010. Deepened snow increases late thaw biogeochemical pulses in mesic low arctic tundra. Biogeochemistry 101: 105–121. doi: 10.1007/s10533-010-9426-5.

Cahill, J.F., and G.G. McNickle. 2011. The behavioral ecology of nutrient foraging by plants. Annu. Rev. Ecol. Evol. Syst. 42(1): 289–311. doi: 10.1146/annurev-ecolsys-102710-145006.

Cain, M.L., S. Subler, J.P. Evans, and M.-J. Fortin. 1999. Sampling spatial and temporal variation in soil nitrogen availability. Oecologia 118: 397–404.

Callaghan, T. V., L.O. Björn, F.S. Chapin III, Y. Chernov, T.R. Christensen, et al. 2005. Arctic tundra and polar desert ecosystems. In: Symon, C., Arris, L., and Heal, B., editors, Arctic climate impact assessment. Cambridge University Press, New York, NY. p. 243–352

Campeau, A.B., P.M. Lafleur, and E.R. Humphreys. 2014. Landscape-scale variability in soil organic carbon storage in the central Canadian Arctic. Can. J. Soil Sci. 94(4): 477–488. doi: 10.4141/cjss-2014-018.

Campioli, M., N. Leblans, and A. Michelsen. 2012. Stem Secondary Growth of Tundra Shrubs: Impact of Environmental Factors and Relationships with Apical Growth. Arctic, Antarct. Alp. Res. 44(1): 16–25. doi: 10.1657/1938-4246-44.1.16.

Cannone, N., M. Guglielmin, and R. Gerdol. 2004. Relationships between vegetation patterns and periglacial landforms in northwestern Svalbard. Polar Biol. 27(9): 562–571. doi: 10.1007/s00300-004-0622-4.

CAVM Team. 2003. Circumpolar Arctic vegetation map. Scale 1:7,500,000. Conservation of Arctic flora and fauna (CAFF) Map No 1. U.S. Fish and Wildlife Service, Anchorage, Alaska.

Chalk, P.M., C.T. Inácio, E.T. Craswell, and D. Chen. 2015. On the usage of absolute (x) and relative (δ) values of 15N abundance. Soil Biol. Biochem. 85: 51–53. doi: 10.1016/j.soilbio.2015.02.027.

Chang, C.-W., D.A. Laird, and C.R. Hurburgh Jr. 2005. Influence of soil moisture on near-infrared reflectance spectroscopic measurement of soil properties. Soil Sci. 170(4): 244–255. doi: 10.1097/01.ss.0000162289.40879.7b.

Chang, C.-W., D.A. Laird, M.J. Mausbach, and C.R. Hurburgh. 2001. Near-infrared reflectance spectroscopy–principal components regression analyses of soil properties. Soil Sci. Soc. Am. J. 65(2): 480–490. doi: 10.2136/sssaj2001.652480x.

Chapin, F.S.I.I.I., N. Fetcher, K. Kielland, K.R. Everett, and A.E. Linkins. 1988. Productivity and nutrient cycling of Alaskan tundra: enhancement by flowing soil water. Ecol. a Publ. Ecol. Soc. Am. (3): 693–702.

Christensen, J.H., B. Hewitson, A. Busuioc, A. Chen, X. Gao, et al. 2007. Regional climate projections. In: Solomon, S., Qin, D., Manning, M., Chen, Z., Marquis, M., et al., editors, Climate change 2007: the physical science basis. Contribution of working group I to the fourth assessment report of the Intergovernmental Panel on Climate Change. Cambridge University Press, Cambridge, United Kingdom and New York, NY, USA. p. 847–940

Christy, C.D. 2008. Real-time measurement of soil attributes using on-the-go near infrared reflectance spectroscopy. Comput. Electron. Agric. 61(1): 10–19. doi: 10.1016/j.compag.2007.02.010.

Craine, J.M., E.N.J. Brookshire, M.D. Cramer, N.J. Hasselquist, K. Koba, et al. 2015. Ecological

interpretations of nitrogen isotope ratios of terrestrial plants and soils. Plant Soil 396(1): 1–26. doi: 10.1007/s11104-015-2542-1.

Cruikshank, J.G. 1971. Soils and terrain units around Resolute, Cornwallis Island. Arctic 24(3): 153–240. doi: https://doi.org/10.14430/arctic3133.

Davidson, E.A., and I.A. Janssens. 2006. Temperature sensitivity of soil carbon decomposition and feedbacks to climate change. Nature 440(7081): 165–73. doi: 10.1038/nature04514.

Davies, A.M.C., and T. Fearn. 2006. Back to basics: calibration statistics. Spectrosc Eur 18(2): 31–32.

Dawson, T.E., S. Mambelli, A.H. Plamboeck, P.H. Templer, and K.P. Tu. 2002. Stable isotopes in plant ecology. Annu. Rev. Ecol. Syst. 33(1): 507–559. doi: 10.1146/annurev.ecolsys.33.020602.095451.

Dennis, J.G. 1977. Distribution patterns of belowground standing crop in Arctic tundra at Barrow, Alaska. Arct. Alp. Res. 9(2): 113–127.

Dickson, L.G. 2000. Constraints to nitrogen fixation by cryptogamic crusts in a polar desert ecosystem , Devon, N.W.T., Canada. Arctic, Antarct. Alp. Res. 32(1): 40–45. doi: 10.2307/1552408.

Ecological Stratification Working Group. 1995. A national ecological framework for Canada. Agriculture and Agri-Food Canada, Research Branch, Centre for Land and Biological Resources Research and Environment Canada, State of the Environment Directorate, Ecozone Analysis Branch, Ottawa/Hull., Ottawa/Hull.

Ekstrøm, C.T. 2018. MESS: Miscellaneous esoteric statistical scripts. R package version 0.5.0.

Elmendorf, S.C., G.H.R. Henry, R.D. Hollister, R.G. Björk, A.D. Bjorkman, et al. 2012. Global assessment of experimental climate warming on tundra vegetation: heterogeneity over space and time. Ecol. Lett. 15(2): 164–75. doi: 10.1111/j.1461-0248.2011.01716.x.

Evans, R.D. 2001. Physiological mechanisms influencing plant nitrogen isotope composition. Trends Plant Sci. 6(3): 121–126. doi: 10.1016/S1360-1385(01)01889-1.

van Everdingen, R., editor. 1998. Multi-language glossary of permafrost and related ground-ice terms. 2005th ed. International Permafrost Association, Calgary, Alberta, Canada.

Frank, D.A., A.W. Pontes, E.M. Maine, J. Caruana, R. Raina, et al. 2010. Grassland root communities: species distributions and how they are linked to aboveground abundance. Ecology 91(11): 3201–3209. doi: 10.1890/09-1831.1.

Frost, G. V., and H.E. Epstein. 2014. Tall shrub and tree expansion in Siberian tundra ecotones since the 1960s. Glob. Chang. Biol. 20(4): 1264–1277. doi: 10.1111/gcb.12406.

Frost, G. V, H.E. Epstein, D.A. Walker, G. Matyshak, and K. Ermokhina. 2013. Patterned-ground facilitates shrub expansion in Low Arctic tundra. Environ. Res. Lett. 8(1): 015035. doi: 10.1088/1748-9326/8/1/015035.

Gillespie, A.W., H. Sanei, A. Diochon, B.H. Ellert, T.Z. Regier, et al. 2014. Perennially and annually frozen soil carbon differ in their susceptibility to decomposition: Analysis of Subarctic earth hummocks by bioassay, XANES and pyrolysis. Soil Biol. Biochem. 68: 106–116. doi: 10.1016/j.soilbio.2013.09.021.

Gold, W.G., and L.C. Bliss. 1995. Water limitations and plant community development in a polar desert. Ecology 76(5): 1558–1568. http://www.jstor.org/stable/1938157.

Grogan, P., A. Michelsen, P. Ambus, and S. Jonasson. 2004. Freeze-thaw regime effects on carbon and nitrogen dynamics in sub-arctic heath tundra mesocosms. Soil Biol. Biochem. 36(4): 641–654. doi: 10.1016/j.soilbio.2003.12.007.

Guerrero, C., B. Stenberg, J. Wetterlind, R.A. Viscarra Rossel, F.T. Maestre, et al. 2014. Assessment of soil organic carbon at local scale with spiked NIR calibrations: effects of selection and extra-weighting on the spiking subset. Eur. J. Soil Sci. 65(2): 248–263. doi: 10.1111/ejss.12129.

Guerrero, C., R. Zornoza, I. Gómez, and J. Mataix-Beneyto. 2010. Spiking of NIR regional models using samples from target sites: Effect of model size on prediction accuracy. Geoderma 158(1–2): 66–77. doi: 10.1016/j.geoderma.2009.12.021.

Guy, A.L., S.D. Siciliano, and E.G. Lamb. 2015. Spiking regional vis-NIR calibration models with local samples to predict soil organic carbon in two High Arctic polar deserts using a vis-NIR probe. Can. J. Soil Sci. 95(3): 237–249. doi: 10.4141/cjss-2015-004.

Haling, R.E., R.J. Simpson, R.A. Culvenor, H. Lambers, and A.E. Richardson. 2012. Field application of a DNA-based assay to the measurement of roots of perennial grasses. Plant Soil 358(1–2): 183–199. doi: 10.1007/s11104-012-1405-2.

Haling, R.E., R.J. Simpson, A.C. McKay, D. Hartley, H. Lambers, et al. 2011. Direct measurement of roots in soil for single and mixed species using a quantitative DNA-based method. Plant Soil 348(1–2): 123–137. doi: 10.1007/s11104-011-0846-3.

Hardy, S.P. 2016. Fertility of frost boils and the effect of diapirism on plant nitrogen uptake in a polar desert ecosystem of the Canadian High Arctic. M.Sc. Thesis, Department of Plant Sciences, University of Saskatchewan. Saskatoon, SK.

Hartley, A.E., C. Neill, J.M. Melillo, R. Crabtree, F.P. Bowles, et al. 1999. Plant performance and soil nitrogen mineralization in response to simulated climate change in subarctic dwarf shrub heath. Oikos 86(2): 331–343.

Hobbie, J.E., and E.A. Hobbie. 2006. 15N in symbiotic fungi and plants estimates nitrogen and carbon flux rates in Arctic tundra. Ecology 87(4): 816–822.

Hodge, A. 2004. The plastic plant: root responses to heterogeneous supplies of nutrients. New Phytol. 162(1): 9–24. doi: 10.1111/j.1469-8137.2004.01015.x.

Högberg, P., L. Högbom, H. Schinkel, M. Högberg, C. Johannisson, et al. 1996. 15N abundance of surface soils, roots and mycorrhizas in profiles of European forest soils. Oecologia 108(2): 207–214. doi: 10.1007/BF00334643.

Horwath Burnham, J., and R.S. Sletten. 2010. Spatial distribution of soil organic carbon in northwest Greenland and underestimates of high Arctic carbon stores. Global Biogeochem. Cycles 24(3): GB3012. doi: 10.1029/2009GB003660.

Horwath, J.L., R.S. Sletten, B. Hagedorn, and B. Hallet. 2008. Spatial and temporal distribution of soil organic carbon in nonsorted striped patterned ground of the High Arctic. J. Geophys. Res. 113(G03S07): G03S07. doi: 10.1029/2007jg000511.

Hudson, J.M.G., G.H.R. Henry, and W.K. Cornwell. 2011. Taller and larger: Shifts in Arctic tundra leaf traits after 16 years of experimental warming. Glob. Chang. Biol. 17(2): 1013–1021. doi: 10.1111/j.1365-2486.2010.02294.x.

Hugelius, G., J.G. Bockheim, P. Camill, B. Elberling, G. Grosse, et al. 2013a. A new data set for estimating organic carbon storage to 3 m depth in soils of the northern circumpolar permafrost region. Earth Syst. Sci. Data 5(2): 393–402. doi: 10.5194/essd-5-393-2013.

Hugelius, G., P. Kuhry, C. Tarnocai, and T. Virtanen. 2010. Soil organic carbon pools in a periglacial landscape: a case study from the central Canadian Arctic. Permafr. Periglac. Process. 21(1): 16–29. doi: 10.1002/ppp.677.

Hugelius, G., J. Strauss, S. Zubrzycki, J.W. Harden, E.A.G. Schuur, et al. 2014. Estimated stocks of circumpolar permafrost carbon with quantified uncertainty ranges and identified data gaps. Biogeosciences 11(23): 6573–6593. doi: 10.5194/bg-11-6573-2014.

Hugelius, G., C. Tarnocai, G. Broll, J.G. Canadell, P. Kuhry, et al. 2013b. The northern circumpolar soil carbon database: Spatially distributed datasets of soil coverage and soil carbon storage in the northern permafrost regions. Earth Syst. Sci. Data 5(1): 3–13. doi: 10.5194/essd-5-3-2013.

IPCC. 2007. Climate change 2007: synthesis report. Contribution of working groups I, II and III to the fourth assessment report of the Intergovernmental Panel on Climate Change. (Core Writing Team, R.. Pachauri, and A. Reisinger, editors). Geneva, Switzerland.

IPCC. 2013. Climate change 2013: the physical science basis. Contribution of working group I to the fifth assessment report of the Intergovernmental Panel on Climate Change (T.F. Stocker, D. Qin, G.-K. Plattner, M. Tignor, S.K. Allen, et al., editors). Cambridge University Press, Cambridge, United Kingdom and New York, NY, USA.

IPCC. 2014. Climate change 2014: impacts, adaptation, and vulnerability. Part b: regional aspects. Contribution of working group II to the fifth assessment report of the Intergovernmental Panel on Climate Change (V.R. Barros, C.B. Field, D.J. Dokken, M.D. Mastrandrea, K.J. Mach, et al., editors). Cambridge University Press, Cambridge, United Kingdom and New York, NY, USA.

Iversen, C.M., V.L. Sloan, P.F. Sullivan, E.S. Euskirchen, A.D. Mcguire, et al. 2015. The unseen iceberg: plant roots in arctic tundra. New Phytol. 205(1): 34–58. doi: 10.1111/nph.13003.

Janik, L.J., R.H. Merry, and J.O. Skjemstaf. 1998. Can mid infrared diffuse reflectance analysis replace soil extractions? Aust. J. Exp. Agric. 38: 681–696. doi: 10.1071/EA97144.

Jeffries, M.O., J.A. Richter-Menge, and J.E. Overland, editors. 2012. Arctic Report Card 2012, www.arctic.noaa.gov/reportcard.

Jobbagy, E.G., and R.B. Jackson. 2000. The vertical distribution of soil organic carbon and its relation to climate and vegetation. Ecol. Appl. 10(2): 423–436.

Johnson, K.D., J. Harden, a. D. McGuire, N.B. Bliss, J.G. Bockheim, et al. 2011. Soil carbon distribution in Alaska in relation to soil-forming factors. Geoderma 167–168: 71–84. doi: 10.1016/j.geoderma.2011.10.006.

Jones, F.A., D.L. Erickson, M.A. Bernal, E. Bermingham, W.J. Kress, et al. 2011. The roots of diversity: Below ground species richness and rooting distributions in a tropical forest

revealed by DNA barcodes and inverse modeling. PLoS One 6(9). doi: 10.1371/journal.pone.0024506.

Jones, M.H., S.E. MacDonald, and G.H.R. Henry. 1999. Sex- and habitat-specific responses of a High Arctic willow, Salix arctica, to experimental climate change. Oikos 87: 129. doi: 10.2307/3547004.

Kalcsits, L.A., H.A. Buschhaus, and R.D. Guy. 2014. Nitrogen isotope discrimination as an integrated measure of nitrogen fluxes, assimilation and allocation in plants. Physiol. Plant. 151(3): 293–304. doi: 10.1111/ppl.12167.

Klaus, M., M. Becher, and J. Klaminder. 2013. Cryogenic soil activity along bioclimatic gradients in Northern Sweden: Insights from eight different proxies. Permafr. Periglac. Process. 24(3): 210–223. doi: 10.1002/ppp.1778.

Kohn, L.M., and E. Stasovski. 1990. The mycorrhizal status of plants at Alexandra Fiord, Ellesmere Island, Canada, a High Arctic site. Mycologia 82(1): 23–35. doi: 10.2307/3759959.

Koven, C.D., D.M. Lawrence, and W.J. Riley. 2015. Permafrost carbon − climate feedback is sensitive to deep soil carbon decomposability but not deep soil nitrogen dynamics. PNAS 112(12): 3752–3757. doi: 10.1073/pnas.1415123112.

Kusumo, B.A., C.B. Hedley, M.J. Hedley, A. Hueni, M.P. Tuohy, et al. 2008. The use of diffuse reflectance spectroscopy for in situ carbon and nitrogen analysis of pastoral soils. Aust. J. Soil Res. 46: 623–635.

Kuznetsova, A., P.B. Brockhoff, and R.H.B. Christensen. 2016. lmerTest: Tests in linear mixed effects models. R package version 2.0-33.

Kweon, G., E. Lund, C. Maxton, P. Drummond, and K. Jensen. 2008. In situ measurement of soil properties using a probe- based VIS- NIR spectrophotometer. St. Joseph, Mich.

Kweon, G.Y., E. Lund, C. Maxton, P. Drummond, and K. Jensen. 2009. Soil profile measurement of carbon contents using a probe-type VIS-NIR spectrophotometer. J Biosyst. Eng 34(5): 382–389.

Kweon, G., and C. Maxton. 2013. Soil organic matter sensing with an on-the-go optical sensor. Biosyst. Eng. 115(1): 66–81. doi: 10.1016/j.biosystemseng.2013.02.004.

Lamb, E.G., S. Han, B.D. Lanoil, G.H.R. Henry, M.E. Brummell, et al. 2011. A High Arctic soil ecosystem resists long-term environmental manipulations. Glob. Chang. Biol. 17(10): 3187–3194. doi: 10.1111/j.1365-2486.2011.02431.x.

Lamb, E.G., T. Winsley, C.L. Piper, S.A. Freidrich, and S.D. Siciliano. 2016. A high-throughput belowground plant diversity assay using next-generation sequencing of the trn L intron. Plant Soil 404: 361–372. doi: 10.1007/s11104-016-2852-y.

Lee, K.S., D.H. Lee, K.A. Sudduth, S.O. Chung, N.R. Kitchen, et al. 2009. Wavelength indentification and diffuse reflectance estimationfor surface and profile soil properties. Trans. ASABE 52(3): 683–695.

Leffler, A.J., and J.M. Welker. 2013. Long-term increases in snow pack elevate leaf N and photosynthesis in Salix arctica: responses to a snow fence experiment in the High Arctic of

NW Greenland. Environ. Res. Lett. 8(2): 025023. doi: 10.1088/1748-9326/8/2/025023.

Legendre, P., and L. Legendre. 2012. Numerical Ecology. 3rd ed. Elsevier.

Lenth, R. V. 2016. Least-squares means: the R package lsmeans. J. Stat. Softw. 69(1): 1–33. doi: doi:10.18637/jss.v069.i01.

Lévesque, E. 1997. Plant distribution and colonization in extreme polar deserts, Ellesmere Island, Canada. PhD Dissertation. Department of Botany, University of Toronto, Canada.

Lützow, M., and I. Kögel-Knabner. 2009. Temperature sensitivity of soil organic matter decomposition—what do we know? Biol. Fertil. Soils 46(1): 1–15. doi: 10.1007/s00374-009-0413-8.

Ma, W.K., A. Schautz, L.-A.E. Fishback, A. Bedard-Haughn, R.E. Farrell, et al. 2007. Assessing the potential of ammonia oxidizing bacteria to produce nitrous oxide in soils of a High Arctic lowland ecosystem on Devon Island, Canada. Soil Biol. Biochem. 39(8): 2001–2013. doi: Doi 10.1016/J.Soilbio.2007.03.001.

Mackay, J.R. 1980. The origin of earth hummocks, western arctic coast, Canada. Can J. Earth Sci 13: 889–897.

Mackelprang, R., M.P. Waldrop, K.M. DeAngelis, M.M. David, K.L. Chavarria, et al. 2011. Metagenomic analysis of a permafrost microbial community reveals a rapid response to thaw. Nature 480(7377): 368–371. doi: 10.1038/nature10576.

Maessen, O., B. Freedman, M.L.N. Nams, and J. Svoboda. 1983. Resource allocation in high-arctic vascular plants of differing growth form. Can. J. Bot. 61(6): 1680–1691. doi: 10.1139/b83-181.

Makarov, M.I. 2009. The nitrogen isotopic composition in soils and plants: Its use in environmental studies (A Review). Eurasian Soil Sci. 42(12): 1335–1347. doi: 10.1134/S1064229309120035.

McNickle, G.G., C.C. St. Clair, and J.F. Cahill. 2009. Focusing the metaphor: plant root foraging behaviour. Trends Ecol. Evol. 24(8): 419–426. doi: 10.1016/j.tree.2009.03.004.

Mevik, B.-H., and R. Wehrens. 2007. The pls package: principal component and partial least squares regression in R. J Stat Softw 18(2): 24 pp.

Michaelson, G.J., C. Ping, and M. Clark. 2013. Soil pedon carbon and nitrogen data for Alaska : an analysis and update. Open J. Soil Sci. 3: 132–142.

Michaelson, G.J., C.L. Ping, H. Epstein, J.M. Kimble, and D. a. Walker. 2008. Soils and frost boil ecosystems across the North American Arctic Transect. J. Geophys. Res. 113(G3): G03S11. doi: 10.1029/2007jg000672.

Michaelson, G.J., C.L. Ping, and J.M. Kimble. 1996. Carbon storage and distribution in tundra soils of Arctic Alaska , U.S.A . Arct. Alp. Res. 28(4): 414–424.

Michaelson, G.J., C.L. Ping, and D.A. Walker. 2012. Soils associated with biotic activity on frost boils in Arctic Alaska. Soil Sci. Soc. Am. J. 76(0): 2265–2277. doi: 10.2136/sssaj2012.0064.

Miller, P.C., R. Kendall, and W.C. Oechel. 1983. Simulating carbon accumulation in northern

ecosystems. Simulation 40(4): 119–131. doi: 10.1177/003754978304000402.

Mishra, U., and W.J. Riley. 2012. Alaskan soil carbon stocks : spatial variability and dependence on environmental factors. : 3637–3645. doi: 10.5194/bg-9-3637-2012.

Morgan, C.L.S., T.H. Waiser, D.J. Brown, and C.T. Hallmark. 2009. Simulated in situ characterization of soil organic and inorganic carbon with visible near-infrared diffuse reflectance spectroscopy. Geoderma 151(3–4): 249–256. doi: 10.1016/j.geoderma.2009.04.010.

Mouazen, A.M., M.R. Maleki, J. De Baerdemaeker, and H. Ramon. 2007. On-line measurement of some selected soil properties using a VIS–NIR sensor. Soil Tillage Res. 93(1): 13–27. doi: 10.1016/j.still.2006.03.009.

Muc, M., B. Freedman, and J. Svoboda. 1989. Vascular plant communities of a polar oasis at Alexandra Fiord (79° N), Ellesmere Island, Canada. Can. J. Bot. 67(4): 1126–1136. doi: 10.1139/b89-147.

Mueller-Dombois, D., and H. Ellenberg. 1974. Aims and methods in vegetation ecology. JohnWiley & Sons Inc., New York, New York, USA, New York, USA.

Mueller, C.W., J. Rethemeyer, J. Kao-Kniffin, S. Löppmann, K.M. Hinkel, et al. 2015. Large amounts of labile organic carbon in permafrost soils of northern Alaska. Glob. Chang. Biol. 21(7): 2804–2817. doi: 10.1111/gcb.12876.

Muller, A.L., S.P. Hardy, S.D. Mamet, M. Ota, E.G. Lamb, et al. 2017. Salix arctica changes root distribution and nutrient uptake in response to subsurface nutrients in High Arctic deserts. Ecology 98(8): 2158–2169. doi: 10.1002/ecy.1908.

Myers-Smith, I.H., S.C. Elmendorf, P.S.A. Beck, M. Wilmking, M. Hallinger, et al. 2015. Climate sensitivity of shrub growth across the tundra biome. Nat. Clim. Chang. 5: 887–891. doi: 10.1038/nclimate2697.

Myers-Smith, I.H., B.C. Forbes, M. Wilmking, M. Hallinger, T. Lantz, et al. 2011. Shrub expansion in tundra ecosystems: dynamics, impacts and research priorities. Environ. Res. Lett. 6(4): 045509. doi: 10.1088/1748-9326/6/4/045509.

Nocita, M., A. Stevens, C. Noon, and B. van Wesemael. 2013. Prediction of soil organic carbon for different levels of soil moisture using Vis-NIR spectroscopy. Geoderma 199: 37–42. doi: 10.1016/j.geoderma.2012.07.020.

Oksanen, J., R. Guillaume Blanchet, F. Kindt, P. Legendre, P.R. Minchin, R.B. O'Hara, et al. 2016. vegan: Community Ecology Package. R package version 2.3-3. https://cran.r-project.org/package=vegan.

Ota, M., S.D. Mamet, A.L. Muller, E.G. Lamb, G. Dhillon, et al. 2020. Could cryoturbic diapirs be key for understanding ecological feedbacks to climate change in high Arctic polar deserts? J. Geophys. Res. Biogeosciences 125(3): 1–13. doi: 10.1029/2019JG005263.

Paré, M.C., and A. Bedard-Haughn. 2013a. Surface soil organic matter qualities of three distinct Canadian Arctic sites. Artic Antarct. Alp. Res. 45(1): 88–98. doi: 10.1657/1938-4246-45.1.88.

Paré, M.C., and A. Bedard-Haughn. 2013b. Soil organic matter quality influences mineralization

and GHG emissions in cryosols: A field-based study of sub- to high Arctic. Glob. Chang. Biol. 19(4): 1126–1140. doi: 10.1111/gcb.12125.

Pebesma, E.J. 2004. Multivariable geostatistics in S: the gstat package. Comput. Geosci. 30: 683–691.

Peterson, R.A., and W.B. Krantz. 2008. Differential frost heave model for patterned ground formation: Corroboration with observations along a North American arctic transect. J. Geophys. Res. 113(G3): G03S04. doi: 10.1029/2007jg000559.

Phillips, M.R. 2011. The depth distribution of organic carbon in mineral cryosols at two sites in the Canadian Arctic. M.Sc. Thesis, Department of Plant Sciences, University of Saskatchewan. Saskatoon, SK. Dep. Soil Sci. Master of.

Ping, C.L., J.G. Bockheim, J.M. Kimble, G.J. Michaelson, and D.A. Walker. 1998. Characteristics of cryogenic soils along a latitudinal transect on Arctic Alaska. J. Geophys. Res. 103(D22).

Ping, C.L., J.D. Jastrow, M.T. Jorgenson, G.J. Michaelson, and Y.L. Shur. 2015. Permafrost soils and carbon cycling. Soil 1: 147–171. doi: 10.5194/soil-1-147-2015.

Ping, C.-L., G.J. Michaelson, M.T. Jorgenson, J.M. Kimble, H. Epstein, et al. 2008. High stocks of soil organic carbon in the North American Arctic region. Nat. Geosci. 1(9): 615–619. doi: 10.1038/ngeo284.

Post, W.M., W.R. Emanuel, P.J. Zinke, and A.G. Stangenberger. 1982. Soil carbon pools and world life zones. Nature 298(5870): 156–159. doi: 10.1038/298156a0.

R Core Development Team. 2015. R: A language and environment for statistical computing. R Foundation for Statistical Computing, Vienna, Austria.

R Core Development Team. 2016. R: a language and environment for statistical computing. http://www.r-project.org/.

Rhoades, C., D. Binkley, H. Oskarsson, and R. Stottlemyer. 2008. Soil nitrogen accretion along a floodplain terrace chronosequence in northwest Alaska: Influence of the nitrogen-fixing shrub Shepherdia canadensis. Ecoscience 15(2): 223–230. doi: 10.2980/15-2-3027.

Riley, I.T., S. Wiebkin, D. Hartley, and A.C. McKay. 2010. Quantification of roots and seeds in soil with real-time PCR. Plant Soil 331(1): 151–163. doi: 10.1007/s11104-009-0241-5.

Rinnan, R., and Å. Rinnan. 2007. Application of near infrared reflectance (NIR) and fluorescence spectroscopy to analysis of microbiological and chemical properties of arctic soil. Soil Biol. Biochem. 39(7): 1664–1673. doi: 10.1016/j.soilbio.2007.01.022.

Robinson, D. 2001. δ 15 N as an integrator of the nitrogen. Trends Ecol. Evol. 16(3): 153–162. doi: 10.1016/s0169-5347(00)02098-x.

Robinson, C.H., P.A. Wookey, J.A. Lee, T. V. Callaghan, and M.C. Press. 1998. Plant community responses to simulated environmental change at a high Arctic polar semi-desert. Ecology 79(3): 856–866. doi: 10.1890/0012-9658(1998)079[0856:PCRTSE]2.0.CO;2.

Sankey, J.B., D.J. Brown, M.L. Bernard, and R.L. Lawrence. 2008. Comparing local vs. global visible and near-infrared (VisNIR) diffuse reflectance spectroscopy (DRS) calibrations for

the prediction of soil clay, organic C and inorganic C. Geoderma 148(2): 149–158. doi: 10.1016/j.geoderma.2008.09.019.

Savile, D.B.. 1979. Ring counts in Salix arctica from northern Ellesmere Island. Can. Field-Nat 93: 81–82.

Savitzky, A., and M.J.. Golay. 1964. Smoothing and differentiation of data by simplified least squares procedures. Anal. Chem. 36(8): 1627–1639.

Schaeffer, S.M., E. Sharp, J.P. Schimel, and J.M. Welker. 2013. Soil-plant N processes in a High Arctic ecosystem, NW Greenland are altered by long-term experimental warming and higher rainfall. Glob. Chang. Biol. 19(11): 484–497. doi: 10.1111/gcb.12318.

Scharlemann, J.P.W., E.V.J. Tanner, R. Hiederer, and V. Kapos. 2014. Global soil carbon: Understanding and managing the largest terrestrial carbon pool. Carbon Manag. 5(1): 81–91. doi: 10.4155/cmt.13.77.

Schmidt, S.K., and D.A. Lipson. 2004. Microbial growth under the snow: Implications for nutrient and allelochemical availability in temperate soils. Plant Soil 259: 1–7. doi: 10.1023/B:PLSO.0000020933.32473.7e.

Schmidtlein, S., H. Feilhauer, and H. Bruelheide. 2012. Mapping plant strategy types using remote sensing (D. Rocchini, editor). J. Veg. Sci. 23(3): 395–405. doi: 10.1111/j.1654-1103.2011.01370.x.

Schuur, E., J. Bockheim, J.G. Canadell, E.E.C. B, S. V Goryachkin, et al. 2008. Vulnerability of permafrost carbon to climate change: implications for the global carbon cycle. Bioscience 58(8): 701–714. doi: 10.1641/B580807.

Schuur, E.A.G., A.D. McGuire, C. Schadel, G. Grosse, J.W. Harden, et al. 2015. Climate change and the permafrost carbon feedback. Nature 520: 171–179. doi: 10.1038/nature14338.

Shaver, G.R., J. Canadell, F.S. Chapin III, J. Gurevitch, J. Harte, et al. 2000. Global warming and terrestrial ecosystems: A conceptual framework for analysis. Bioscience 50(10): 871. http://10.0.6.105/0006-3568(2000)050[0871:GWATEA]2.0.CO.

Shilts, W.W. 1978. Nature and genesis of mudboils, Central Keewatin, Canada. Can J Earth Sci 15(7): 1053–1068. doi: https://doi.org/10.1139/e78-113.

Sila, A., and T. Terhoeven-Urselmans. 2013. soil.spec: soil spectral file conversion, data exploration and regression

Sistla, S.A., J.C. Moore, R.T. Simpson, L. Gough, G.R. Shaver, et al. 2013. Long-term warming restructures Arctic tundra without changing net soil carbon storage. Nature 497: 615–618. doi: 10.1038/nature12129.

Skjemstad, J.O., and J.A. Baldock. 2007. Total and organic carbon. In: Carter, M.R. and Gregorich, E.G., editors, Soil Sampling and Methods of Analysis. 2nd ed. CRC Press, Boca Raton, FL. p. 225–237

Soil Classification Working Group. 1998. The Canadian system of soil classification. 3rd ed. Agric. and Agri-Food Can. Publ 1646.

Sombroek, W.G., F.O. Nachtergaele, and A. Hebel. 1993. Amounts, dynamics and sequestering of carbon in tropical and subtropical soils. Ambio 22(7): 417–426. doi: 10.2307/4314120.

Soriano-Disla, J.M., L.J. Janik, R. a. Viscarra Rossel, L.M. MacDonald, and M.J. McLaughlin. 2014. The performance of visible, near-, and mid-infrared reflectance spectroscopy for prediction of soil physical, chemical, and biological properties. Appl. Spectrosc. Rev. 49(2): 139–186. doi: 10.1080/05704928.2013.811081.

Stenberg, B. 2010. Effects of soil sample pretreatments and standardised rewetting as interacted with sand classes on Vis-NIR predictions of clay and soil organic carbon. Geoderma 158(1–2): 15–22. doi: 10.1016/j.geoderma.2010.04.008.

Stenberg, B., R.A. Viscarra Rossel, A.M. Mouazen, and J. Wetterlind. 2010. Visible and Near Infrared Spectroscopy in Soil Science. Adv. Agron. 107(10): 163–215. doi: 10.1016/S0065-2113(10)07005-7.

Stevens, A., and L.R. Lopez. 2013. An introduction to the prospectr package. R package version 0.1.3

Stewart, K.J., M.E. Brummell, R.E. Farrell, and S.D. Siciliano. 2012. N2O flux from plant-soil systems in polar deserts switch between sources and sinks under different light conditions. Soil Biol. Biochem. 48(0): 69–77. doi: 10.1016/j.soilbio.2012.01.016.

Stewart, K.J., D. Coxson, and S.D. Siciliano. 2011a. Small-scale spatial patterns in N2-fixation and nutrient availability in an arctic hummock-hollow ecosystem. Soil Biol. Biochem. 43(1): 133–140. doi: 10.1016/j.soilbio.2010.09.023.

Stewart, K.J., E.G. Lamb, D.S. Coxson, and S.D. Siciliano. 2011b. Bryophyte-cyanobacterial associations as a key factor in N2-fixation across the Canadian Arctic. Plant Soil 344(1): 335–346. doi: 10.1007/s11104-011-0750-x.

Sullivan, P.F., M. Sommerkorn, H.M. Rueth, K.J. Nadelhoffer, G.R. Shaver, et al. 2007. Climate and species affect fine root production with long-term fertilization in acidic tussock tundra near Toolik Lake, Alaska. Oecologia 153(3): 643–652. doi: 10.1007/s00442-007-0753-8.

Swanson, D.K., C.L. Ping, and G.J. Michaelson. 1999. Diapirism in soils due to thaw of ice-rich material near the permafrost table. Permafr. Periglac. Process. 10(4): 349–367.

Tarnocai, C. 1998. The amount of organic carbon in various soil orders and ecological provinces in Canada. In: Lal, R., Kimble, J.M., Follett, R.F., and Stewart, B.A., editors, Soil processes and the carbon cycle. CRC Press, Boca Raton, FL. p. 81–92

Tarnocai, C., J.G. Canadell, E.A.G. Schuur, P. Kuhry, G. Mazhitova, et al. 2009. Soil organic carbon pools in the northern circumpolar permafrost region. Glob. Biogeochem Cycles 23(2): GB2023. doi: 10.1029/2008GB003327.

Tedrow, J.C.F. 1966. Polar desert soils. Soil Sci Soc Amer Proc 30: 381–387.

Templer, P.H., M.C. Mack, F.S. Chapin III, L.M. Christenson, J.E. Compton, et al. 2012. Sinks for nitrogen inputs in terrestrial ecosystems: a meta-analysis of 15N tracer field studies. 93: 1816–1829. doi: 10.1890/11-1146.1.

Tolvanen, A., and G.H.R. Henry. 2001. Responses of carbon and nitrogen concentrations in High Arctic plants to experimental warming. Can. J. Bot. 79(6): 711–718. doi: 10.1139/cjb-79-6-711.

Tye, A.M., S.D. Young, N.M.J. Crout, H.M. West, L.M. Stapleton, et al. 2005. The fate of 15N

added to high Arctic tundra to mimic increased inputs of atmospheric nitrogen released from a melting snowpack. Glob. Chang. Biol. 11(10): 1640–1654. doi: 10.1111/j.1365-2486.2005.01044.x.

Ugolini, F.C., G. Corti, and G. Certini. 2006. Pedogenesis in the sorted patterned ground of Devon Plateau, Devon Island, Nunavut, Canada. Geoderma 136(1–2): 87–106. doi: 10.1016/j.geoderma.2006.03.030.

Vandenberghe, J. 1992. Cryoturbations: A sediment structural analysis. Permafr. Periglac. Process. 3: 343–352.

Varmuza, K., and P. Filzmoser. 2009. Introduction to multivariate analysis in chemometrics. CRC Press.

Vasques, G.M., S. Grunwald, and J.O. Sickman. 2008. Comparison of multivariate methods for inferential modeling of soil carbon using visible/near-infrared spectra. Geoderma 146(1–2): 14–25. doi: 10.1016/j.geoderma.2008.04.007.

Viscarra Rossel, R.A., and T. Behrens. 2010. Using data mining to model and interpret soil diffuse reflectance spectra. Geoderma 158(1–2): 46–54. doi: 10.1016/j.geoderma.2009.12.025.

Viscarra Rossel, R.A., S.R. Cattle, A. Ortega, and Y. Fouad. 2009. In situ measurements of soil colour, mineral composition and clay content by vis–NIR spectroscopy. Geoderma 150(3–4): 253–266. doi: 10.1016/j.geoderma.2009.01.025.

Viscarra Rossel, R.A., Y.S. Jeon, I.O.A. Odeh, and A.B. McBratney. 2008. Using a legacy soil sample to develop a mid-IR spectral library. Aust. J. Soil Res. 46: 1–16. doi: 10.1071/SR07099.

Viscarra Rossel, R.A., D.J.J. Walvoort, A.B. McBratney, L.J. Janik, and J.O. Skjemstad. 2006. Visible, near infrared, mid infrared or combined diffuse reflectance spectroscopy for simultaneous assessment of various soil properties. Geoderma 131(1–2): 59–75. doi: 10.1016/j.geoderma.2005.03.007.

Walker, D.A., H.E. Epstein, W.A. Gould, A.M. Kelley, A.N. Kade, et al. 2004. Frost-boil ecosystems: complex interactions between landforms, soils, vegetation and climate. Permafr. Periglac. Process. 15(2): 171–188. doi: 10.1002/ppp.487.

Walker, D.A., H.E. Epstein, M.K. Raynolds, P. Kuss, M.A. Kopecky, et al. 2012. Environment, vegetation and greenness (NDVI) along the North America and Eurasia Arctic transects. Environ. Res. Lett. 7: 015504. doi: 10.1088/1748-9326/7/1/015504.

Walker, D.A., H.E. Epstein, V.E. Romanovsky, C.L. Ping, G.J. Michaelson, et al. 2008. Arctic patterned-ground ecosystems: A synthesis of field studies and models along a North American Arctic transect. J. Geophys. Res. 113(G3): G03S01. doi: 10.1029/2007JG000504.

Walker, D.A., M.K. Raynolds, F.J.A. Daniëls, E. Einarsson, A. Elvebakk, et al. 2005. The circumpolar Arctic vegetation map. J. Veg. Sci. 16: 267–282. doi: doi:10.1111/j.1654-1103.2005.tb02365.x.

Walker, M.D., H.C. Wahren, R.D. Hollister, G.H.R. Henry, L.E. Ahlquist, et al. 2006. Plant community responses to experimental warming across the tundra biome. Proc. Natl. Acad. Sci. U. S. A. 103(5): 1342–1346. doi: 10.1073/pnas.0503198103.

Walkley, A., and I.A. Black. 1934. An examination of the Degtjareff method for determining soil organic matter, and a proposed modification of the chromic acid titration method. Soil Sci. 37(1): 29–38. doi: 10.1097/00010694-193401000-00003.

Washburn, A.L. 1956. Classification of patterned ground and review of suggested origins. Geol. Soc. Am. Bull. 67(7): 823–866. doi: 10.1130/0016-7606(1956)67[823:copgar]2.0.co;2.

Wenjun, J., S. Zhou, H. Jingyi, and L. Shuo. 2014. In situ measurement of some soil properties in paddy soil using visible and near-infrared spectroscopy. PLoS One 9(8): 11 pp. doi: 10.1371/journal.pone.0105708.

Wetterlind, J., and B. Stenberg. 2010. Near-infrared spectroscopy for within-field soil characterization: small local calibrations compared with national libraries spiked with local samples. Eur. J. Soil Sci. 61(6): 823–843. doi: 10.1111/j.1365-2389.2010.01283.x.

Wild, B., N. Gentsch, P. Čapek, K. Diáková, R.J.E. Alves, et al. 2016. Plant-derived compounds stimulate the decomposition of organic matter in arctic permafrost soils. Sci. Rep. 6(April): 25607. doi: 10.1038/srep25607.

Wild, B., J. Schnecker, R.J.E. Alves, P. Barsukov, J. Bárta, et al. 2014. Input of easily available organic C and N stimulates microbial decomposition of soil organic matter in arctic permafrost soil. Soil Biol. Biochem. 75: 143–151. doi: 10.1016/j.soilbio.2014.04.014.

Wold, S., M. Sjöström, and L. Eriksson. 2001. PLS-regression: a basic tool of chemometrics. Chemom. Intell Lab 58: 109–130.

Yano, Y., G.R. Shaver, A.E. Giblin, E.B. Rastetter, and K.J. Nadelhoffer. 2010. Nitrogen dynamics in a small arctic watershed: Retention and downhill movement of15N. Ecol. Monogr. 80(2): 331–351. doi: 10.1890/08-0773.1.

Yeh, K.C., and K.C. Kwan. 1978. A comparison of numerical integrating algorithms by trapezoidal, Lagrange, and spline approximation. J. Pharmacokinet. Biopharm. 6(1): 79–98. doi: 10.1007/BF01066064.

Zhang, X., J. He, J. Zhang, I. Polyakov, R. Gerdes, et al. 2012. Enhanced poleward moisture transport and amplified northern high-latitude wetting trend. Nat. Clim. Chang. 3(1): 47–51. doi: 10.1038/nclimate1631.

APPENDICES

APPENDIX A

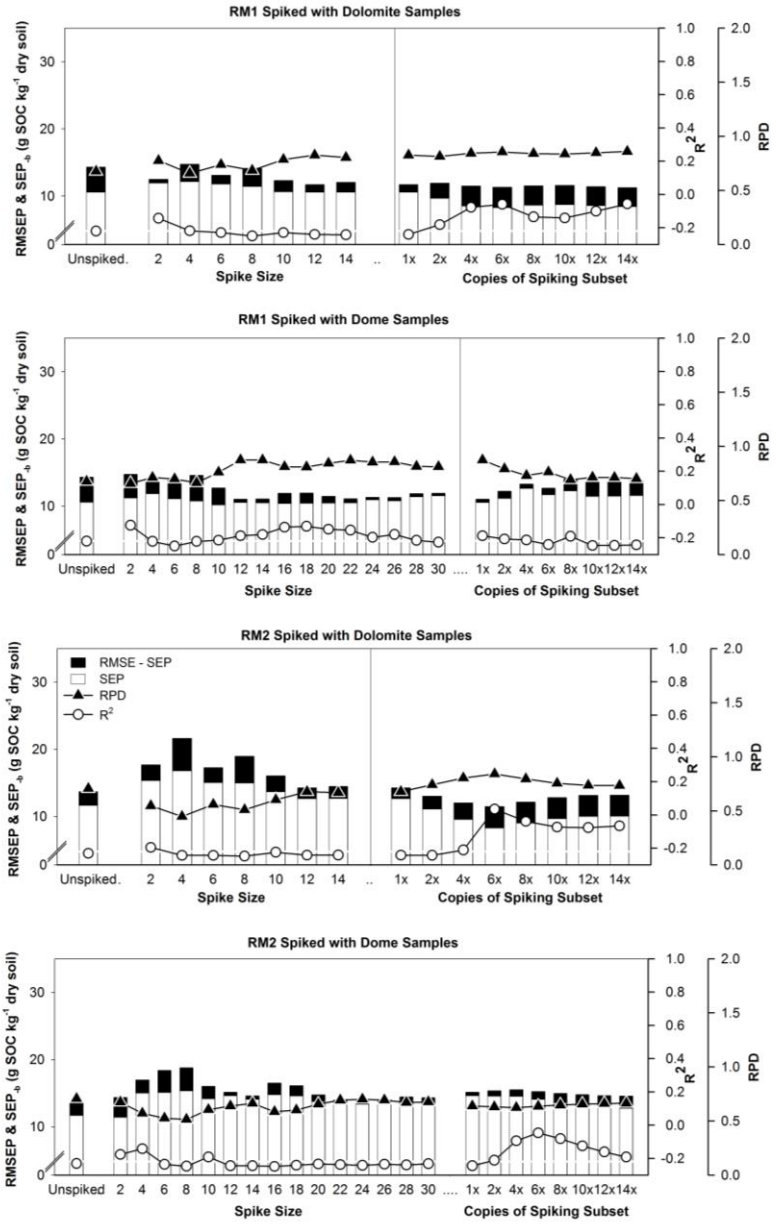

Fig. A.1 Model performance parameters of regional models RM1 and RM2 predicting the Dolomite target test set for: unspiked regional models, regional models spiked with Dolomite and Dome spiking subsets, and regional models spiked with additional copies of the Dolomite and Dome spiking subsets (SS12).

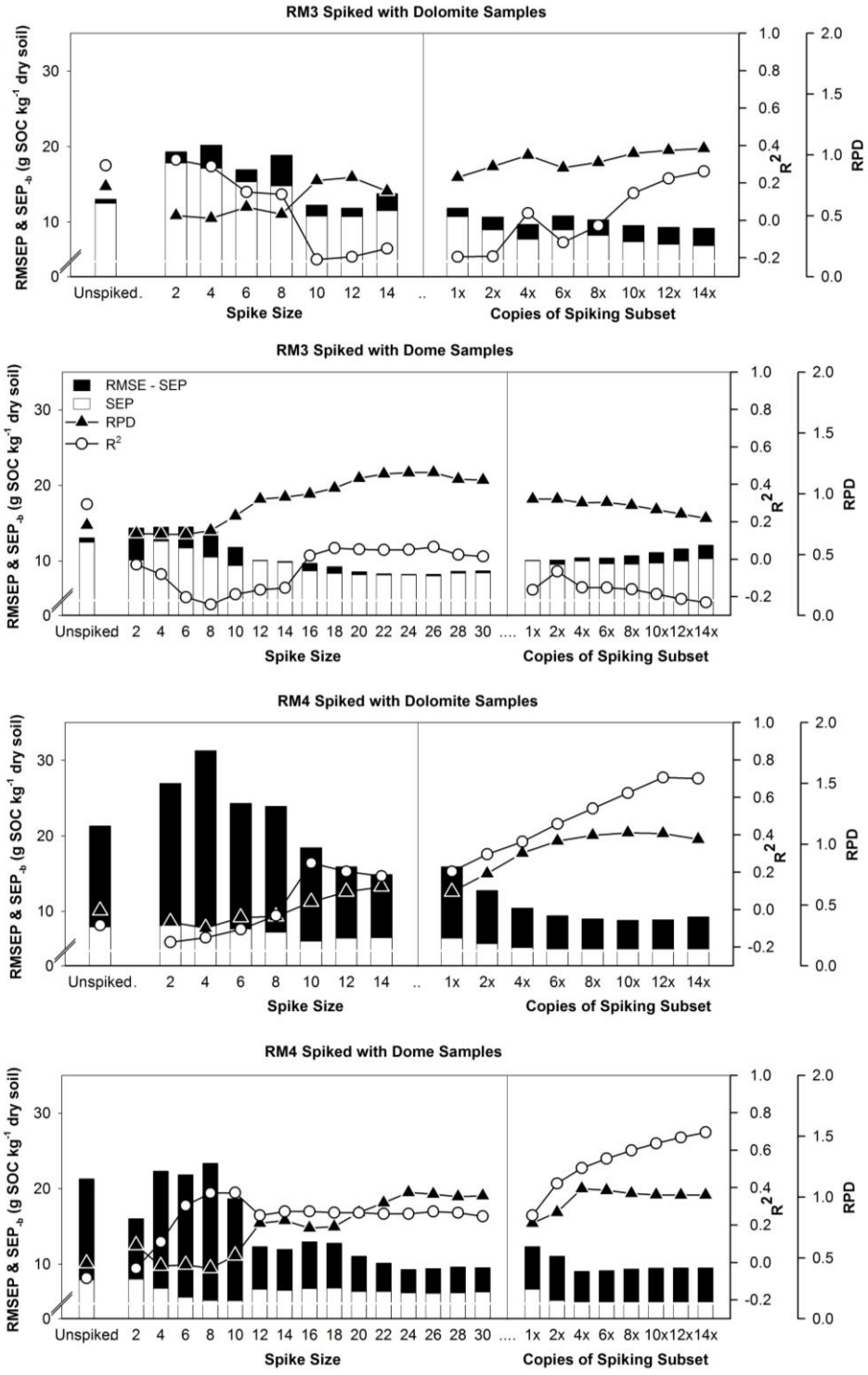

Fig. A.2 Model performance parameters of regional models RM3 and RM4 predicting the Dolomite target test set for: unspiked regional models, regional models spiked with Dolomite and Dome spiking subsets, and regional models spiked with additional copies of the Dolomite and Dome spiking subsets (SS12).

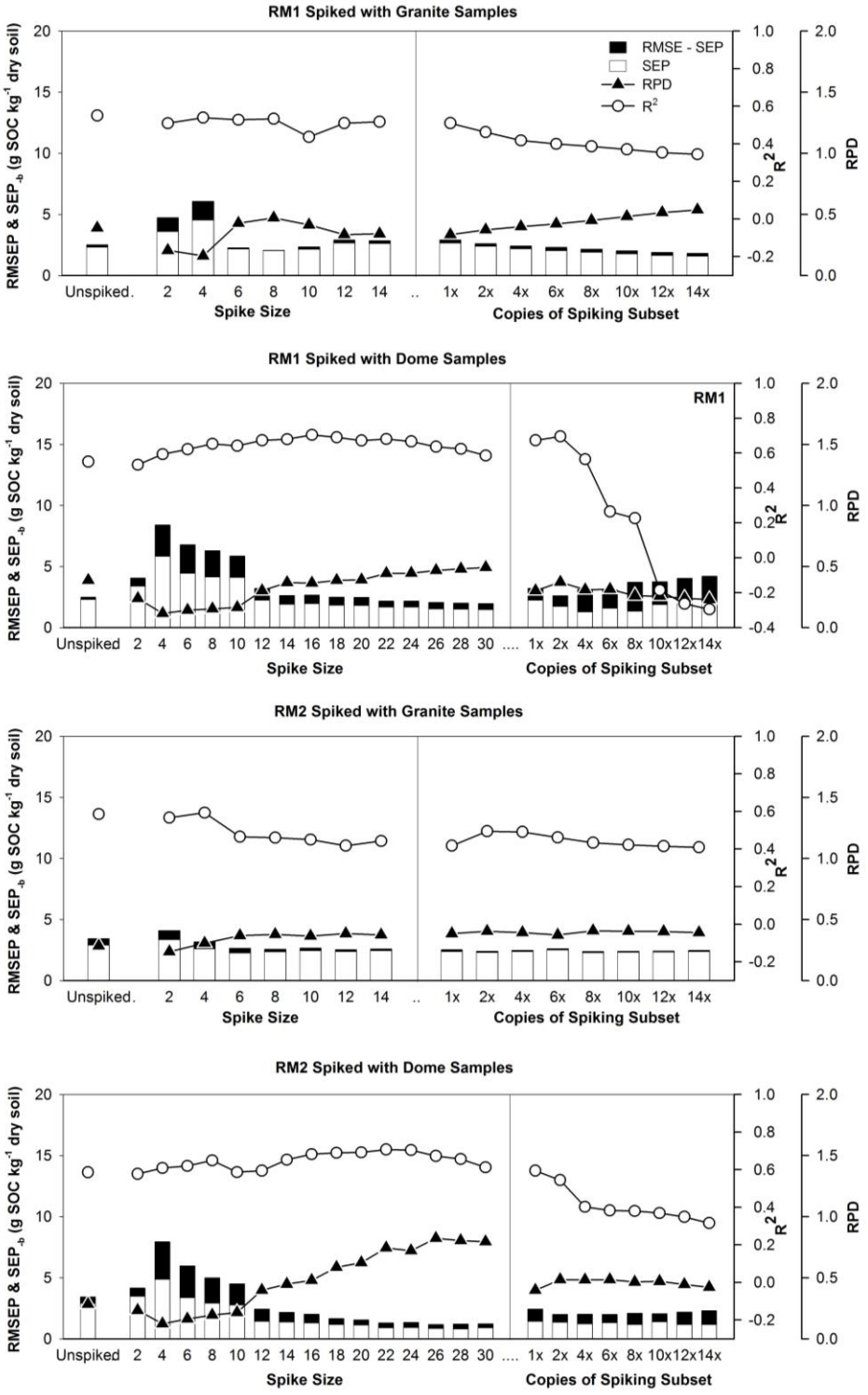

Fig. A.3 Model performance parameters of regional models RM1 and RM2 predicting the Granite target test set for: unspiked regional models, regional models spiked with Granite and Dome spiking subsets, and regional models spiked with additional copies of the Granite and Dome spiking subsets (SS12).

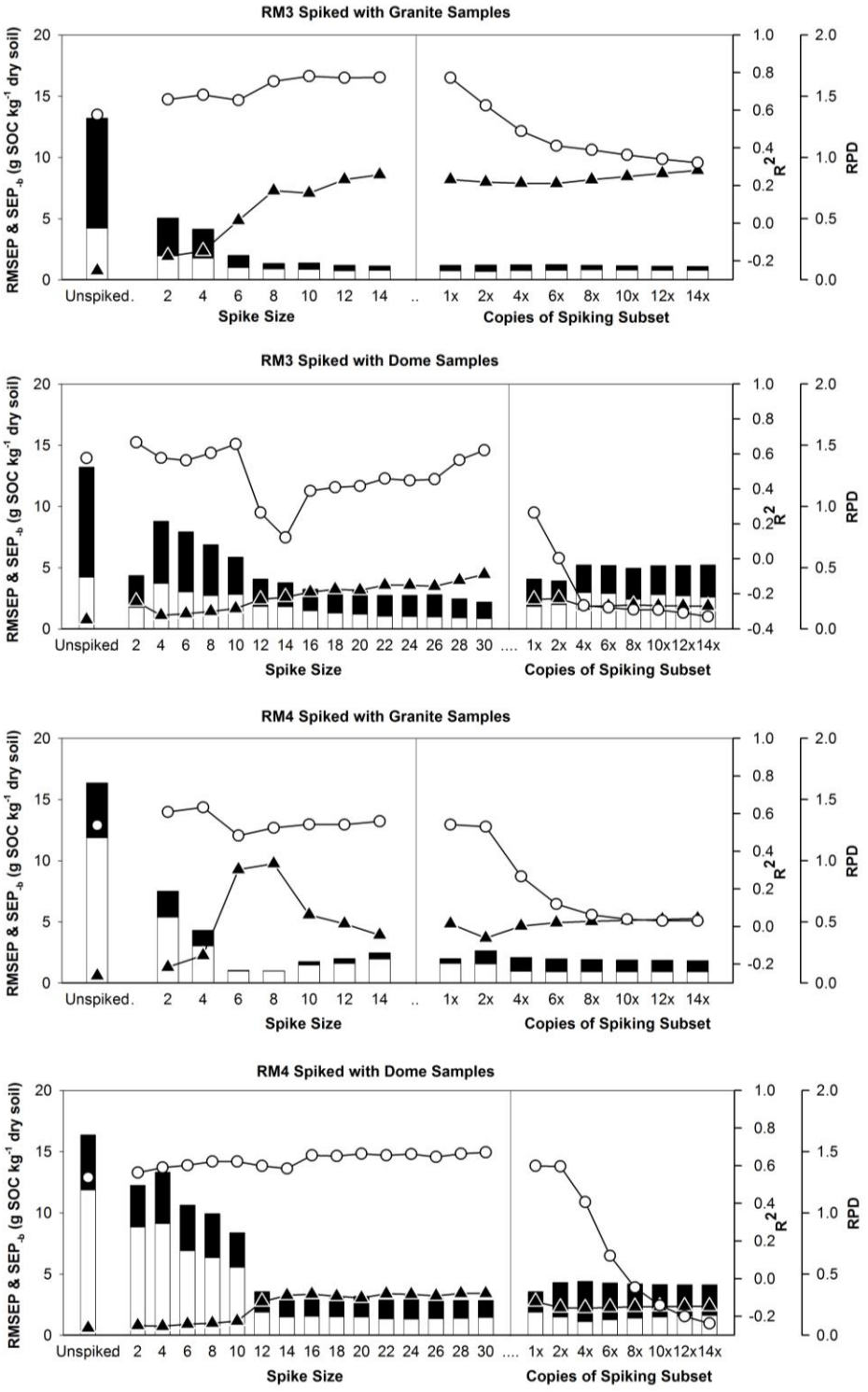

Fig. A.4 Model performance parameters of regional models RM3 and RM4 predicting the Granite target test set for: unspiked regional models, regional models spiked with Granite and Dome spiking subsets, and regional models spiked with additional copies of the Granite and Dome spiking subsets (SS12).

APPENDIX B

Table B.1 Surface cover characteristics of frost boils (n=52) in surface cover groups (I and II) and summary statistics testing for differences between the groups. The surface cover groups were determined by clustering the sampling blocks using Ward's minimum variance clustering and principal component analysis (PCA). Group I is characterized by high bryophyte cover and Group II is characterized by higher bare ground and lichen cover. *S. arctica* is the dominant vascular plant species in both groups.

Surface cover group	Blocks	All Vascular plant	Rock	Gravel	Bare ground	Lichen	Bryophytes	Litter	*S. arctica*
					(% cover)†				
I	1, 4, 7-12	9 ± 1	11 ± 1	9 ± 1	13 ± 2	12 ± 1	44.6 ± 2	16 ± 1	8 ± 1
II	2, 3, 5, 6	8 ± 1	14 ± 2	7 ± 1	23 ± 2	18 ± 2	28.4 ± 2	13 ± 2	7 ± 1
Summary statistics of surface cover group as a main effect									
df		1, 50	1, 50	1, 50	1, 50	1, 50	1, 50	1, 50	1, 50
F		2.12	2.26	1.13	13.57	9.21	27.06	2.62	1.50
P > F		0.15	0.14	0.29	<0.01	<0.01	<0.01	0.11	0.23

† Mean ± standard error for vegetation groups are calculated based on mean % surface cover on frost boils within vegetation groups.

Table B.2 Relationship between natural abundance of $\delta^{15}N$ in leaves versus soil $\delta^{15}N$. Regression statistics are shown for the ground surface, high SOC (Bhy in diapirs), and low SOC subsurface areas in non-diapir and diapir frost boils. Significant p-values are indicated by ** ($P < 0.01$).

Frost boil type	SOC region	Coefficient	SE	adjR^2	df	F	$P > F$
Non-diapir	Surface	1.285	0.349	0.533	1,10	13.540	0.004**
	High	0.020	0.696	-0.100	1,10	0.001	0.977
	Low	0.898	0.553	0.129	1,10	2.630	0.136
Diapir	Surface	0.517	0.335	0.112	1,10	2.391	0.153
	High	0.865	0.197	0.625	1,10	19.310	0.001**
	Low	1.216	0.296	0.591	1,10	16.900	0.002**

Table B.3 Gross mineralization and nitrification rates for diapir and non-diapir frost boils sampled on dolomitic and granitic parent material from July 12-22 sampling period. Values are means ± SE of each frost boil type within the polar semi-deserts.

Parent Material	Frost boil type	Initial $^{15}NH_4$†‡ APE_0	Mineralization‡ mg NH_4 kg^{-1} dry soil d^{-1}	Initial $^{15}NO_3$†‡ APE_0	Nitrification‡ mg NO_3 kg^{-1} dry soil d^{-1}
Dolomite	*Non-diapir*	63.2 ± 4.3	0.04 ± 0.02	20.1 ± 1.6	0.25 ± 0.07
	Diapir	42.6 ± 8.7	0.01 ± 0.13	19.7 ± 0.6	0.09 ± 0.04
Granite	*Non-diapir*	53.9 ± 3.5	0.11 ± 0.03	16.1 ± 0.6	0.16 ± 0.05
	Diapir	46.9 ± 5.8	0.04 ± 0.02	17.0 ± 0.7	0.41 ± 0.11
Summary statistics of mixed effects models with frost boil type as a main effect §					
Dolomite	*n=16*	$F_{(1,12)} = 1.19$, $P = 0.30$	$F_{(1,12)} = 0.90$, $P = 0.36$	$F_{(1,6)} = 0.04$, $P = 0.85$	$F_{(1,11)} = 2.53$, $P = 0.13$
Granite	*n=16*	$F_{(1,10)} = 4.57$, $P = 0.06$	$F_{(1,12)} = 4.34$, $P = 0.06$	$F_{(1,12)} = 0.59$, $P = 0.46$	$F_{(1,12)} = 4.09$, $P = 0.07$

† APE_0 = atom % ^{15}N excess of NH_4^+/NO_3^- pool at time zero

‡ In-field gross mineralization rate and gross nitrification rates were each measured on a pair of 200 cm^3 soil cores for each frost boil using the ^{15}N isotope-dilution technique (Hart et al. 1994). Each soil core was labeled with 10.4 mL of $(^{15}NH_4)_2SO_4$ or $K^{15}NO_3$ solution (15 µg/mL N at 98% ^{15}N enrichment), for mineralization and nitrification, respectively. ^{15}N and ^{14}N were collected using the diffusion disk technique (Stark and Hart 1996), and samples were analyzed using a Costech ECS4010 elemental analyzer coupled to a Delta V mass spectrometer (Department of Soil Science, University of Saskatchewan) and a Technicon Autoanalyzer (Technicon Industrial Systems, 1978). Negative values outside of three standard deviations from the mean were excluded from the analysis (For gross mineralization - 2 dolomite and 1 granite samples; for gross nitrification -3 dolomite and 1 granite sample), negative values within three standard deviations were truncated to zero.

§ Mixed effects models were fit with frost boil type ("non-diapir" or "diapir") as a main effect and sampling blocks as a random effect. Models were fit using the lmerTest package in R version 3.2.3 (R Core Team 2016, Kuznetsova et al. 2016)

References

Hart, S., J. Stark, E. Davidson, and M. Firestone. 1994. Nitrogen mineralization, immobilization, and nitrification. Pages 985–1018 Methods of Soil Analysis, Part 2 - Microbiological and Biochemical Properties. SSSA Book Series, no. 5, Madison, WI.

Kuznetsova, A., P. B. Brockhoff, and R. H. B. Christensen. 2016. lmerTest:Tests in linear mixed effects models. R package version 2.0-32. https://CRAN.R-project.org/package=lmerTest.

R Core Team. 2016. R: a language and environment for statistical computing. R Foundation for Statistical Computing. http://www.r-project.org/, Vienna, Austria.

Stark, J. M., and S. C. Hart. 1996. Diffusion technique for preparing salt solutions, Kjeldahl digests, and persulfate digests for Nitrogen-15 analysis. Soil Sci. Soc. Am. J. **60**:1846-1855.

APPENDIX C

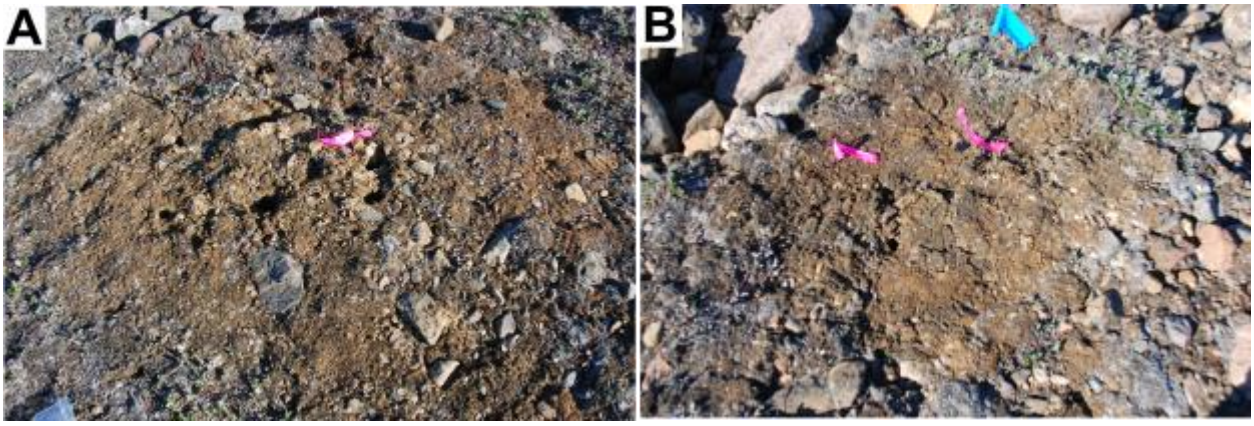

Fig. C.1 Frost boils varied from (A) weakly developed circles with poor sorting of coarse material to the edge, to (B) highly developed, sorted circles with a fine-grained material concentrated near the centre**.**

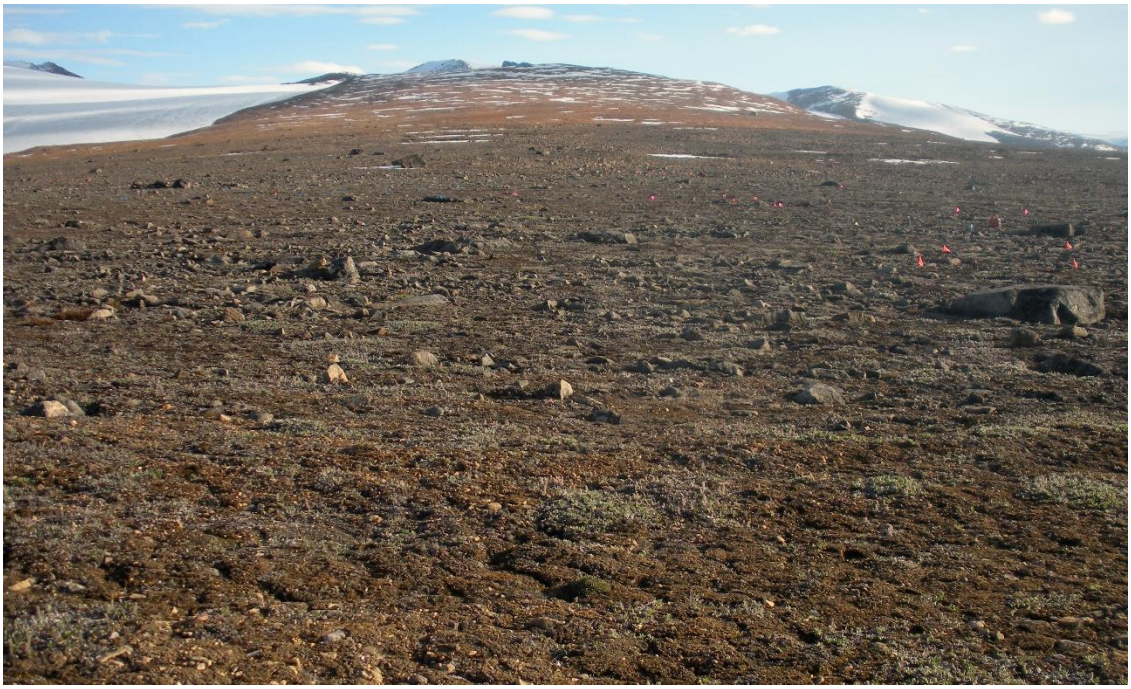

Fig. C.2 A polar semi-desert site at Alexandra Fiord, NU, CA (78°51′N, 76°06′W). Soils were sorted into patterned ground features from cryoturbation processes that affect the distribution of plant cover on the landscape (Photo credit: Sarah Hardy)**.**

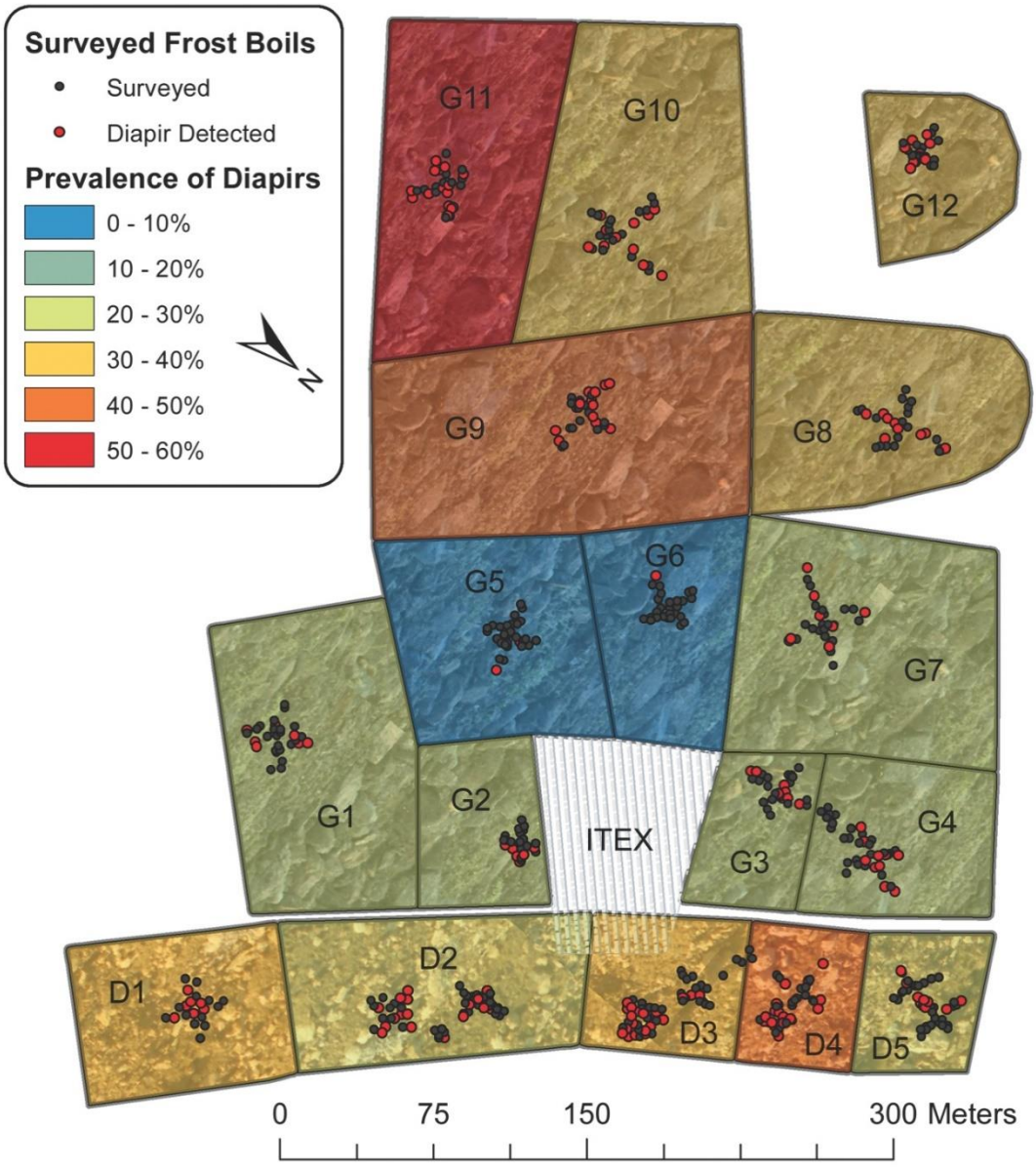

Fig. C.3 Map of field site showing the blocking design and frost boil sample transects. Frost boils with subsurface soil organic carbon peaks detected by visible near-infrared reflectance spectrometry indicate diapir presence (red points). Blocks are coloured to represent the relative abundance of diapir frost boils detected in the randomly positioned perpendicular transects located in each block. Alpha-numeric codes differentiate dolomitic (D) and granitic (G) deserts. The ITEX (international tundra exchange experiment) was not surveyed.

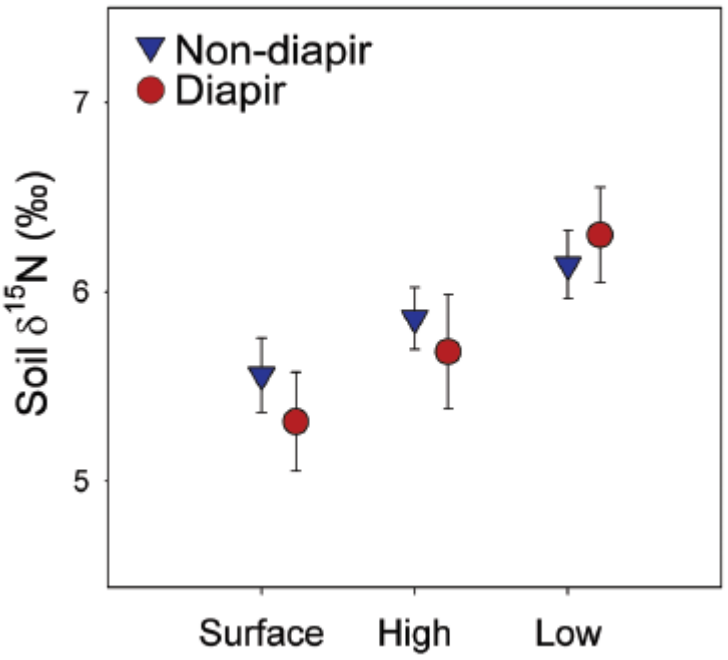

Fig. C.4 Natural abundance soil $\delta^{15}N$ signatures ± SE in non-diapir (blue triangle) and diapir (red circle) frost boils from three different soil organic carbon (SOC) sources in the soil. SOC carbon sources were determined by selecting the surface soils, and the maximum (high) and minimum (low) subsurface SOC concentration for each frost boil using the SOC profiles predicted using vis-NIR spectrophotometry.

APPENDIX D

Analysis of fine scale grids

This appendix outlines the general procedure of fitting 3D variogram models and kriging SOC within the active layer of 24 frost boils.

General Procedure for fitting variogram models

1. Isolate the frost boil of interest.
2. Plot a sample variogram using the variogram function of the gstat package, and fit a model to the sample variogram. Fit variograms using spherical models. If models do not converge, exponential or Gaussian models may be suitable depending on the structure of the data
    a. Sample variograms will initially capture the spatial structure at a cutoff of only 25cm, thus only captures spatial correlation within the soil profile of a single sample point.
3. Adjust the parameters of the sample variogram to explore the spatial structure of SOC (g/kg) on each frost boil.
    a. Adjust the cutoff of distance to encompass approximately ½ to ¾ of the sample site. Within the fine-scale grids the maximum distance between two points at the same depth is 70 cm. The maximum distance between any two points within the sampling grid would be 78 cm. Thus, a maximum cutoff distance would be 60 cm. In some cases, cutoff distance will need to be adjusted for models to converge.
    b. Adjust the lag distances/ width of the lag bins. There should be at least 30 pairs of points per lag distance. Wider lag distances are required to detect spatial structure

between the sample points in different quadrats, however wider lag distance tends to reduce structure for the shortest distances which results in a larger nugget effect. Start with a width of 4 and increase width as needed to capture the wider scale spatial structure.

Table D.1 Variogram model fitting parameters and

Block	Frost boil	Model	Parameters	Nugget	Sill	Nugget:Sill	Range
G2	556.2	Spherical	width = 4; cutoff = 60	0.030	0.119	0.252	37.7 cm
G2	578.2	Spherical	width = 4; cutoff = 60	0.029	0.094	0.309	24.5 cm
G3	543	Spherical	width = 4; cutoff = 60	0.013	0.033	0.394	19.8 cm
G3	547	Spherical	width 4; cutoff = 60	0.021	0.049	0.429	35.6 cm
G4	517	Spherical	width = 10; cutoff = 55	0.030	0.057	0.526	24.9 cm
G4	533	Spherical	width = 10; cutoff = 60	0.050	0.079	0.633	14.5 cm
G4	1002	Spherical	width = 4; cutoff = 60	0.020	0.046	0.438	46.3 cm
G4	1003	Spherical	width = 4; cutoff = 60	0.027	0.069	0.394	35.8 cm
G5	568.2	Spherical	width = 6; cutoff = 60	0.015	0.040	0.375	36.4 cm
G5	593.2	Spherical	width = 5; cutoff = 60	0.011	0.066	0.167	41.5 cm
G6	634.2	Spherical	width = 4; cutoff = 60	0.011	0.071	0.155	39.0 cm
G6	642.2	Spherical	width = 4; cutoff = 60	0.023	0.088	0.261	24.0 cm
G7	599.2	Exponential	width = 2; cutoff = 45	0.020	0.082	0.244	26.4 cm
G7	619.2	Gaussian	width = 4; cutoff = 50	0.018	0.080	0.225	26.6 cm
G8	1160	Spherical	width = 4; cutoff = 60	0.003	0.048	0.063	41.3 cm
G8	1172	Spherical	width = 4; cutoff = 60	0.003	0.022	0.136	12.0 cm
G9	486.2	Gaussian	width = 4; cutoff = 50	0.020	0.112	0.179	46.2 cm
G9	1018	Spherical	width = 4; cutoff = 60	0.012	0.044	0.273	25.9 cm
G10	1103	Spherical	width = 8; cutoff = 60	0.028	0.091	0.308	23.1 cm
G10	1104	Spherical	width = 4; cutoff = 60	0.028	0.093	0.301	18.6 cm
G11	1130	Spherical	width = 8; cutoff = 60	0.044	0.074	0.595	21.6 cm
G11	1133	Spherical	width = 4; cutoff = 60	0.021	0.051	0.412	5.2 cm
G12	1217	Spherical	width = 8; cutoff = 45	0.004	0.119	0.034	20.3 cm
G12	1218	Spherical	width = 6; cutoff = 60	0.003	0.018	0.167	18.9 cm

Supplemental figures of fine-scale SOC on frost boils by sampling block

Block 2

Frost boils 578.2 and 556.2 had decreasing SOC with depth in the center of the frost boil, with no apparent subsurface peak.

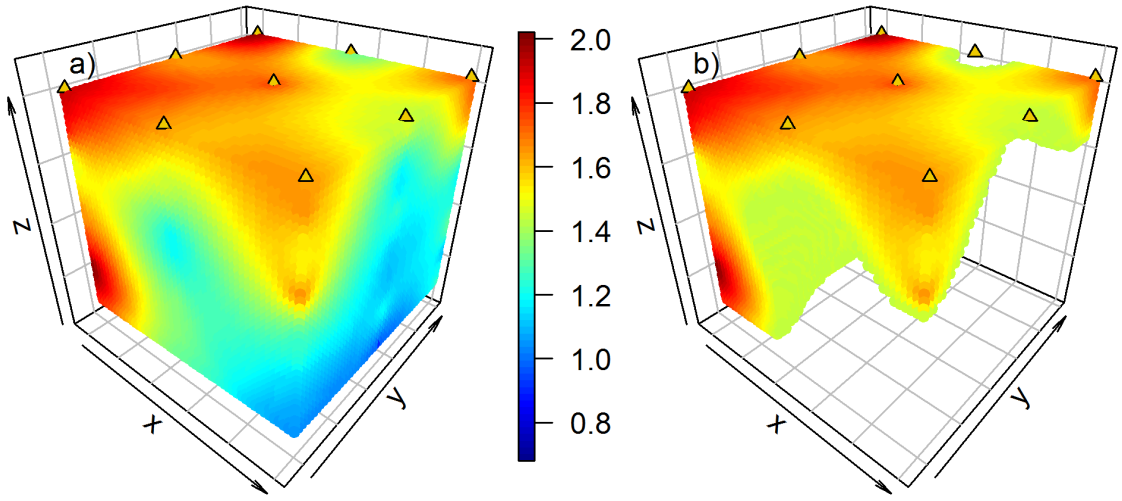

Figure D.1. Frost boil 578.2 displaying all kriged log transformed SOC (g k^{-1}) values (a), and the values in the top quartile of the frost boil (b). The x-axis extends from the edge of the frost boil toward the center and the y-axis is parallel to the edge. Triangular points show the vis-NIR sampling locations.

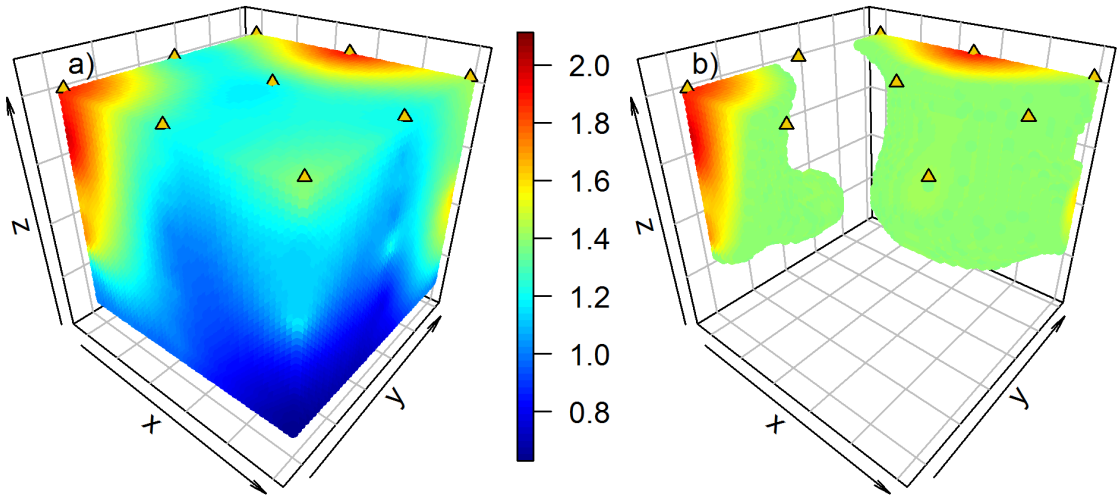

Figure D.2. Frost boil 556.2 displaying all kriged log transformed SOC (g k-1) values (a), and the values in the top quartile of the frost boil (b). The x-axis extends from the edge of the frost boil toward the center and the y-axis is parallel to the edge. Triangular points show the vis-NIR sampling locations.

Block 3

Frost boil 547 had decreasing SOC with depth in its center, whereas frost boil 543 had a strong subsurface peak detected near the soil surface. Frost boil 543 had a narrow variogram range of 19.8 cm which limited the ability to krige between vis-NIR subplot sampling points. An additional figure is included of the raw data.

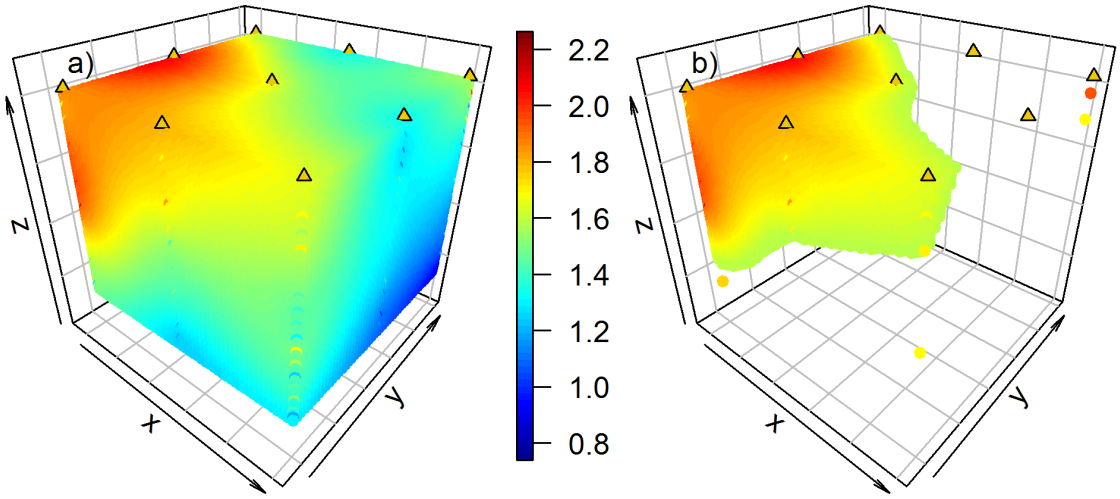

Figure D.3. Frost boil 547 displaying all kriged log transformed SOC (g k^{-1}) values (a), and the values in the top quartile of the frost boil (b). The x-axis extends from the edge of the frost boil toward the center and the y-axis is parallel to the edge. Triangular points show the vis-NIR sampling locations.

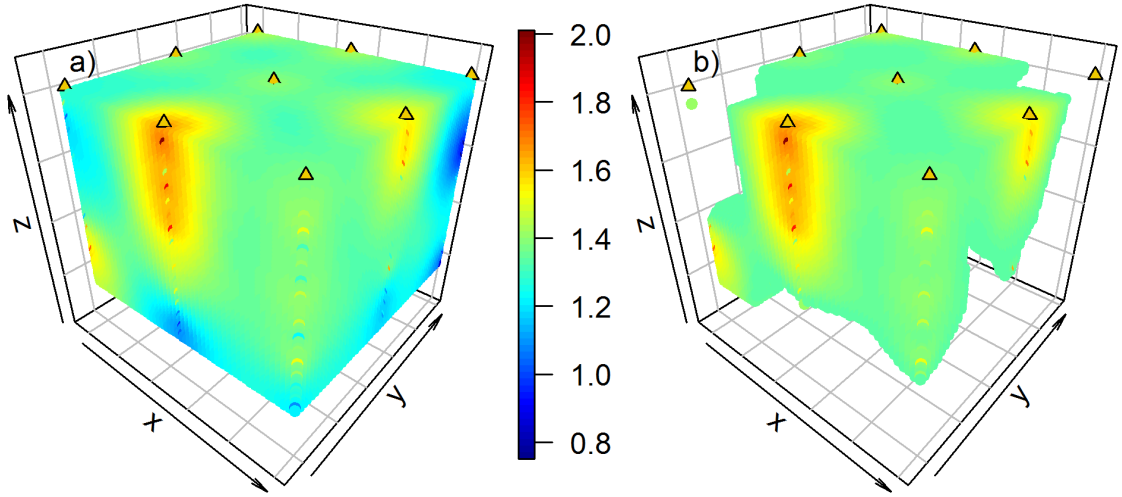

Figure D.4. Frost boil 543 displaying all kriged log transformed SOC (g k^{-1}) values (a), and the values in the top quartile of the frost boil (b). The x-axis extends from the edge of the frost boil toward the center and the y-axis is parallel to the edge. Triangular points show the vis-NIR sampling locations.

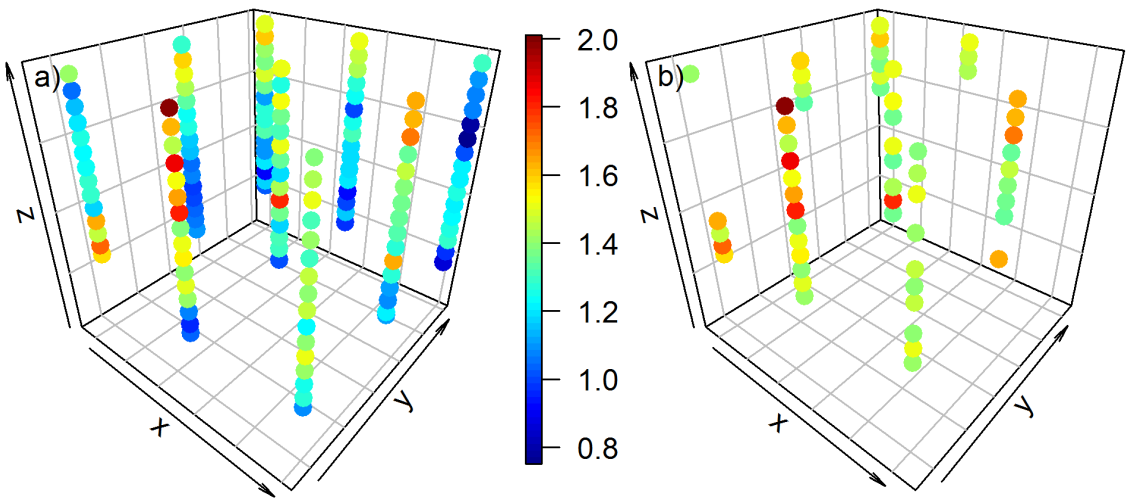

Figure D.5. Frost boil 543 displaying vis-NIR predicted log transformed SOC (g k^{-1}) displaying all values (a), and the values in the top quartile of the frost boil (b). The x-axis extends from the edge of the frost boil toward the center and the y-axis is parallel to the edge. Triangular points show the vis-NIR sampling locations.

Block 4

Frost boil 533 has a strong subsurface peak near the top of the active layer in its center. Frost boil 517 had no significant change in SOC throughout the soil profile at its center. Frost boil 533 had a narrow variogram range of 10.8 cm which limited the ability to krige between vis-NIR subplot sampling points. An additional figure is included of the raw data.

Frost boil 1002 had a weak sub surface peak in the middle of the active layer in its center and frost boil 1003 had decreasing SOC with depth with no evidence of a subsurface peak.

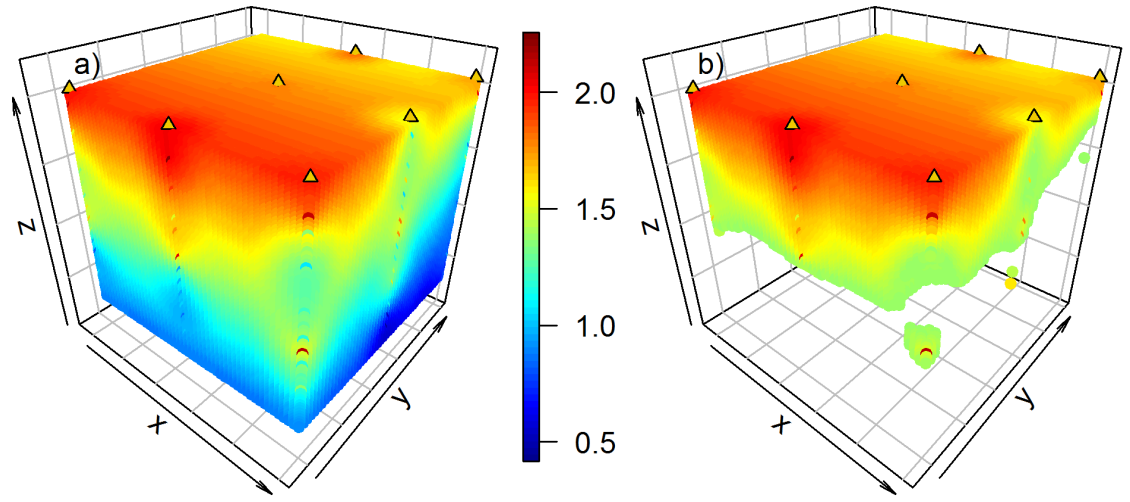

Figure D.6. Frost boil 533 displaying all kriged log transformed SOC (g k^{-1}) values (a), and the values in the top quartile of the frost boil (b). The x-axis extends from the edge of the frost boil toward the center and the y-axis is parallel to the edge. Triangular points show the vis-NIR sampling locations.

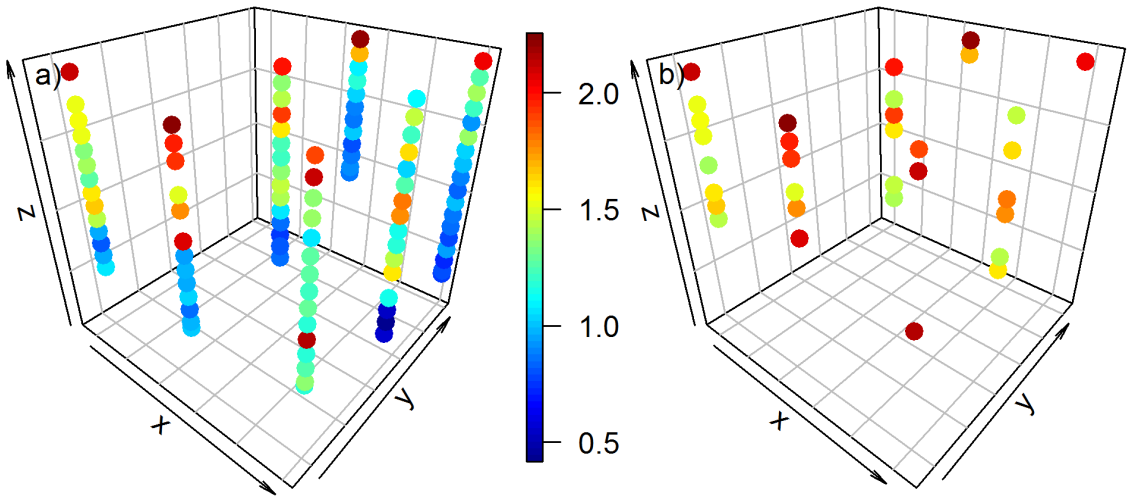

Figure D.7. Frost boil 533 displaying vis-NIR predicted log transformed SOC (g k^{-1}) displaying all values (a), and the values in the top quartile of the frost boil (b). The x-axis extends from the edge of the frost boil toward the center and the y-axis is parallel to the edge. Triangular points show the vis-NIR sampling locations.

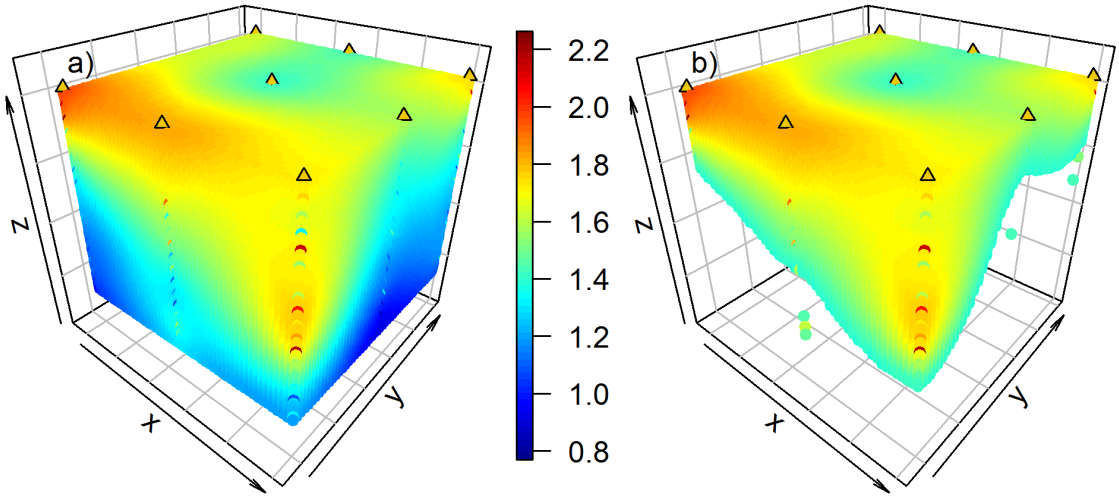

Figure D.8. Frost boil 517 displaying all kriged log transformed SOC (g k-1) values (a), and the values in the top quartile of the frost boil (b). The x-axis extends from the edge of the frost boil toward the center and the y-axis is parallel to the edge. Triangular points show the vis-NIR sampling locations.

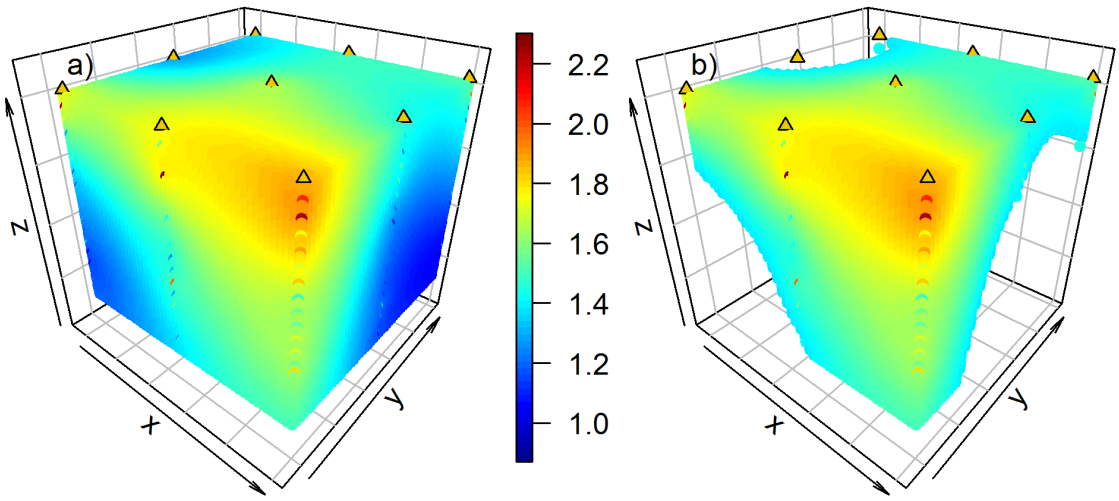

Figure D.9. Frost boil 1002 displaying all kriged log transformed SOC (g k-1) values (a), and the values in the top quartile of the frost boil (b). The x-axis extends from the edge of the frost boil toward the center and the y-axis is parallel to the edge. Triangular points show the vis-NIR sampling locations.

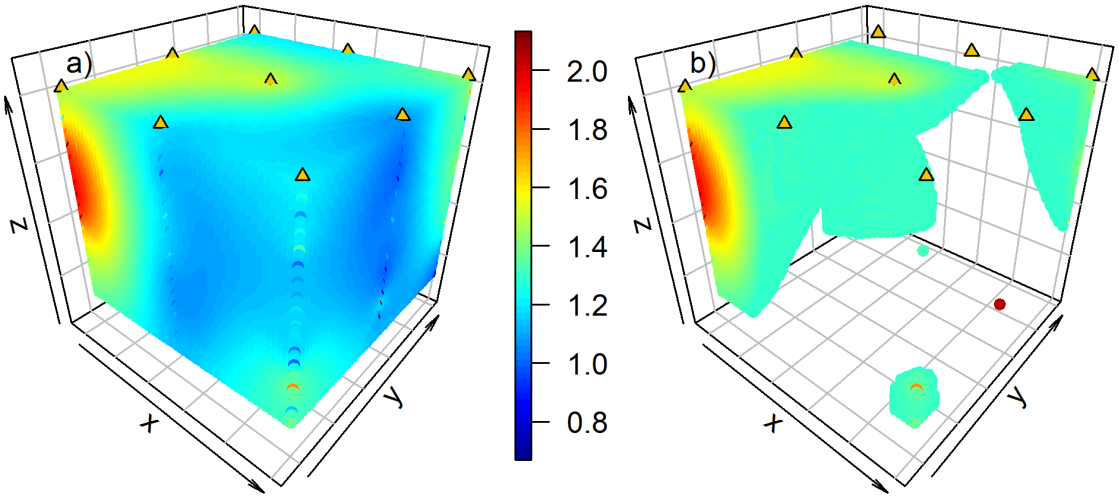

Figure D.10. Frost boil 1003 displaying all kriged log transformed SOC (g k-1) values (a), and the values in the top quartile of the frost boil (b). The x-axis extends from the edge of the frost boil toward the center and the y-axis is parallel to the edge. Triangular points show the vis-NIR sampling locations.

Block 5

Frost boil 593.2 had no change in SOC throughout the soil profile in its center and FB 568.2 had decreasing SOC with depth.

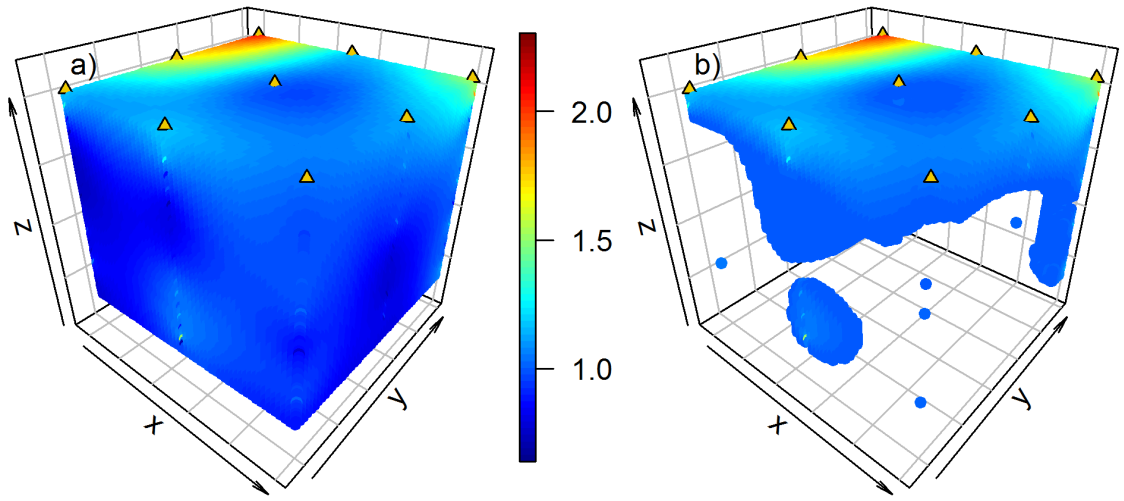

Figure D.11. Frost boil 593.2 displaying all kriged log transformed SOC (g k^{-1}) values (a), and the values in the top quartile of the frost boil (b). The x-axis extends from the edge of the frost boil toward the center and the y-axis is parallel to the edge. Triangular points show the vis-NIR sampling locations.

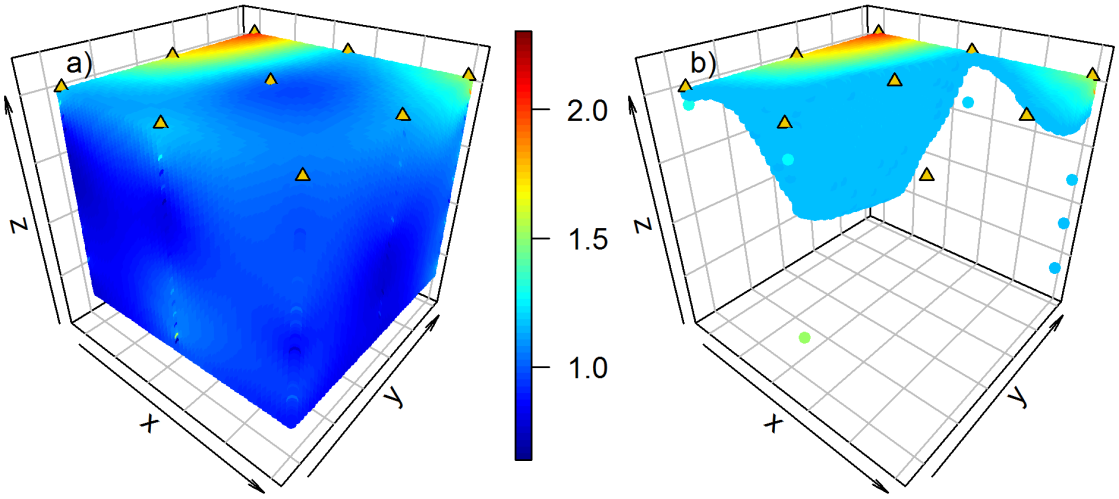

Figure D.12. Frost boil 593.2 all displaying kriged log transformed SOC (g k^{-1}) values (a), and the regions enriched in at least 10 g SOC kg^{-1} relative to the minimum SOC detected on his frost boil (b). The x-axis extends from the edge of the frost boil toward the center and the y-axis is parallel to the edge. Triangular points show the vis-NIR sampling locations.

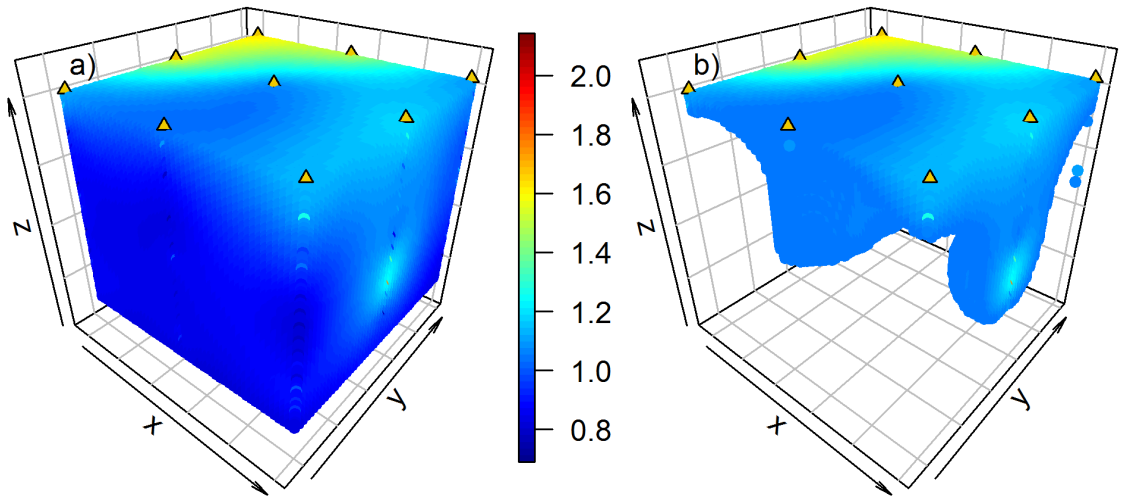

Figure D.13. Frost boil 568.2 displaying all kriged log transformed SOC (g k^{-1}) values (a), and the values in the top quartile of the frost boil (b). The x-axis extends from the edge of the frost boil toward the center and the y-axis is parallel to the edge. Triangular points show the vis-NIR sampling locations.

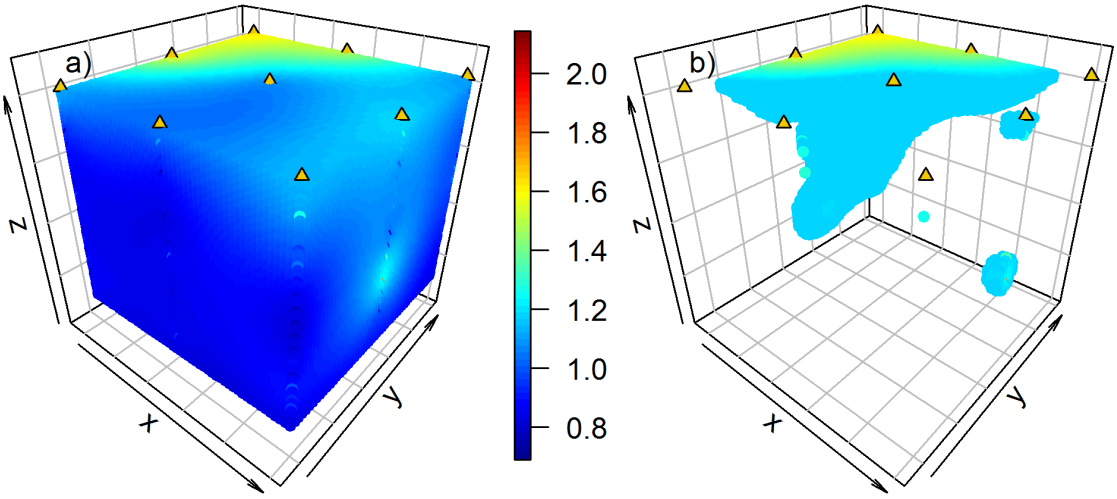

Figure D.14. Frost boil 568.2 all displaying kriged log transformed SOC (g k^{-1}) values (a), and the regions enriched in at least 10 g SOC kg^{-1} relative to the minimum SOC detected on his frost boil (b). The x-axis extends from the edge of the frost boil toward the center and the y-axis is parallel to the edge. Triangular points show the vis-NIR sampling locations.

Block 6

Frost boil 642.2 had no change in SOC throughout its soil profile in its center and frost boil 634.2 had decreasing SOC with depth.

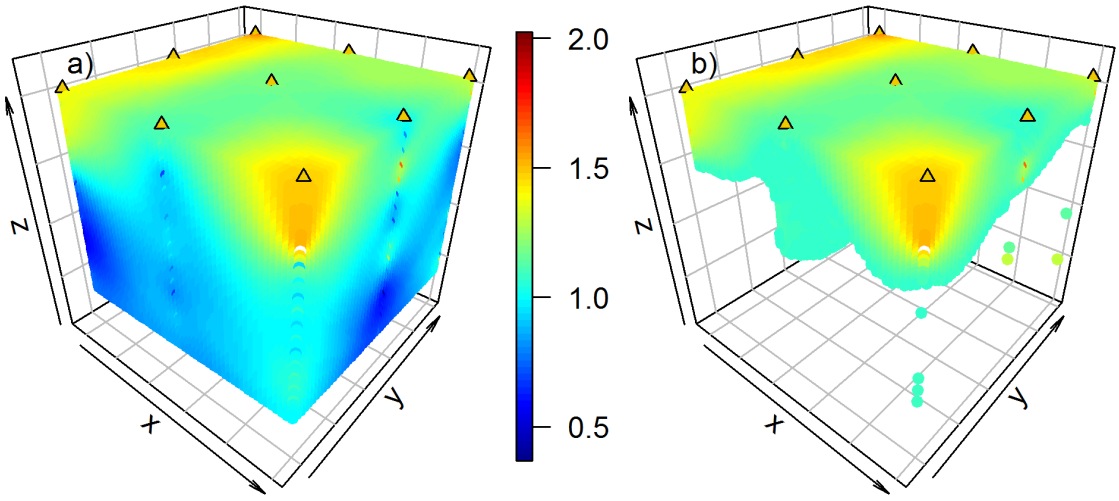

Figure D.15. Frost boil 642.2 displaying all kriged log transformed SOC (g k^{-1}) values (a), and the values in the top quartile of the frost boil (b). The x-axis extends from the edge of the frost boil toward the center and the y-axis is parallel to the edge. Triangular points show the vis-NIR sampling locations.

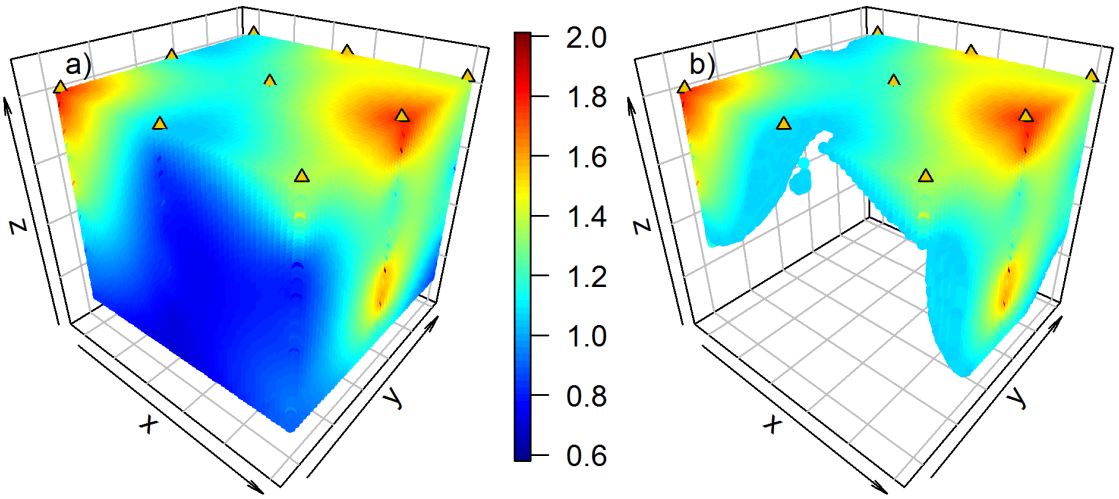

Figure D.16. Frost boil 634.2 displaying all kriged log transformed SOC (g k^{-1}) values (a), and the values in the top quartile of the frost boil subsurface (<= 5 cm) (b). The x-axis extends from the edge of the frost boil toward the center and the y-axis is parallel to the edge. Triangular points show the vis-NIR sampling locations.

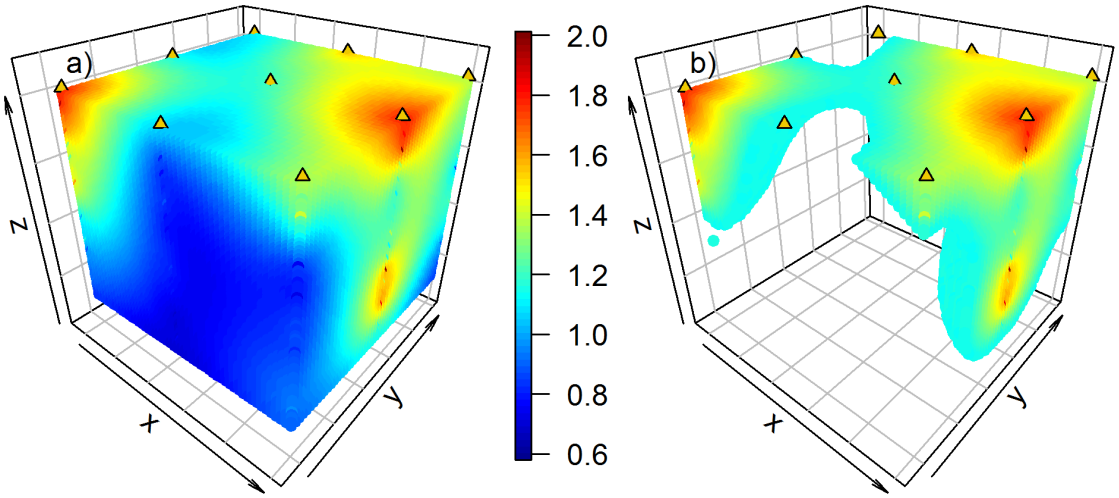

Figure D.17. Frost boil 634.2 all displaying kriged log transformed SOC (g k^{-1}) values (a), and the regions enriched in at least 10 g SOC kg^{-1} relative to the minimum SOC detected on his frost boil (b). The x-axis extends from the edge of the frost boil toward the center and the y-axis is parallel to the edge. Triangular points show the vis-NIR sampling locations.

Block 7

Frost boil 619.2 had decreasing SOC with depth detected in its center and frost boil 599 has a strong peak detected near the bottom of the active layer in its center.

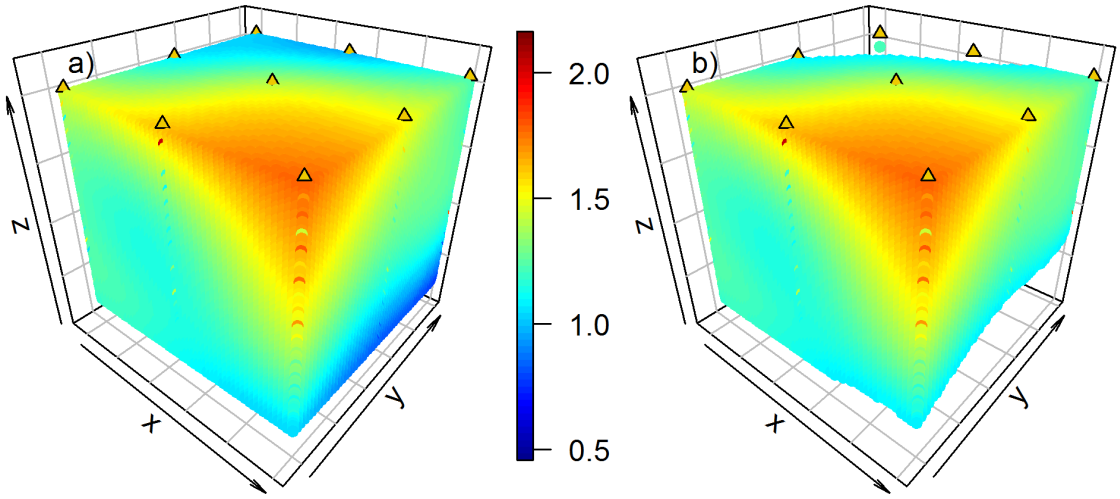

Figure D.18. Frost boil 619.2 displaying all kriged log transformed SOC (g k^{-1}) values (a), and the values in the top quartile of the frost boil (b). The x-axis extends from the edge of the frost boil toward the center and the y-axis is parallel to the edge. Triangular points show the vis-NIR sampling locations.

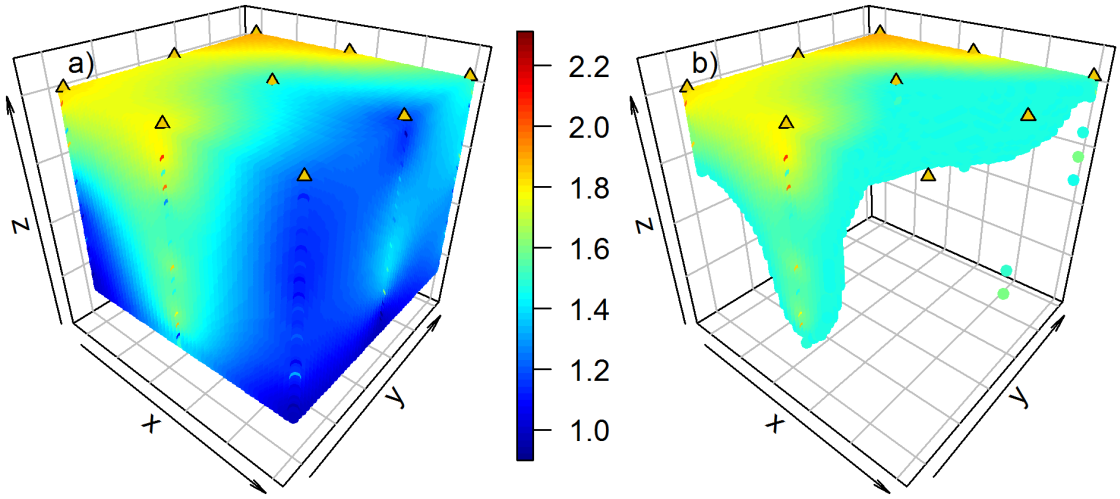

Figure D.19. Frost boil 599.2 displaying all kriged log transformed SOC (g k^{-1}) values (a), and the values in the top quartile of the frost boil (b). The x-axis extends from the edge of the frost boil toward the center and the y-axis is parallel to the edge. Triangular points show the vis-NIR sampling locations.

Block 8

Frost boil 1172 has no change in SOC detected in its center, frost boil had a strong enrichment in SOC mid-active layer.

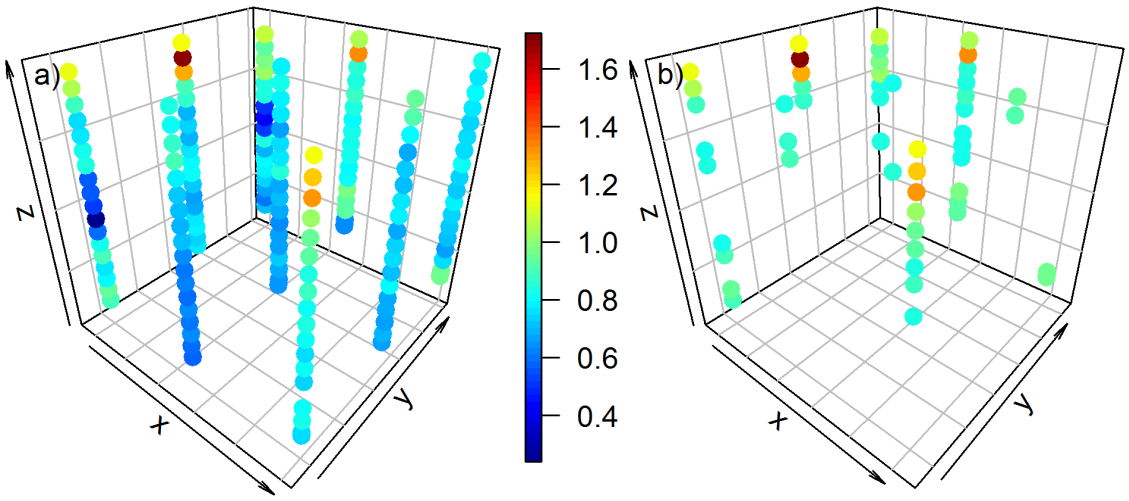

Figure D.20. Frost boil 1172 displaying vis-NIR predicted log transformed SOC (g k^{-1}) displaying all values (a), and the values in the top quartile of the frost boil (b). The x-axis extends from the edge of the frost boil toward the center and the y-axis is parallel to the edge. Triangular points show the vis-NIR sampling locations.

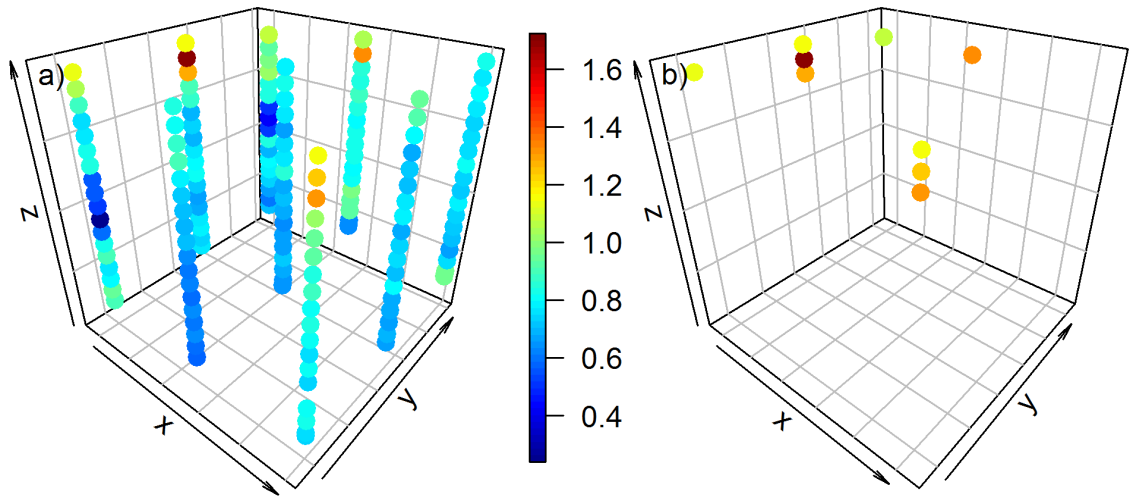

Figure D.21. Frost boil 1172 displaying vis-NIR predicted log transformed SOC (g k^{-1}) displaying all values (a), and the values with greater than 10 g kg-1 contrast with the minimum SOC detected on the frost boil (b). The x-axis extends from the edge of the frost boil toward the center and the y-axis is parallel to the edge. Triangular points show the vis-NIR sampling locations.

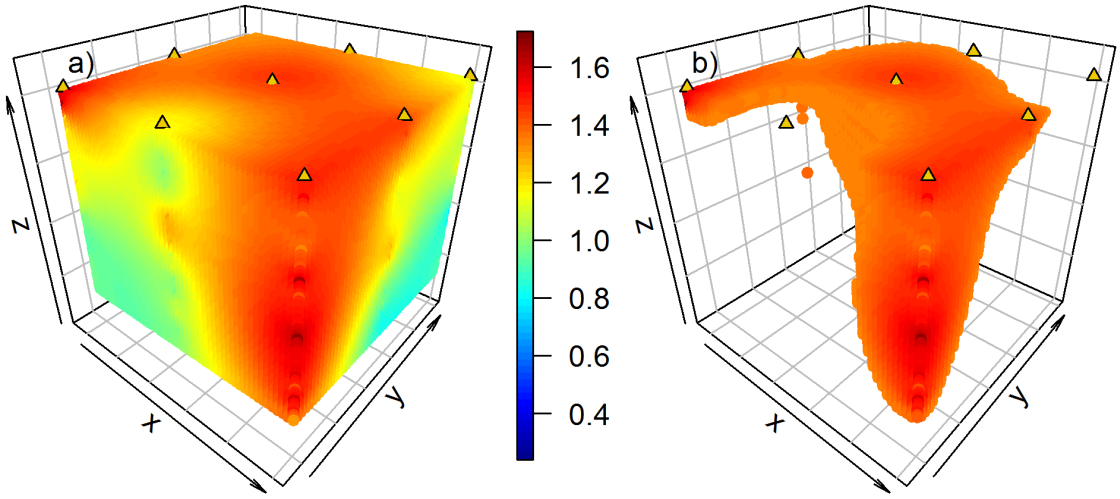

Figure D.22. Frost boil 1160 displaying all kriged log transformed SOC (g k^{-1}) values (a), and the values in the top quartile of the frost boil (b). The x-axis extends from the edge of the frost boil toward the center and the y-axis is parallel to the edge. Triangular points show the vis-NIR sampling locations.

Block 9

Frost Boil 1018 had a strong subsurface peak of carbon at a depth of 29.5 to 34 cm in its Center. Frost Boil 486.2 had decreasing SOC with depth and no subsurface peak detected in its Center.

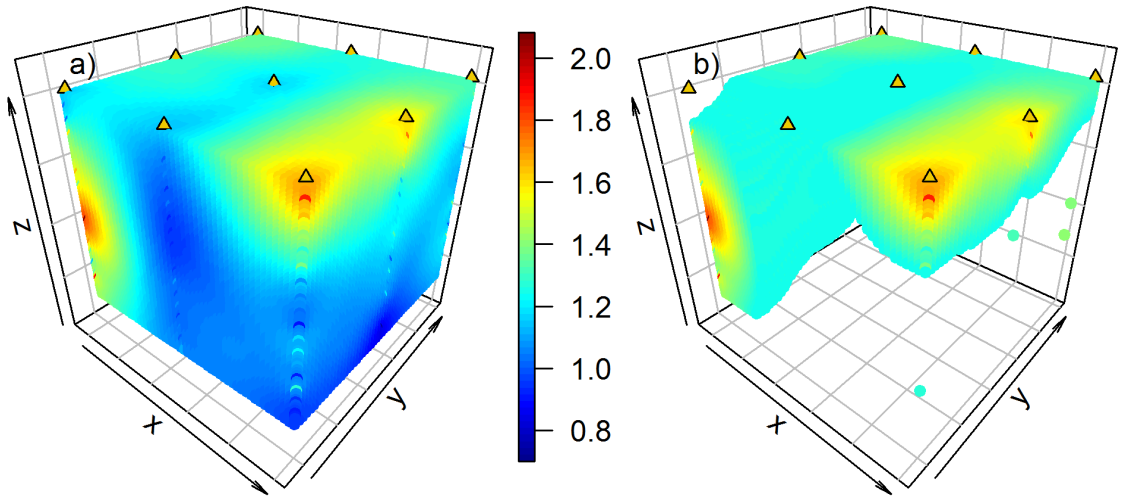

Figure D.23. Frost boil 1018 displaying all kriged log transformed SOC (g k^{-1}) values (a), and the values in the top quartile of the frost boil (b). The x-axis extends from the edge of the frost boil toward the center and the y-axis is parallel to the edge. Triangular points show the vis-NIR sampling locations.

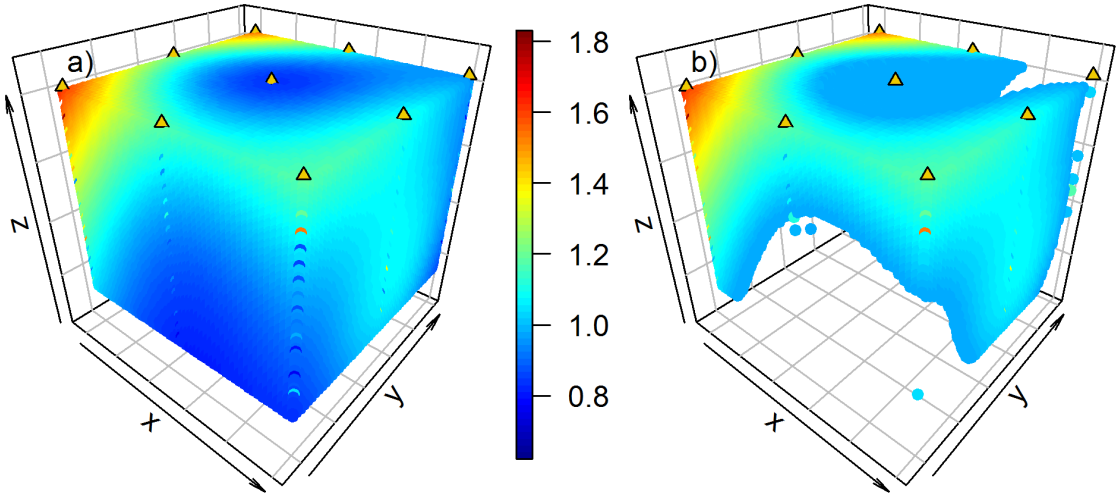

Figure D.24. Frost boil 486.2 displaying all kriged log transformed SOC (g k^{-1}) values (a), and the values in the top quartile of the frost boil (b). The x-axis extends from the edge of the frost boil toward the center and the y-axis is parallel to the edge. Triangular points show the vis-NIR sampling locations.

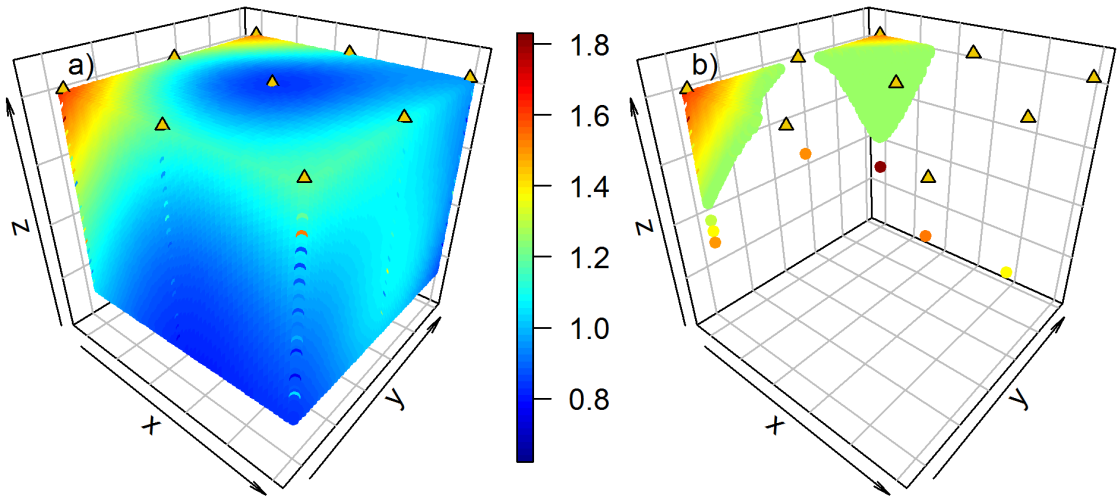

Figure D.25. Frost boil 486.2 all displaying kriged log transformed SOC (g k^{-1}) values (a), and the regions enriched in at least 10 g SOC kg^{-1} relative to the minimum SOC detected on his frost boil (b). The x-axis extends from the edge of the frost boil toward the center and the y-axis is parallel to the edge. Triangular points show the vis-NIR sampling locations.

Block 10

Both frost boil 1103 and 1104 had decreasing SOC with depth at their centers, with no evidence of subsurface enrichments

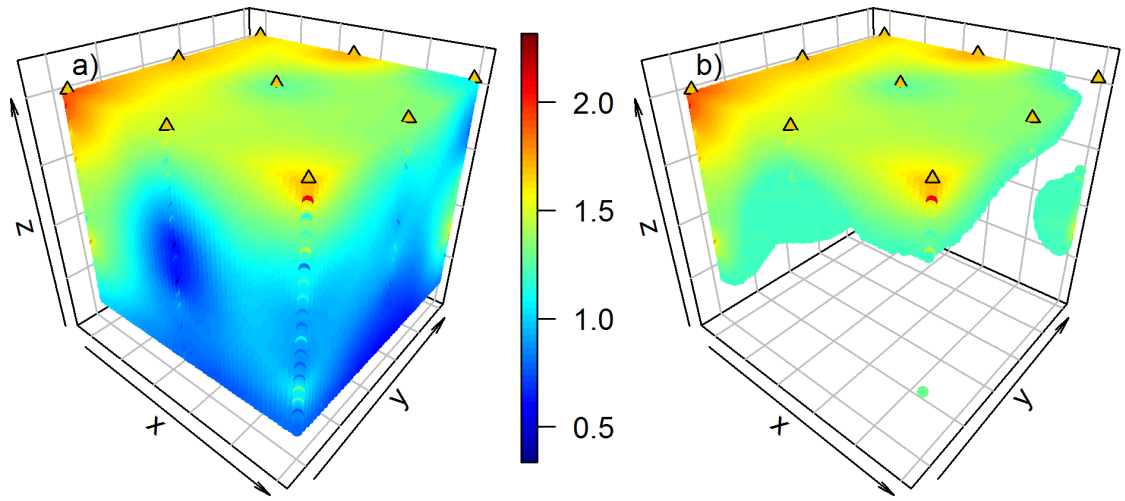

Figure D.26. Frost boil 1103 displaying all kriged log transformed SOC (g k^{-1}) values (a), and the values in the top quartile of the frost boil (b). The x-axis extends from the edge of the frost boil toward the center and the y-axis is parallel to the edge. Triangular points show the vis-NIR sampling locations.

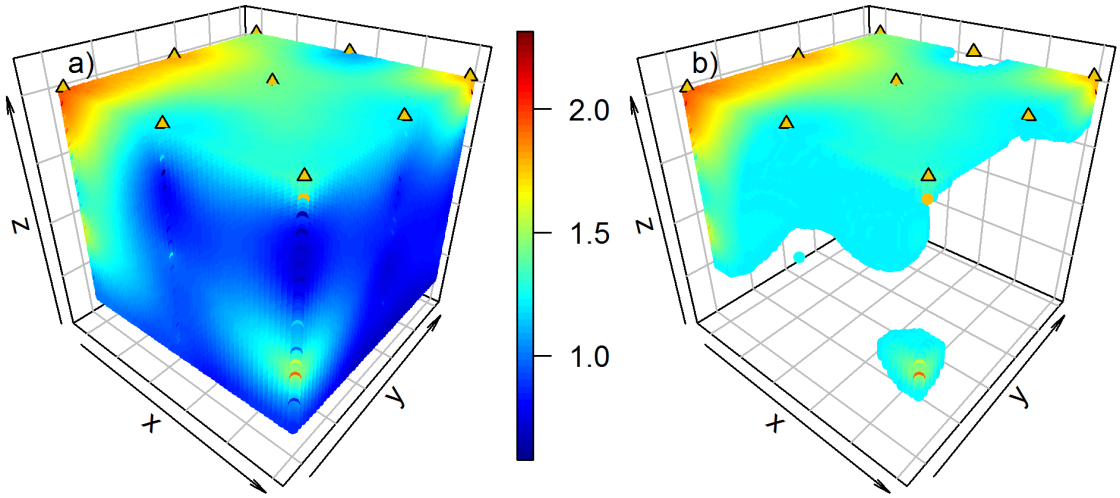

Figure D.27. Frost boil 1104 displaying all kriged log transformed SOC (g k^{-1}) values (a), and the values in the top quartile of the frost boil (b). The x-axis extends from the edge of the frost boil toward the center and the y-axis is parallel to the edge. Triangular points show the vis-NIR sampling locations.

Block 11

Frost boil 1133 had a strong subsurface enrichment near the top of the active layer in its center, and frost boil 1130 had a strong enrichment near the bottom of the active layer at its center.

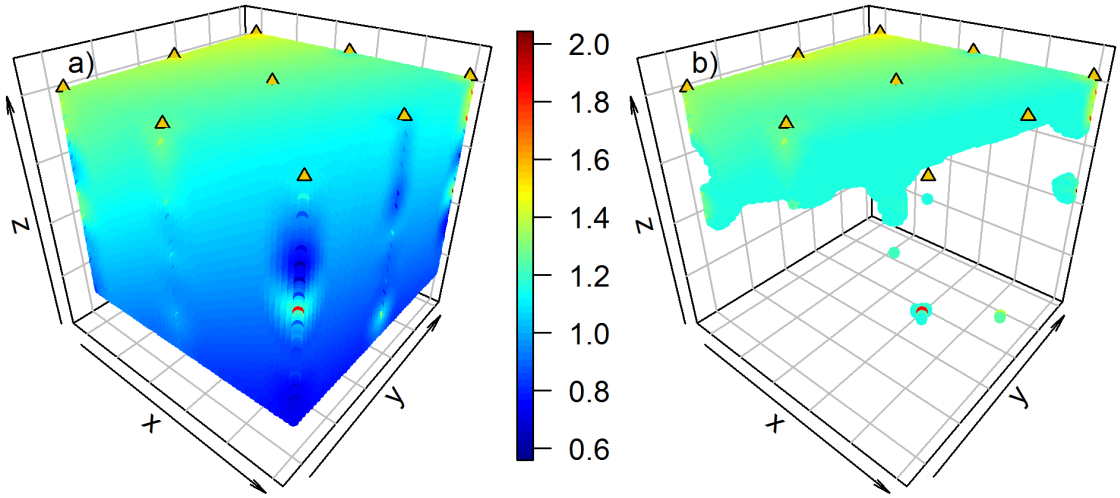

Figure D.28. Frost boil 1133 displaying all kriged log transformed SOC (g k^{-1}) values (a), and the values in the top quartile of the frost boil (b). The x-axis extends from the edge of the frost boil toward the center and the y-axis is parallel to the edge. Triangular points show the vis-NIR sampling locations.

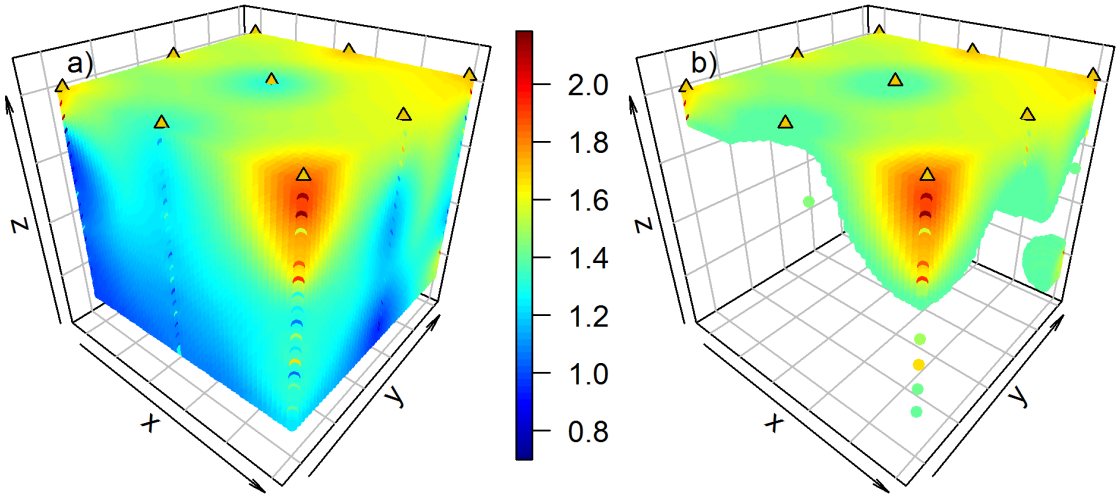

Figure D.29. Frost boil 1130 displaying all kriged log transformed SOC (g k^{-1}) values (a), and the values in the top quartile of the frost boil (b). The x-axis extends from the edge of the frost boil toward the center and the y-axis is parallel to the edge. Triangular points show the vis-NIR sampling locations.

Block 12

Frost boil 1218 had no change in SOC detected throughout its soil profile in its center and frost boil 1217 had a moderate strength enrichment at the bottom of the active layer at its center.

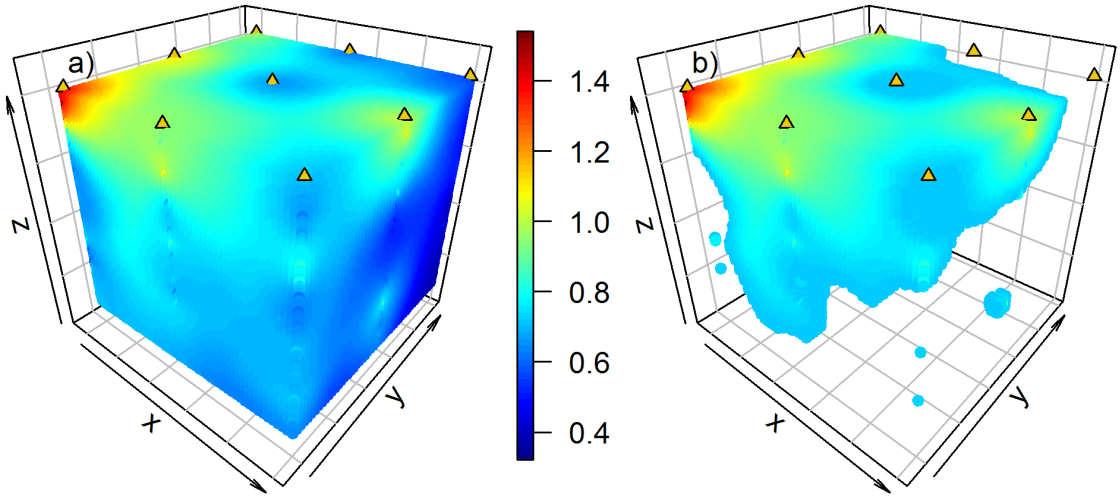

Figure D.30. Frost boil 1218 displaying all kriged log transformed SOC (g k^{-1}) values (a), and the values in the top quartile of the frost boil (b). The x-axis extends from the edge of the frost boil toward the center and the y-axis is parallel to the edge. Triangular points show the vis-NIR sampling locations.

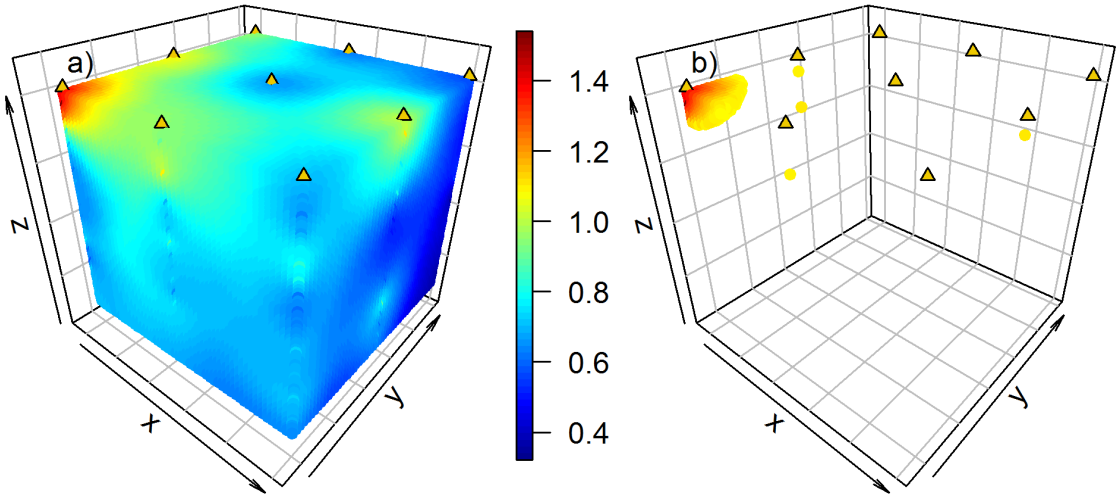

Figure D.31. Frost boil 1218 all displaying kriged log transformed SOC (g k^{-1}) values (a), and the regions enriched in at least 10 g SOC kg^{-1} relative to the minimum SOC detected on his frost boil (b). The x-axis extends from the edge of the frost boil toward the center and the y-axis is parallel to the edge. Triangular points show the vis-NIR sampling locations.

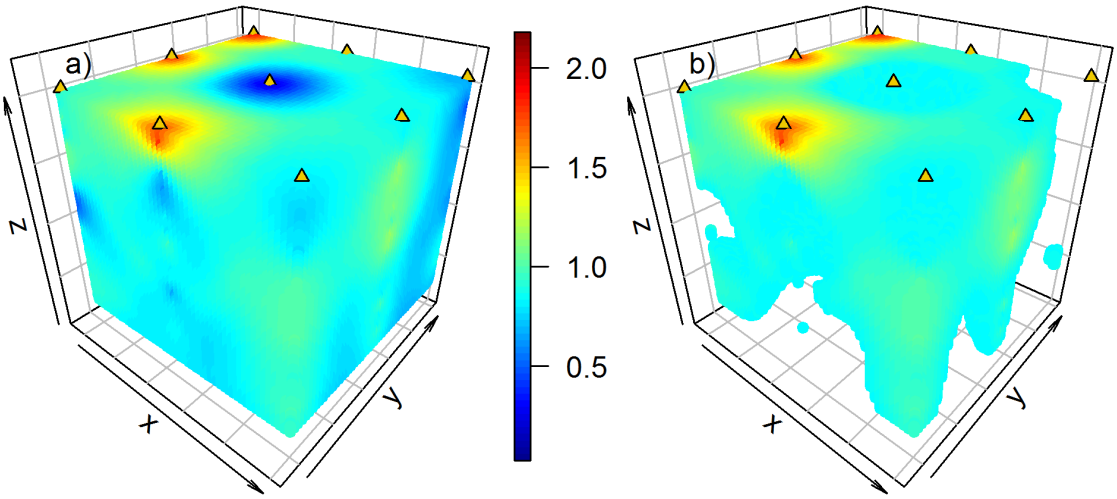

Figure D.32. Frost boil 1217 displaying all kriged log transformed SOC (g k^{-1}) values (a), and the values in the top quartile of the frost boil (b). The x-axis extends from the edge of the frost boil toward the center and the y-axis is parallel to the edge. Triangular points show the vis-NIR sampling locations.

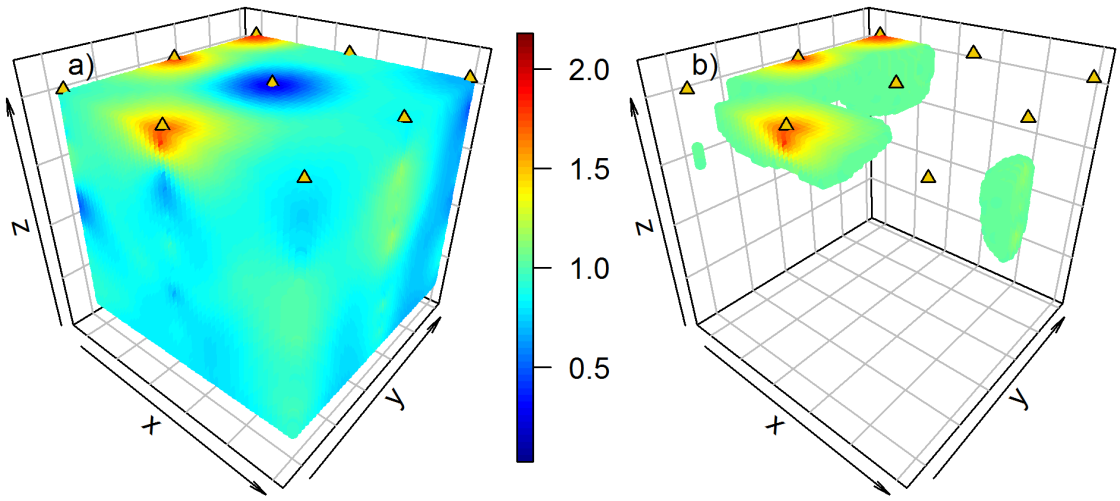

Figure D.33. Frost boil 1217 all displaying kriged log transformed SOC (g k^{-1}) values (a), and the regions enriched in at least 10 g SOC kg^{-1} relative to the minimum SOC detected on his frost boil (b). The x-axis extends from the edge of the frost boil toward the center and the y-axis is parallel to the edge. Triangular points show the vis-NIR sampling locations.

References

(https://vsp.pnnl.gov/help/Vsample/Kriging_Variogram.htm ; https://support.esri.com/en/technical-article/000004923)

APPENDIX E

Above and below-ground plant community composition and structure in response to heterogeneous distribution of SOC in the frost boils of a High Arctic granitic polar desert

Purpose and Justification

The purpose of this work was to investigate whether vascular plants in polar deserts respond to the presence of subsurface pockets of nutrients (diapir Bhy horizons) in frost boils. Given that frequency of diapirs is linked to broad scale differences in plant community and we know that *S. arctica* is able to access nutrients from diapirs when they are present (Muller et al., 2017, Chapter 4), I speculated that there would be distinct differences in the above and below ground plant community structure and composition between diapir and non-diapir frost boils. These data were collected in the course of my thesis, but full analysis is out of scope for the thesis. Methods are detailed here to facilitate future use of this dataset.

Field Sampling

We surveyed relative abundance (n= 52 frost boils) and presence – absence (n = 131 frost boils) of plant species across the 12 granitic blocks (Mueller-Dombois and Ellenberg, 1974). Vegetation cover was assessed in a 0.75 x 0.75 m plot containing a grid of nine contiguous 0.25 x 0.25 m (0.0625-m^2) subplots. The grid was randomly positioned on the vegetated edge and extended to the frost boil center. We recorded the cover of vascular plants, lichens and bryophytes, and physical descriptors such as rock, gravel, litter, and bare ground in each subplot.

We dug soil pits cross sectioning the centre to the edge of 12 diapir and 12 non-diapir frost boils, this cross section corresponded with the vis-NIR sampling points in subplots of the

vegetation sampling grid. In each of those subplots, soil samples were collected in 5 cm increments from the soil surface to a depth of 35 cm (n= ~21/frost boil).

Aboveground plant community progress

At the landscape and individual frost boil scales, we have been attempting to link the presences of diapirs and frost boil types depicted in Figure 3.8 to average sampling block and frost boil differences in plant community composition. Thus far we have used mixed effect models, various ordination and constrained ordination approaches to visualize this data set and an indicator species analysis. In Chapter 4, we observed that more diapirs were detected in blocks with greater bryophyte cover compared to blocks with more bare ground and lichen cover. However, when it comes to comparing diapir and non-diapir frost boils very little difference in average above ground plant community has been observed.

Once the data-analysis of the fine-scale distribution of SOC is completed in section 3.3 and we better understand how the different SOC distributions in frost boil centers and the within frost boil variation contributes to subsurface pockets of carbon, we will look more closely at the relationship between fine-scale SOC distribution and above ground plant community on the frost boil surface.

Belowground plant community progress

For this portion of the project we are really interested in linking the plant root community composition and distribution within frost boils to the distribution of carbon within frost boils. Specifically, linking the plant root community to the presence of diapirs. Are there any specific plant species that are able to access these subsurface nutrient rich patches? Are there other species that are restricted to the surface carbon? If one or both of these cases is true, what does that mean

in a changing climate? Does this give certain plant species a competitive advantage over others? Could this be one mechanism that shrubs are greening the arctic?

Materials and Methods

Eight frost boils (4 diapir / 4 non-diapir) were selected to look at the fine scale root distribution of vascular plants using next generation sequencing. Samples were taken in 5 cm depth increments from 0 to 35 cm at three locations within each frost boil (n=21/frost boil). For this study, we have decided to extract DNA from the soil to get the plant root DNA for this study as well as archaea, bacterial and fungal DNA for a whole community analysis for another study. However, while there are field studies that have extracted DNA from mixed root communities and successfully used next-generation sequencing (Frank et al., 2010; Jones et al., 2011; Lamb et al., 2016), few studies have extracted plant root DNA from soils (Riley et al., 2010; Haling et al., 2011, 2012; Bithell et al., 2014), and none that I've found thus far have dealt with mixed root samples. We identified several challenges associated with extracting plant root DNA from these Arctic soils that resulted in several pre-processing steps prior to extracting DNA:

- *Rocky soils* – high coarse fragments in arctic soils require that they be sieved prior to DNA extraction
- *Low root density* – low root density in arctic soils means that the volume/weight of soil used in the standard protocol to extract DNA from soil may not be sufficient to detect the full root community in our soil samples. Therefore, large roots will be picked from the samples while sieving and a 3 g of sub-sample of the sieved soil will be collected to capture the fine-roots in the soil. The soil and roots will be freeze-dried and homogenized using a ball-grinder prior to DNA extraction.

- *Background soil plant DNA*- Haling et al. (2011) found that when extracting plant root DNA from agricultural soils, you must account for the soil seed bank. Due to the cold climate in the arctic, the soil seed bank, plant roots, and other plant parts redistributed in the soil are likely to persist in the soil (Iversen et al., 2015). To account for the background soil plant DNA we will select ~18 soil samples.
- *Differences in DNA recovery between samples* – Additionally, Haling et al. (2011) suggests using an internal plant standard added to each sample to account for varying DNA recovery due to variable soil properties. We will select a readily available non-Arctic plant that has already been sequenced and is in a different taxonomic family from those found at the field site as an internal plant standard.

To briefly summarize the procedure, prior to extracting DNA picked large roots, sieve soils to remove coarse fragments, freeze dry and grind soil samples. We will add an internal plant standard to our soil samples and extract plant root DNA following the protocols provided in the Power Plant Pro DNA Isolation Kit (Qiagen). The DNA was quantified, standardised, amplified using trnL primers and barcoded following the protocol provided by Illumina.

- Approximately 168 soil samples from 8 frost boils have had all large root picked and were sieved to remove coarse fragments. Picked roots were placed in sterile glass vials and three grams of soil was added to ensure fine plant root community was captured in the samples. Samples were then freeze-dried and homogenized with a ball grinder.

Root Processing SOP

Sieving Soils and Picking Roots

We are sieving soils prior to freeze drying the soils to remove the large % of coarse fragments found in Arctic soils. Because these roots are going to be processed by molecular methods we need to be sure that the materials we work with are sterile and there is no carry-over between samples.

Materials

- Arctic Soil Samples in 50 ml Falcon Tubes
- Styrofoam cooler with Ice
- 2 mm Sieves
- Glass vials
- Small falcon tubes
- 2 Plastic Wash basins
- 10% Bleach Solution
- 70% Ethanol Solution
- Solvent – Acetone
- 1 Plastic or glass waste container
- 1 glass waste container in fume hood
- Kimwipes
- Elastics (Ask Katrina)
- Forceps/tweezers
- Metal sample scoops

Methods

Cleaning Glass Vials

1. Prepare a plastic wash basin with distilled water and a second wash basin with a 10% bleach solution.
2. If dirty (with soil), clean small glass vials that will be used to freeze dry the soil samples in the sink with soap and water. Rinse with distilled water to remove soap residue. Place vials in bleach solution and soak for the 10 minute contact time. Rinse with MilliQ water and place vials to dry in the MilliQ rinsed materials area.
3. Store glass vials covered with aluminium foil in 'Amanda' Drawer

Cleaning Sieves

4. You can use the same basins for the sieves as for the glass vials however don't wash glass vials after you have washed sieves to avoid cross contamination.
5. Wash sieves with soap and water, rinse with distilled water.
6. Dip sieve in 10% bleach solution to ensure all surfaces have contact with bleach and place on clean drying area to allow ~ 5 minute contact time.
7. Re-dip sieve in 10% bleach solution and allow to sit for another 5 minutes.
8. Rinse with acetone in the fume hood and let dry in the fume hood.

9. If not being used immediately, store in the sterile sieve drawer.

Sieving Soils

10. Prepare your work station by wiping the area with water, followed by a 70% ethanol solution.
11. Collect soil samples from the freezer and place in Styrofoam cooler.
12. Label glass vial using lab tape and unique sample number.
13. Tare glass vial on the scale and/or record the weight of the glass vial
14. Dump soil sample in sterile sieve, pick out any roots that do not pass through the sieve and place in the sterile glass vial.
15. Push sample as best you can through the sieve using metal tools or clean glove. Discard rocks.
16. Record weight of roots. Tare.
17. Weigh out 3 g of soil and record exact weight.
18. Cover sample with a kimwipe and wrap the elastic to secure. Return to cooler or place in freezer.
19. Return remaining sample to falcon tube and place label.

Freeze Dry Soils

20. Follow manual operating procedures for the free-drying machine.
21. Be sure to rub silicon gel (found on top shelf on the green cabinet) on the rubber-door seals to ensure proper seal.

Grinding Soils

22. Follow the attached Retsch MM400 Capsule Grinding and Cleaning SOP that was prepared by Samantha Chomyshen.
23. Only modification is that we will be grinding and weighing the full sample that has been freeze-dried (approximately 3 g)
24. Gently scrape sample from the grinding tube and place sample in the micro-centrifuge tube for storage.

DNA Extraction – Using the PowerPlant Pro Kit

Preparing the internal standard

We are using an internal standard to track any differences in sample extraction between the soil + root samples.

1. Grind dry material
2. Extract DNA
3. Sanger sequence species

Testing background DNA concentration

- Select 3 FBs with 1 high, 1 med, 1 low vascular plant cover. 3 depths (Surface soils, 10-20, 20-30). FB center and FB edge. Total 18 samples.
- Pick roots and plant parts from select soil subsamples samples
- Extract DNA from the soil.

APPENDIX F

The following data resulting from this dissertation will be appended as supplemental data:

1. DOME2013_vis_NIR.xlsx : This excel sheet contains the vis-NIR soil spectra taken in the center of frost boils as well as in the fine-scale grids used to visualize SOC distribution in 2-3 dimensions for Chapters 4 and 5.
2. PlantCommunityData_Dome_2013.xlsx : This excel sheet contains the percent plant cover data used in chapter 4 and additional presence-absence data taken on polar desert frost boils that was not assessed in this dissertation.
3. Root Sequencing Data (zip) : These zip folders contain the fastq files and sample information for the root sequencing described in Appendix 5.